

AD-751 928

**DAMAGE THRESHOLD STUDIES IN LASER
CRYSTALS**

Concetto R. Giuliano, et al

Hughes Research Laboratories

Prepared for:

Air Force Cambridge Research Laboratories

September 1972

DISTRIBUTED BY:

NTIS

**National Technical Information Service
U. S. DEPARTMENT OF COMMERCE
5285 Port Royal Road, Springfield Va. 22151**

DAMAGE THRESHOLD STUDIES IN LASER CRYSTALS

C. R. GIULIANO, D. F. DuBOIS,
R. W. HELLWARTH, L. D. HESS, and G. R. RICKEL

HUGHES RESEARCH LABORATORIES
3011 MALIBU CANYON ROAD
MALIBU, CALIFORNIA 90265

Details of Illustrations in
this document may be better
studied on microfiche

FINAL TECHNICAL REPORT
CONTRACT F19628-69-C-0277
PROJECT: 8693

SEPTEMBER 1972

PERIOD COVERED: 16 JUNE 1969 through 15 JUNE 1972

CONTRACT MONITOR: ERLAN S. BLISS, CAPT, USAF
OPTICAL PHYSICS LABORATORY

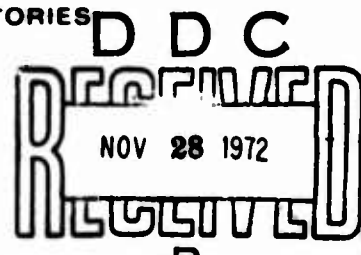
Reproduced by
NATIONAL TECHNICAL
INFORMATION SERVICE
U S Department of Commerce
Springfield VA 22151

Sponsored by
ADVANCED RESEARCH PROJECTS AGENCY
ARPA ORDER 1434

Monitored by
AIR FORCE CAMBRIDGE RESEARCH LABORATORIES
AIR FORCE SYSTEMS COMMAND
UNITED STATES AIR FORCE
BEDFORD MASSACHUSETTS 01730

DISTRIBUTION STATEMENT A

Approved for public release;
Distribution Unlimited



AD751928

Program Code No. 1D10
 Effective Date of Contract 21 May 1969
 Contract Expiration Date 15 July 1972
 Principal Investigator and Phone No.. Concetto R. Giuliano;
 213 456-6411, Ext. 208
 Project Monitor and Phone No. . . . Capt. Erlan S. Bliss;
 617 861-2600

ACCESSION FOR	
NTIS	White Section <input checked="" type="checkbox"/>
DOC	Ext. Section <input type="checkbox"/>
UNANNOUNCED	<input type="checkbox"/>
JUSTIFICATION	
BY	
DISTRIBUTION/AVAILABILITY CODES	
Doc.	Avail. & T. Sec.
A	

Qualified requestors may obtain additional copies from the
 Defense Documentation Center. All others should apply to
 the National Technical Information Service.

DOCUMENT CONTROL DATA - R&D

(Security classification of title, body of abstract and indexing annotation must be entered when the overall report is classified)

1. ORIGINATING ACTIVITY (Corporate author) Hughes Research Laboratories 3011 Malibu Canyon Road Malibu, California 90265		2a. REPORT SECURITY CLASSIFICATION Unclassified	
		2b. GROUP	
3. REPORT TITLE DAMAGE THRESHOLD STUDIES IN LASER CRYSTALS			
4. DESCRIPTIVE NOTES (Type of report and inclusive dates) Scientific Final. Period Covered: 16 June 1969 through 15 June 1972. Approved: September 1972.			
5. AUTHOR(S) (First name, middle initial, last name) Concetto R. Giuliano Robert W. Hellwarth Gerald R. Rickel Donald F. DuBois LaVerne D. Hess			
6. REPORT DATE September 1972		7a. TOTAL NO. OF PAGES 118 125	7b. NO. OF REFS 11
8a. CONTRACT OR GRANT NO. Arpa Order 1434 F19628-69-C-0277		9a. ORIGINATOR'S REPORT NUMBER(S)	
a. PROJECT, TASK, WORK UNIT NOS. 8693 N/A N/A			
c. DOD ELEMENT 61101D		9b. OTHER REPORT NO(S) (Any other numbers that may be assigned this report) AFCRL-72-0485	
d. DOD SUBELEMENT N/A			
10. DISTRIBUTION STATEMENT Approved for public release: distribution unlimited. (A)			
11. SUPPLEMENTARY NOTES This research was supported by the Advanced Research Projects Agency.		12. SPONSORING MILITARY ACTIVITY Air Force Cambridge Research Laboratories (OP) L. G. Hanscom Field Bedford, Massachusetts 01730	
13. ABSTRACT This report contains a cumulative summation of a three-year experimental and theoretical program on laser induced damage in ruby and sapphire at 6943 Å. Both bulk and surface damage were studied, using a well-characterized single transverse and longitudinal mode Q-switched ruby laser and amplifier. Temporal studies of the development of internal damage tracks using a high speed streak camera have been correlated with self-focusing theory with good agreement and constitute the first direct evidence for moving self-foci in solids. It has been found that beams with elliptical spatial cross-sections have higher self-focusing thresholds than circular beams. This result indicates that problems that arise from self-focusing of high power optical beams can be avoided by proper choice of beam shape. An investigation into the relation between surface damage and surface plasmas is described. The study of temporal and spatial surface plasma differentiation shows that the entrance plasma consists of two components: an air plasma and an explosion plasma, while the exit surface plasma is of the explosion type. The surface plasmas are shown to be a result rather than a cause of the surface damage. Surface damage experiments on samples polished by energetic Ar ⁺ ion beams have shown a marked increase (up to 10x) in damage threshold indicating that surface finish and/or crystallinity are very important in determining damage resistance. Theoretical efforts have developed a new model for optical breakdown in materials based on a transfer of optical energy to photoelectrons which undergo rapid energy transfer to acoustic phonons via optical phonons. Also, a theoretical framework has been developed describing the momentum distribution of conduction electrons in a polar lattice driven by strong optical fields. Models of self-focusing mechanisms are discussed, and nondamaging methods are suggested for measuring surface absorption which can result in distinguishing between surface damage mechanisms.			

UNCLASSIFIED

Security Classification

14.	KEY WORDS	LINK A		LINK B		LINK C	
		ROLE	WT	ROLE	WT	ROLE	WT
	Bulk Damage						
	Surface Damage						
	Ruby and Sapphire						
	Self-Focusing						
	Elliptical Beams						
	Single Mode Lasers						
	Surface Plasmas						
	Entrance and Exit Damage						
	Ion Beam Polishing						
	Streak Camera Experiments						
	Electron Heating Theory						
	Avalanche Theory						
	Surface Absorption						
	Nonlinear Refractive Index						

UNCLASSIFIED

Security Classification

ib

AFCRL-72-0485

DAMAGE THRESHOLD STUDIES IN LASER CRYSTALS

Concetto R. Giuliano, Donald F. DuBois, Robert W. Hellwarth,
LaVerne D. Hess, Gerald R. Rickel

HUGHES RESEARCH LABORATORIES
a division of hughes aircraft company
Malibu, California 90265

Contract F19628-69-C-0277
Project 8693

Final Technical Report
September 1972

Period Covered: 16 June 1969 through 15 June 1972

Contract Monitor: Erlan S. Bliss, Capt. USAF
Optical Physics Laboratory

Sponsored by
Advanced Research Projects Agency
ARPA Order 1434

Monitored by
AIR FORCE CAMBRIDGE RESEARCH LABORATORIES
AIR FORCE SYSTEMS COMMAND
UNITED STATES AIR FORCE
Bedford, Massachusetts 01730

Approved for public release: Distribution unlimited

Details of illustrations in
this document may be better
studied on microfiche

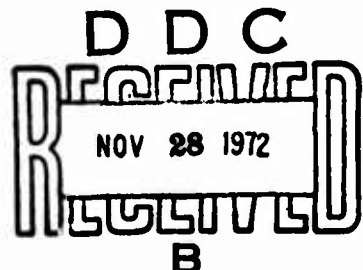


TABLE OF CONTENTS

	FOREWORD	vii
	ABSTRACT	ix
	LIST OF ILLUSTRATIONS	xi
I	EXPERIMENTAL STUDIES: OPTICAL DAMAGE	1
	A. Introduction and Summary	1
	B. Self-Focusing Bulk Damage in Ruby and Sapphire	3
	1. Streak Camera Studies	4
	2. Dynamics of Track Formation in Ruby	12
	3. Further Discussion of Theory Compared with Experiment	12
	4. Summary of Streak Camera Experiments	14
	5. Damage Threshold as a Function of Beam Radius	15
	6. Bulk Damage and Self-Focusing for Noncircular Beams	18
	7. Further Comments on Elliptical Beams	24
	8. Use of Elliptical Beams for Determining Intrinsic Damage Threshold Power Densities	24
	9. Optical Pumping Experiments	26
	C. Surface Damage Studies	28
	1. Relation between Surface Damage and Plasma Formation	28
	2. Surface Damage Threshold for Ruby as a Function of Beam Size and Divergence	40

	3.	Morphology of Entrance and Exit Damage	40
	4.	Attempts to Increase Surface Damage Threshold by Ion Beam Polishing	46
	5.	Comments on Fluctuations of Surface Damage Threshold Values	49
	D.	Beam Profile and Spot Size Measurements	50
	1.	Survey of Early Work	50
	2.	Spot Size Measurements Inside Samples	53
	3.	Ring Structure in the Focused Single Mode Laser Beam Beyond Beam Waist	57
	E.	Experimental Apparatus used in Damage Threshold Studies	63
II		THEORETICAL STUDIES: OPTICAL DAMAGE	69
	A.	Bulk Damage	69
	1.	Breakdown Mechanisms	69
	2.	Mechanisms Governing Self-Focusing	70
	B.	Surface Damage	75
	1.	Heating from Linear Absorption	75
	2.	Heating from Nonlinear Absorption	80
	3.	Electron Avalanche Ionization	81
III		SUMMATION OF EXPERIMENTAL AND THEORETICAL STUDIES	83

IV	RECOMMENDATIONS FOR FUTURE WORK	85
V	PRESENTATIONS AND PUBLICATIONS	89
A.	Presentations	89
B.	Publications	90
	REFERENCES	93
	APPENDIX A - Role of Photo-Electrons in Optical Damage	95
	APPENDIX B - Theory of Electron Velocity Distribution in Crystal Irradiated by a Strong Optical Beam	105
	DD FORM 1473	119

FOREWORD

This is the final technical report on Contract F19628-69-C-0277, Project 8693. The work reported herein was accomplished by Hughes Research Laboratories, Malibu, California. This report covers the study period 16 June 1969 through 15 June 1972.

Principal investigator for the program was C. R. Giuliano. L. D. Hess and G. R. Rickel contributed to the experimental phase. Principal contributor to the theoretical aspect of the program was R. W. Hellwarth, with D. F. DuBois providing additional input.

This document was submitted by the authors September 1972. The Air Force contract monitor was Erlan S. Bliss, Capt. USAF.

Preceding page blank

ABSTRACT

This report contains a cumulative summation of a three-year experimental and theoretical program on laser induced damage in ruby and sapphire at 6943 Å. Both bulk and surface damage were studied, using a well-characterized single transverse and longitudinal mode Q-switched ruby laser and amplifier. Temporal studies of the development of internal damage tracks using a high speed streak camera have been correlated with self-focusing theory with good agreement and constitute the first direct evidence for moving self-foci in solids. It has been found that beams with elliptical spatial cross-sections have higher self-focusing thresholds than circular beams. This result indicates that problems that arise from self-focusing of high power optical beams can be avoided by proper choice of beam shape. An investigation into the relation between surface damage and surface plasmas is described. The study of temporal and spatial surface plasma differentiation shows that the entrance plasma consists of two components: an air plasma and an explosion plasma, while the exit surface plasma is of the explosion type. The surface plasmas are shown to be a result rather than a cause of the surface damage. Surface damage experiments on samples polished by energetic Ar^+ ion beams have shown a marked increase (up to 10x) in damage threshold indicating that surface finish and/or crystallinity are very important in determining damage resistance. Theoretical efforts have developed a new model for optical breakdown in materials based on a transfer of optical energy to photoelectrons which undergo rapid energy transfer to acoustic phonons via optical phonons. Also, a theoretical framework has been developed describing the momentum distribution of conduction electrons in a polar lattice driven by strong optical fields. Models of self-focusing mechanisms are discussed, and nondamaging methods are suggested for measuring surface absorption which can result in distinguishing between surface damage mechanisms.

Preceding page blank

LIST OF ILLUSTRATIONS

Fig. I-1.	Example of Typical Damage Track in Ruby Caused by Temporally Smooth Pulse	13
Fig. I-2.	Threshold Power Density Versus Beam Radius for Ruby and Sapphire Samples	16
Fig. I-3.	Relative Bulk Damage Threshold as a Function of Optical Pumping for Different Samples	27
Fig. I-4.	Beam Area and Entrance Surface Damage Threshold as a Function of Surface Distance from Beam Waist	41
Fig. I-5.	Exit Surface Damage Threshold Power for Sapphire and Ruby Samples	42
Fig. I-6.	Optical and Scanning Electron Micrographs of Vacuum Entrance Surface Damage for Beam at Normal Incidence	44
Fig. I-7.	Optical Micrograph of Vacuum Entrance Surface Damage for Beam Incident at 45°	45
Fig. I-8.	Schematic Representation of Setup used in Beam Profile Measurements	52
Fig. I-9.	Multiple Lens Camera Photograph of Beam Profile Inside Ruby Sample for Different Incident Energies and Arbitrary Relative Exposures	54
Fig. I-10.	Multiple Lens Camera Photographs of Beam Profile Inside Sapphire Sample	55
Fig. I-11.	Beam Profile at Different Distances from 30.5 cm Lens	59
Fig. I-12.	Schematic Representation of Experimental Apparatus	64
Fig. I-13.	Typical Photo Monitoring Fabry-Perot Interferogram	66
Fig. I-14.	Tektronix 519 Oscilloscope Traces	66

SECTION I

EXPERIMENTAL STUDIES: OPTICAL DAMAGE

A. INTRODUCTION AND SUMMARY

This report represents the culmination of a three year program on laser induced damage in ruby and sapphire. The broad goals of the program were to perform experiments designed to elucidate the nature of the damage mechanism or mechanisms and to provide means of avoiding or eliminating damage. A parallel theoretical effort was to be carried out, the function of which was to examine present theories of damage and to explore new theories for damage mechanisms in the light of the experimental observations.

The main experimental emphasis in this program has been placed on bulk damage. In the early stages, bulk damage thresholds were measured on a number of samples from different sources. There has been much indirect evidence that bulk damage in inclusion-free solids is initiated by self-focusing. We have studied the temporal evolution of damage tracks in sapphire and ruby using a high speed streak camera and correlated the damage evolution with the theory for a moving catastrophic self-focus. These results, which are presented in Section I-B-1 through 4, constitute the first direct evidence for a moving self-focus in solids and give direct confirmation that the initiating mechanism for bulk damage is self-focusing. Further results on damage threshold for different focusing conditions presented in I-B-5 indicate as do the above mentioned results that both electrostrictive and electronic self-focusing mechanisms are operative for the pulse durations and spot sizes employed in these studies. Damage thresholds as a function of optical pumping in ruby samples are discussed in Section I-B-9.

Surface damage threshold studies undertaken in the latter stages of this program have attempted to provide an understanding of the relation between surface damage and surface plasmas (Section I-C-1) and have shown that the plasmas are a result of rather than the cause of surface damage; although some features of surface damage (especially on the entrance surface) are shown to result from the interaction of the plasma with the surface (Section I-C-3). Also contained in Sections I-C-1 and 2 are the result of surface damage threshold measurements as a function of beam size and divergence. These results show that both entrance and exit damage mechanisms are power density (or energy density) dependent and are not complicated by nonlinear propagation phenomena (except for ruby exit damage which is discussed in Section I-C-2). Surface damage morphology is also discussed in Section I-C, and differences between entrance and exit damage are illustrated by the use of scanning electron micrographs.

In the interest of avoiding or eliminating damage, we have discovered two very promising areas for pursuit. First, for bulk damage, it has been found during this work that the threshold for self-focusing is greater for beams having an elliptical spatial cross-section than for circular beams. This effect is discussed in Section I-B-6. For unfocused elliptical beams, the self-focusing threshold increases linearly as the ratio of major to minor elliptic axes. Hence, one can avoid problems that arise from self-focusing by appropriately choosing the beam shape. The second promising area involves the increase of surface damage thresholds with ion beam polishing. At this time, these threshold increases of up to 10x and greater have been realized, but the nature of the improvement is not understood in detail. The phenomenon can be explained in terms of a distinct improvement in surface finish or crystallinity or a combined influence of both. The results of these observations are discussed in Section I-C-4.

The theoretical effort in this program has given interpretation of experimental results, developed new theories for damage mechanisms, and suggested new experiments to further elucidate possible mechanisms for surface damage. Early in the program a new model

was developed for the optical breakdown of a material based on a transfer of the optical energy to photoelectrons which undergo rapid transfer to acoustic phonons via optical phonons. This treatment is presented in Appendix A. In Appendix B we present the development of a theoretical framework for the study of the momentum distribution of conduction electrons in a polar lattice being driven by a strong optical field. Although we have not expended the considerable computational effort necessary to obtain numerical estimates of numbers of high energy electrons, we have been able to show that many ad hoc hypotheses that have been put forward are without theoretical basis.

In Section II-A we discuss the development of models of the mechanisms responsible for the self-focusing that triggers bulk damage. We have found evidence that electronic hyperpolarizability is not the dominant mechanism in laser glass, sapphire, and YAG but probably is in the alkali halides. We have pointed out ways of establishing the mechanisms by standard, nondamaging optical measurements.

Surface damage is discussed in Section II-B. Here we have studied the three types of mechanisms most likely to be central in surface damage: heating by linear surface absorption, heating by photoelectron absorption, and avalanche ionization. We have isolated eight methods which we show can achieve nondamaging measurements of surface absorption and distinguish among the mechanisms.

B. SELF-FOCUSING BULK DAMAGE IN RUBY AND SAPPHIRE

The early stages of this program were devoted to measuring thresholds for bulk damage in ruby and sapphire. We obtained samples from different suppliers and carried out damage threshold measurements. In the early measurements a long focal length lens (48 cm) was used almost exclusively for creating damage. The results of the early threshold measurements are presented in Semiannual Reports 1 and 2. Most of the work done at that time was exploratory; many of the results had to be subsequently modified in the light of information obtained later in the program. The early period was of great value, mainly as

a time for gathering clues to be pursued later and for refining the apparatus and experimental techniques as well as gaining experience and familiarity with the various phenomena encountered.

In the following sections we present the more significant results obtained in our studies of bulk damage. Most of the emphasis is centered on the phenomenon of self-focusing, which is the initiating mechanism for bulk damage in inclusion-free sapphire and ruby and most other transparent materials. Many of the results presented here have contributed to a deeper understanding of the self-focusing phenomenon.

1. Streak Camera Studies

Some of the more significant results of this study have arisen from a series of experiments in which we observed the temporal development of damage tracks using a fast image converter camera operating in the streaking mode. The results of these experiments are understood in terms of self-focusing as the initiating mechanism for bulk filamentary damage; our experiments constitute the first direct observation of a moving self-focused spot in solids. Shortly after we performed our first streak camera experiments we came in contact with J. H. Marburger of the University of Southern California who has been working with the theory of self-focusing for some time. A treatment of our experimental measurements in the framework of his theory has yielded a satisfying picture of the dynamics of self-focusing and its connection to the damage tracks. This collaboration has led to publication in *Physical Review Letters* and the proceedings of the 1971 Third ASTM Symposium on Damage in Laser Materials. The latter paper, which is somewhat more detailed than the former, is reproduced in the following pages, as published.

Time Evolution of Damage Tracks in Sapphire and Ruby*

Concetto R. Giuliano

Hughes Research Laboratories
Malibu, California 90265

A fast streaking camera has been employed to observe the time-evolution of bulk damage filaments in sapphire and ruby on a nanosecond time scale. Externally focused light from a mode controlled ruby laser and amplifier was used to induce damage in the samples studied. Either side-scattered light at 6943 \AA or blue-green light from the self-luminous damage sites was detected by the streaking camera. It was found that damage first occurs at or near the natural focus of the lens, and that the damage track grows in an upstream direction toward the laser. The damage filament is formed during the rising portion of the incident laser pulse, reaching its full length at the peak of the pulse. The relationship between the location of the damage at a given instant and the corresponding instantaneous laser power will be discussed in the context of a possible self-focusing mechanism.

Key Words: Bulk damage, filamentary damage, dynamics, moving focus, sapphire, self-focusing, streak photography.

1. Introduction

The causes of laser induced damage can be divided into three separate steps. First, the initiating step, in which the intensity is built up in the medium by a mechanism such as self-focusing. Second, the medium responds to these high intensities by undergoing any of a number of nonlinear processes such as multiphoton absorption and/or phonon generation. Third, the local power dissipation is high enough to exceed the elastic limits of the material, causing catastrophic breakdown.

Much indirect evidence has existed for supporting self-focusing as the initiating mechanism for laser-induced bulk damage. [1,2].¹ However, different interpretations for the phenomenon have been postulated such as self-trapped filaments of light, repetitive focusing, and moving foci. We have observed the time-development of damage tracks in sapphire and ruby and found that it is most logically explained in terms of a moving focus. This is the first direct observation in support of a moving focus in solids.

We will concern ourselves here with the phenomenon of bulk damage in sapphire, although much of the discussion applies in general for most transparent dielectrics in which filamentary damage is observed. The damage is characterized by a long track, as shown in Fig. 1. Here we see a typical damage track formed by a single pulse from a laser operating in a single longitudinal and transverse mode. The damage filament is characterized by a "head" at the part of the track nearest the sample entrance and a tapering "tail," the end of which occurs at or very near the focal plane of the lens used to focus the laser light in the material. The track often, but not always, displays a region of relatively dense damage at or near the tip of the tail, usually in the form of a crack or "damage star." As we examine the regions of the damage track upstream from the tail (Fig. 1 (b)), we begin to see some subsidiary fracturing alongside the damage filament. This fracturing is randomly located and becomes increasingly dense toward the head of the track where the extent of subsidiary fracturing is maximum (Fig. 1 (c)). If the incident light pulse is not temporally smooth the damage track shows the same filamentary behavior, but in addition, there are occasional regions of more dense damage along the track. An example of this is shown in Fig. 2, where we see a track formed by a pulse in which the laser was oscillating in two longitudinal modes. If the depth of modulation of the incident pulse is large, the filamentary character of the damage track may not be present. Instead, one may see only a series of fractured regions spaced along the light path with gaps of undamaged material between them. We also notice the

*This work was supported by the Advanced Research Projects Agency under ARPA Order 434 with Air Force Cambridge Research Laboratories.

¹ Numerals in square brackets indicate literature references appearing at the end of this paper.

general feature that the damage filament itself is narrower at the tail of the track (~ 2 to $5\ \mu\text{m}$) and broader at the head (several tens of microns). We will later explain these qualitative features of bulk damage in the light of our recent observation of the time-evolution of these damage tracks.

2. Experimental

The experimental setup is shown in Fig. 3. The oscillator employs a 4 inch long x $1/4$ inch diameter ruby pumped by two linear lamps in a double elliptical pump cavity. The ruby crystal is water-cooled by a closed-cycle refrigeration system maintained at 0°C . The high reflectivity mirror is coated with a 99% reflectivity high field damage coating from Perkin Elmer Corporation. Q-switching is accomplished with a solution of cryptocyanine in methanol in a 1 mm path length cell whose transmission is 30% at $6943\ \text{\AA}$.

The temperature controlled (34°C) resonant reflector that was designed to optimize longitudinal mode control consists of two quartz etalons and a quartz spacer, whose combined effect is to enhance cavity modes separated by $2\ \text{cm}^{-1}$ and to discriminate against intermediate modes.

Portions of the laser beam are split off in various ways (see Fig. 3), so that the power output, near- and far-field patterns, and Fabry-Perot patterns can be monitored for each shot. This is accomplished in the following way. Light reflecting from wedged beamsplitter W_1 gives two diverging beams; one of them hits the magnesium oxide diffuser, where the scattered light is monitored by a biplanar photodiode used as our power monitor. The second beam from W_1 hits ground-glass screen G, where it is photographed through lens L and the 1 m focal length camera focused at infinity. This gives a magnified ($\sim 5\times$) near-field picture. Another portion of the light is removed by beamsplitter B_1 and hits mirror M_2 , which can be placed in or out of position depending on the use of the alignment laser. From M_2 the light either goes to the Fabry-Perot interferometer or can be partially reflected from wedged beamsplitter W_2 , where it results in a pair of far-field patterns. A 0.6 neutral density filter is placed near the focal plane of the camera so that the far-field pattern and the Fabry-Perot pattern can be seen at two different exposures. The two Glan prisms are used as a variable attenuator after the amplifier. Beamsplitter B_2 samples the light to photodiode No. 2, which monitors the power incident upon the focusing lens, which was designed for minimum spherical aberration (Special Optics). Photodiode No. 3 monitors the light after the sample. The signals from the two detectors are integrated and displayed on a dual-beam oscilloscope.

The water cooled amplifier ruby is 6 inches long x 0.5 inches diameter, with one end wedged relative to the other by about 0.5° . The input end of the amplifier rod is antireflection coated to minimize the chances of oscillation within the amplifier itself. The ruby rod is closely coupled to a helical flashlamp, which is pumped with a power supply capable of delivering 8 kJ in a 3 msec pulse. The power supply employs a pulse shaping network of 20 sections, each section pumping for 150 μsec . The maximum gain obtained with the amplifier is about 10 dB.

In all experiments described in this paper, the amplifier flashlamp pumping was held constant, and the amount of light incident on the sample was varied by rotating the first of the two Glan prisms. We found that our amplifier acts as a weak negative lens whose focal length depends on optical pumping [3]. Thus we fixed the amplifier pumping to minimize the shot-to-shot variations in the beam characteristics. Typical output from the oscillator plus amplifier is about 150 mJ in pulses which can range from about 15 to 30 nsec. The far-field beam profile was measured to be gaussian down to 8% of the peak using a modified multiple-lens camera technique [4].

The streak camera experimental setup is shown in Fig. 4. We used an STL image converter camera operating in the streaking mode to photograph the self-luminous damage tracks during their formation. The camera was triggered either by the sync pulse from the Pockels cell, when it was used as the Q-switch, or from the laser light itself, when the cryptocyanine Q-switch was employed. For all the experiments described, the light was focused inside the sample using a lens ($f = 19\ \text{cm}$) which was designed for minimum spherical aberration. In the latter experiments a portion of the incident light was split off and allowed to enter the camera directly to give a marker streak which gives the relation between the time of formation of a particular point on the damage track and the peak of the incident pulse. In the experiments described here, a Corning 4-94 filter was placed in front of the camera lens. This served to block the laser light which was scattered from the damage sites while passing the self-luminous light in the blue-green part of the spectrum. When the scattered light at $6943\ \text{\AA}$ is allowed to enter the camera, essentially the same behavior is observed when it is blocked. However, scattered laser light from previously formed damage tracks in the sample constitutes an inconvenient background which interferes with the observation of the track of interest. After each streak photograph was taken, the position of the head and tail of the damage track was determined by examining the crystal using a measuring microscope. These measurements were found to be consistent with the location and extent of the damage inferred from the streak photos.

3. Results of Streak Measurements

Typical streak photographs of the damage in sapphire are shown in Figs. 5 and 6. In Fig. 5 we see the time development of the damage track when an unmodulated pulse is incident on the sample. In Fig. 6 we see the streak photo for a modulated input pulse. (The 750 MHz modulation occurs when the Pockels cell Q-switch is used.) The essential features of these results to be noted are the following.

1. The track first appears at or very near the location of the beam waist.*
2. The track grows in the upstream direction moving toward the sample entrance.
3. The track reaches its maximum length when the incident pulse reaches its peak.

The qualitative behavior of the time evolution of these damage tracks can be described in terms of moving self-focus as follows. At a certain critical power P_c , a self-focus first appears at the beam waist where the damage first occurs. As the power increases the distance z_f required to form a self-focus decreases, and the damage track grows in the upstream direction. The minimum z_f corresponds to the maximum power, thus the head of the track will occur at the peak of the incident pulse. The rate of growth of the track depends on the temporal shape of the laser pulse. The self-focused spot sweeps through the downstream part of the track more quickly than the upstream part, hence the extent of damage is greater at the head than at the tail.

When the incident pulse is modulated, we expect to see local regions of heavy damage associated with the passage of local maxima on the leading edge of the pulse. Each consecutive peak has slightly more power than the preceding one, and therefore causes a self-focus which dwells at slightly smaller z . A glance at the damage track formed from a modulated pulse (Fig. 6) shows the spacing between the heavily damaged regions to decrease toward the head of the track, as one might expect from the above qualitative explanation. Thus, what might appear to be evidence for multiple or repeated focusing could be simply an artifact of temporal spiking on the input pulse, which causes a single focus to pause occasionally as it sweeps upstream.

Streak photographs of damage tracks in ruby show the same qualitative behavior as that seen in sapphire, but the comparison with the self-focusing theory below was not carried out. The general features of damage in ruby are not the same as those in sapphire, and the location and lengths of damage tracks are not as reproducible. One may attribute this to the absorption in ruby at 6943 Å, but the differences have not been investigated in detail (see ref. [3]).

The reduction of data taken from streak and oscilloscope photographs was accomplished by tracing the photographs onto graph paper at a convenient magnification using an opaque projector and picking off values of instantaneous power and damage location at specific times. The two time scales were synchronized by locating the center (most intense region) of the marker streak and allowing this to coincide with the peak of the incident laser pulse. The center of the marker streak was determined "by eye" and was found to be reproducibly locatable to within about 1 nsec (1 mm on the streak photographs). Thus, we obtain values of distance of a particular point on the damage track from the entrance surface z_f and the corresponding instantaneous laser power. An example of the traces is shown in Fig. 7.

4. Comparison of Experiment with Theory

We will now attempt to correlate the above experimental results with the self-focusing theory of Marburger and coworkers [5,6]. Many of the details of this theory are presented in a following paper [7], and we will only dwell on the results as applicable to our experimental results.

The above referenced theory assumes that the induced refractive index in the medium δn responds instantly to local changes in the optical intensity. The following equation is obtained from numerical solutions of the nonlinear wave equation (for $P > P_c$).

$$\left((P/P_c)^{1/2} - 0.858 \right)^2 = 0.0202 + 0.136 [ka_0^2/z_f(\omega)]^2 \quad (1)$$

and

$$z_f^{-1}(\omega) = z_f^{-1}(R) + R^{-1} \quad (2)$$

Here, for an incident gaussian equiphase beam, a is the e^{-1} radius of the intensity profile at the sample entrance, k is the wave vector in the medium, R is the distance from the crystal entrance to the low intensity beam waist, $z_f(R)$ is the distance from the sample entrance to the self-focus when the incident beam has phase curvature R ($R < 0$ for a converging beam); P and P_c are the incident power and

*In many of the photographs the intensity of the light from the tail of the track is too weak to record. However, subsequent examination of the tracks show that the location of tail is very reproducible from shot to shot.

the critical power for self-focusing, respectively. The theory predicts that two self-foci are formed; they coincide at the low intensity beam focus at $P = P_c$ and at higher power they separate, one moving downstream at the speed of light and the other moving upstream at a rate which depends on the temporal shape of the input pulse. We will deal here with a comparison of the theory and experiment for the backward moving self-focus.

Equation 1 is a hyperbola whose asymptote is

$$(P/P_c)^{1/2} = 0.858 + 0.369 ka_0^2 \left(\frac{1}{R} + \frac{1}{z_f(R)} \right). \quad (3)$$

Thus, for powers greater than about $2P_c$ at plot of $P^{1/2}$ versus z_f^{-1} should give a straight line. Figure 8 shows that this is nearly so.^c Here we present data taken from a number of streak camera measurements for different peak powers and at two different pulse widths τ .

The evident curvature of the plots in Fig. 8 and their dependence on peak power and pulse duration can be explained by including the slow response of the index change δn which was ignored in the above analysis.

Of the various possible mechanisms for δn , those arising from nonlinearity of electronic response [8] and libration [9] are essentially instantaneous. The largest noninstantaneous mechanism for δn is electrostriction, which leads to an effective nonlinear index of refraction n_2 , which decreases as the dimensionless quantity $x = a/u\tau$ increases [10]. Here, a is the spatial beam radius, τ the effective pulse width, and u is the longitudinal sound velocity in the medium. Thus, there is a characteristic time a/u for the electrostrictive nonlinearity to develop, and hence the critical power required to obtain a self-focus will depend on beam size and pulse duration.

The index change leading to a self-focus at a particular distance z_f can only be induced by that portion of the pulse which has passed z_f before the self-focus is formed. Thus, the effective τ should be considered a decreasing function of z_f when considering points along an evolving damage track formed on the leading edge of the pulse. For a converging beam, the beam width a increases with decreasing z . Thus, it becomes increasingly difficult for electrostrictive self-focusing to occur as z_f decreases for a given input pulse; a self-focus formed upstream from the low intensity beam waist cannot take advantage of the small beam radius at the natural focus.

We can crudely account for the effect of electrostriction by replacing P_c^{-1} in (1) by $P_{c1}^{-1} + [P_{c2}f(x)]^{-1}$, where f is an increasing function of x , P_{c1} is the critical power due to instantaneous mechanisms, and $P_{c2}f(x)$ is the critical power for electrostriction.

For our particular conditions of pulse lengths and focusing, the fractional change in a from the tail to head of the track is substantially larger than the fractional change in τ . Therefore, we expect $f(x)$ to be a decreasing function of z_f causing positive curvature in a plot of $P^{1/2}$ versus z_f^{-1} according to (1). This is consistent with the data shown in Fig. 8.

Since the first self-focus occurs at the low intensity beam focus, a is the same for all curves at $z_f = |R|$. Therefore, we would expect that x would decrease for pulses of longer duration. This means that the self-focus forms more easily (i.e., at lower powers) for a longer pulse, everything else being equal. This explains the vertical separation between the two groups of curves in Fig. 8. Similarly, one would expect that pulses of different peak power, but the same duration, would form an initial self-focus at different incident powers. In this case the critical power is less for lower peak power than for higher peak power pulses of the same duration. Take, for example, an incident pulse for which the self-focus occurs just at the peak, as compared with a pulse of the same width but much higher peak power. One would expect the self-focus to first occur at a higher power for the latter pulse, because not enough time would have elapsed for a self-focus to have occurred at the same power as for the first pulse. This accounts for the separation at the lower power end between curves of the same pulse width in Fig. 8.

The slight negative curvature seen at the high power ends of the curves in Fig. 8 is very sensitive to the "synchronization" of the pulse profile with the streak photographs. Because of the slow response of the electrostrictive mechanism, the maximum upstream excursion of the damage track would be expected to lag the pulse peak by an amount somewhat less than the response time. We did not attempt to take this into account in plotting the data. This could explain the negative curvature seen at the high power ends of several of the curves in Fig. 8. A relative shift between the oscilloscope traces and the streak photographs of the order of nanoseconds will remove this curvature. The direction of the adjustment is consistent with this explanation.

We see from (3) that the straight line plot of $P^{1/2}$ versus z_f^{-1} should have a slope of $0.369 ka_0^2 P_c^{-1/2}$. Hence we can obtain values for P_c from the slopes of the curves in Fig. 8. Values for a at the crystal entrance were obtained by measurement of the beam profile at a number of points beyond

the focusing lens. The range of critical powers obtained from the slopes in Fig. 8 is 180 kW to 5.4 MW, which is consistent at one extreme with the predictions of electrostrictive self-focusing for sapphire [10] and at the other with values of n_2 inferred from other manifestations of electronic distortion [11].

The author acknowledges the skilled technical assistance of G. R. Rickel.

5. References

- [1] Budin, J.P. and Raffy, J., Appl. Phys. Letters 9, 291 (1966).
- [2] Zverev, G.M., Mikhailova, T.N., Pashkov, V.A., Solov'eva, N.M., Plasma Zh, Eksp. Teor. Fiz. 5, 391, (1967); JETP Letters 5, 319 (1967).
- [3] Giuliano, C.R., DuBois, D.F., Hellwarth, R.W., and Rickel, G.R., "Damage Threshold Studies in Laser Crystals," Semiannual Report No. 3, January 1971 - ARPA Order No. 1434.
- [4] Winer, I.M., Appl. Optics 5, 1437 (1966).
- [5] Dawes, E.L., and Marburger, J.H., Phys. Rev. 179, 862 (1969).
- [6] White, D.R., Marburger, J.H., and Dawes, E.L., (to be published).
- [7] Marburger, J.H., these Proceedings.
- [8] Brewer, R.G., and Lee, C.H., Phys. Rev. Letters 121, 267 (1968).
- [9] Polloni, R., Sacchi, C.A., and Svelto, O., Phys. Rev. Letters 23, 690 (1969); Cubeddu, R., Polloni, R., Sacchi, C.A., and Svelto, O., Phys. Rev. A 2, 1955(1970).
- [10] Kerr, E.L., "Damage in Laser Glass," Glass, A., Guenther, A., Stickley, C., and Myers, J., Ed., Amer. Soc. Testing and Materials, Technical Publication 469, p 23 (1969).
- [11] Wang, C.C., and Baardson, E.L., Phys. Rev. 185, 1079 (1969).

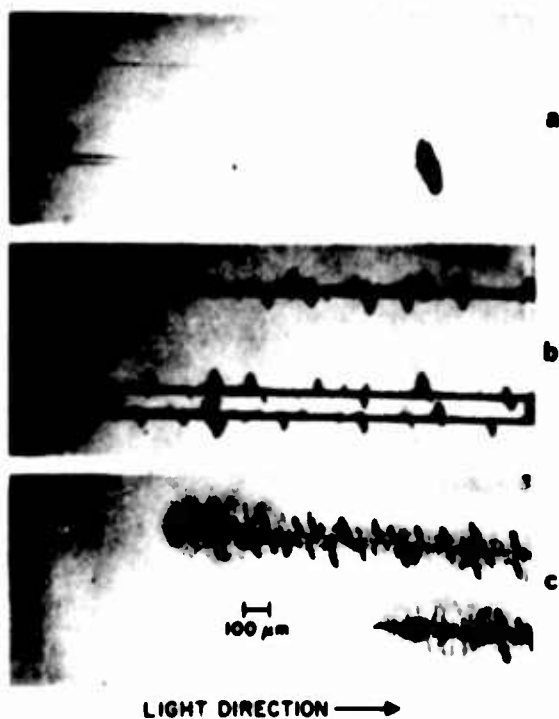


Fig. 1 Typical examples of damage tracks in sapphire caused by a temporally smooth pulse showing damage at (a) the tail, (b) the intermediate region, (c) the head.

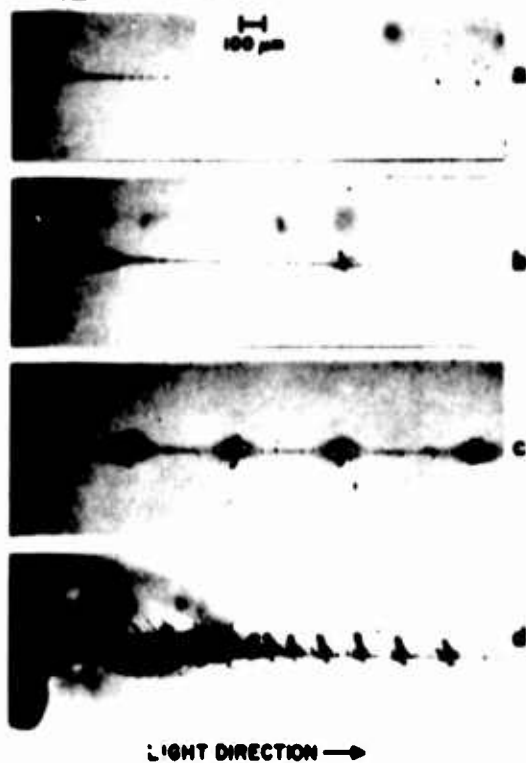


Fig. 2 Examples of damage tracks in sapphire caused by a temporally modulated pulse, (a) through (d) progressing from the tail to the head.

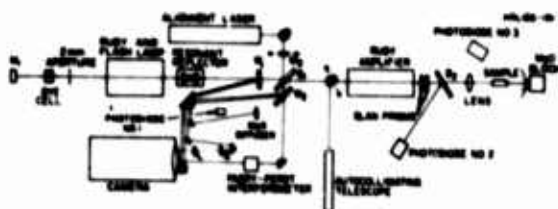


Fig. 3 Schematic representation of laser amplifier and associated monitoring apparatus.

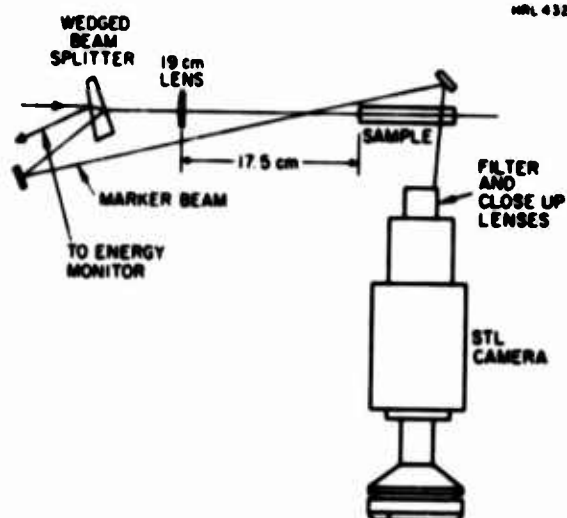


Fig. 4 Streak camera experimental setup.

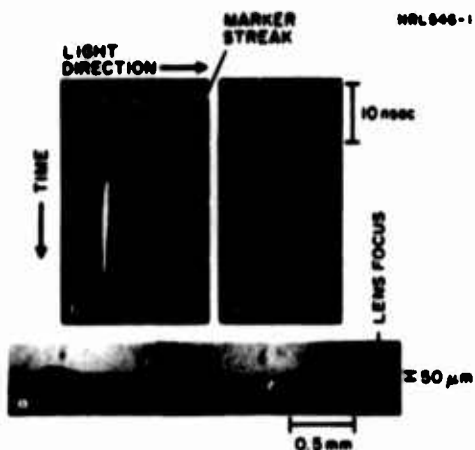


Fig. 5 Typical examples of (a) damage filament, (b) streak photograph, (c) oscilloscope trace for a temporally smooth incident pulse.

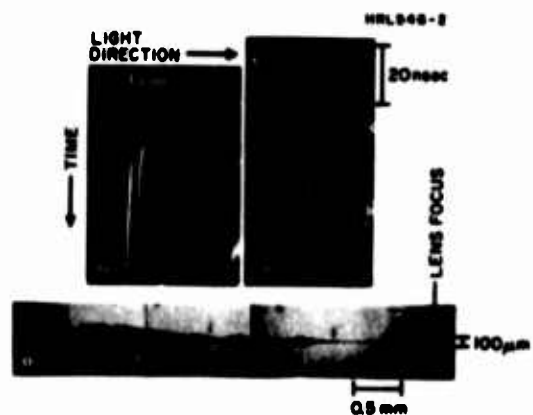


Fig. 6 Typical example of (a) damage filament, (b) streak photograph, (c) oscilloscope trace for a modulated (~750 MHz) incident pulse.

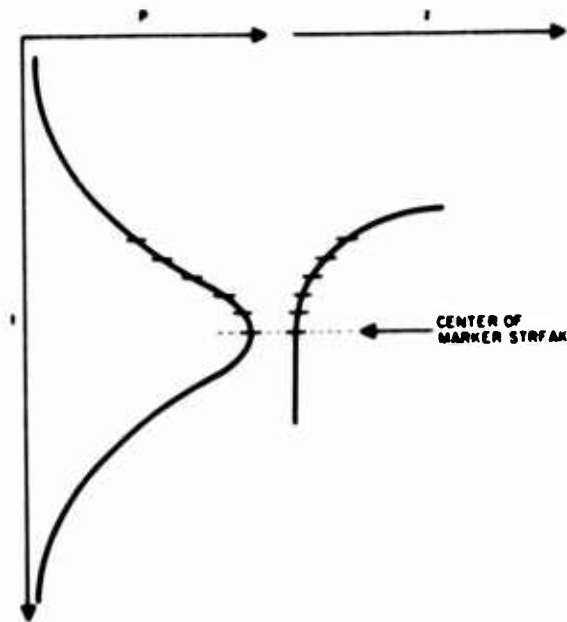


Fig. 7 Juxtaposition of oscilloscope trace and streak photograph showing method of obtaining instantaneous powers and corresponding damage location.

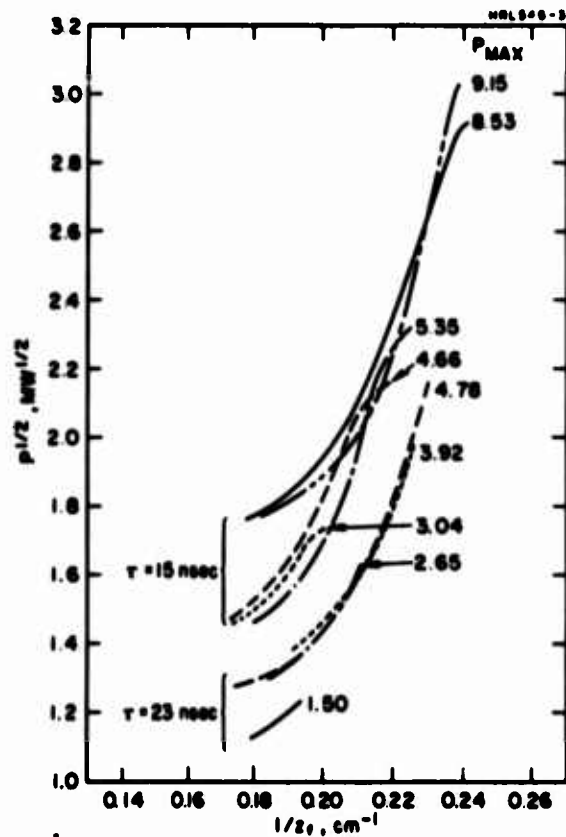


Fig. 8 Plot of $P^{1/2}$ versus z_0^{-1} from data taken from streak and oscilloscope photographs for different incident peak powers and pulse widths.

2. Dynamics of Track Formation in Ruby

The results obtained with ruby are qualitatively similar in some respects to those of sapphire. However, there are a few differences which emphasize a definite contrast between the damage phenomena in both materials. A quantitative comparison of the dynamical data was not made in this program. Because the length of the damage track in ruby is about one-third as long as that in sapphire for the same incident power and focusing, the resolution in the streak photographs is less for the same magnification. In addition, the full length of the track in ruby generally is not visible in the streak photographs, since the downstream end does not glow brightly enough to be detected. Consequently, the visible portion of the tracks is very short and at the magnification used it is very difficult to make reliable measurements from the streak photographs.

In addition to the difference in track length, another feature that distinguishes ruby from sapphire is that the track in ruby is not a continuous filament even when the incident pulse is temporally smooth. An example of this is given in Fig. I-1. This phenomenon which illustrates another of the many distinctions between ruby and sapphire damage and which might be linked to the absorption in ruby remains unexplained.

3. Further Discussion of Theory Compared with Experiment

The conclusion that the damage under the conditions of our experiments is the result of a moving self-focus rather than a trapped filament or a repetitive focus is an essential feature of this work. A close quantitative agreement with the self-focusing theory of Marburger and coworkers would predict that all the curves in Fig. 8 of the preceding manuscript would lie on top of one another and be essentially coincident with the curve of the manuscript eq. (1), substituting the proper values of a_0 , R , and P_c . Obviously, this is not the case, but the reasons are qualitatively understood, and a plausible explanation for the differences between the curves lies in the consideration that the

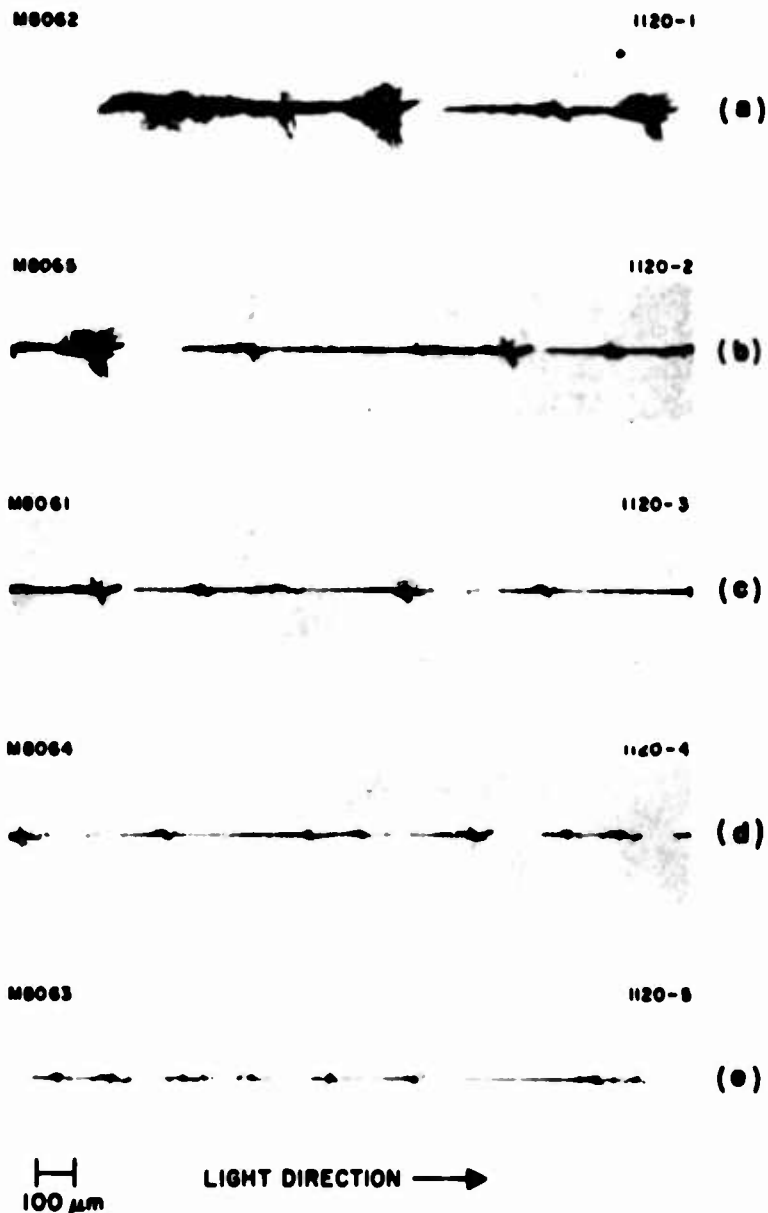


Fig. I-1. Example of typical damage track in ruby caused by temporally smooth pulse ($f = 19$ cm lens), (a) through (e) progressing from tail to head. Note breaks in damage track in contrast to unbroken track in sapphire.

nonlinearity does not respond instantaneously to the optical fields. The curvature of the plots, the shift between the two sets of curves for different pulse widths, and the differences in the low power ends of the curves with the same pulse width can be qualitatively understood by invoking a noninstantaneous response. In attempting to account for this empirically, P_c^{-1} in manuscript eq. (1) may be replaced by $P_{c1}^{-1} + [P_{c2}f(x)]^{-1}$, where P_{c1} is the critical power for an instantaneous response, and $P_{c2}f(x)$ is the critical power for electrostriction. As mentioned in the manuscript, $f(x)$ is essentially a function which makes it harder to get self-focusing if the pulse is short or if the beam size is large. This says then, that for focused beams self-focusing becomes more difficult as the track progresses back toward the entrance, at least for pulses of roughly the width and temporal shape with which we are concerned.

However, it may be possible with our present data to determine $f(x)$, thus obtaining a more satisfactory quantitative agreement than exists at this time. This possibility was not explored during this program.

4. Summary of Streak Camera Experiments

In summarizing essential results of the dynamics of formation of the damage filaments, there are several important features on which the theory and experiment agree.

As the incident power reaches a critical value, a self-focus occurs at the low power lens focus. This is the first point where a self-focus is expected to occur. As the power is increased the distance necessary to obtain a self-focus is less, and the self-focus moves toward the entrance of the medium. Therefore, the damage track has one end at, or very near the lens focus and the other end between the focus and the crystal entrance. The rate at which the self-focus moves, and consequently, the rate at which the damage filament grows depends on the rate of change of intensity with time. The faster the intensity grows, the faster the self-focused spot moves upstream. When the

incident pulse reaches its peak, the damage track reaches its maximum length. As the intensity decreases, the self-focused spot will tend to move back downstream. However, since the damage has already been created, it interferes with the propagation back downstream. As a result, the head of the track shows more heavy damage. If the amplitude of the incident light pulse varies with time, the self-focused spot will move in an irregular fashion, going rapidly upstream when the intensity is rapidly increasing and pausing at local peaks. The damage resulting from this kind of pulse will show local regions of more heavy damage, formed during local maxima, separated by narrow filaments that form when the self-focus is moving rapidly. If the depth of modulation is large, the connecting filamentary characteristic may not be observed, but only the regions of high local damage along a line separated by regions of no damage. Thus, what appear to be evidence for repetitive or multiple focusing can be shown to be a result of temporal structure on the rising portion of the input pulse.

5. Damage Threshold as a Function of Beam Radius

In Semiannual Report 4 we presented the results of some measurements of bulk damage threshold in ruby and sapphire for different focal length lenses. The data are plotted in Fig. 1-2 as a log-log plot of threshold power density versus beam radius, both evaluated at the beam waist inside the sample. A slope of minus two in these plots would indicate a constant power threshold, independent of lens focal length that is consistent with a self-focusing mechanism in a material with an instantaneous nonlinear response such as that arising from electronic distortion. Instantaneous response implies that the steady state conditions for self-focusing apply. In the case of electrostrictive self-focusing as a dominant mechanism, this would correspond to long pulses or small beams. For pulses of constant length, the steady state condition for electrostriction is approached as the beam size gets smaller. The case of large beams or short pulses corresponds to the transient situation for electrostrictive self-focusing.

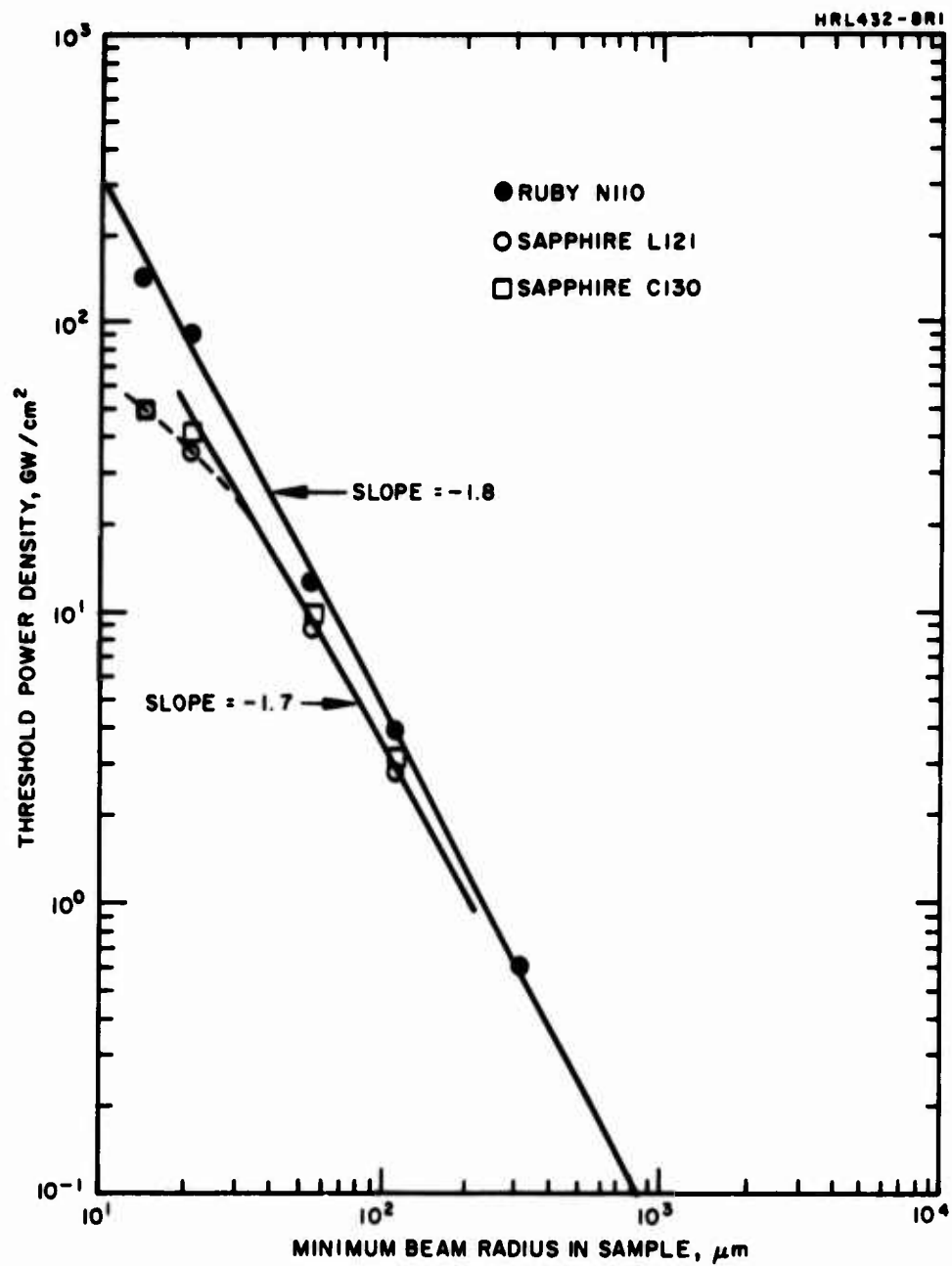


Fig. I-2. Threshold power density versus beam radius for ruby and sapphire samples.

In the extreme of the transient regime, a constant power density threshold is expected, giving a slope of zero for large beam sizes in the plot in Fig. I-2. If self-focusing by electrostriction were the sole cause of bulk damage, we would expect to see a slope of minus two in the small beam radius region, tailing off to zero slope at large radii. A combination of contributions from both slow and fast self-focusing mechanisms would give a slope less than minus two which we observe.

Of course, the above discussion really applies to situations where the light incident on the medium is unfocused, or slightly focused, because the self-focusing phenomenon depends on a nonlinearity which takes place continuously along the beam. That is, the phenomena which take place at a certain plane affect the self-focusing at points farther downstream in the material.

What will be expected then for sharply focused beams compared with gently focused beams? If the beam is sharply focused inside a material that is long compared with the length of the focal region, the beam size is rapidly decreasing with distance on the approach to the low power focus. This means that the region over which a phenomenon such as electrostriction is effective in creating self-focusing is less than if the beam radius were constant and the same size as at the waist. The material responds to create a kind of continuous acoustic lens all along the beam. But for a certain range of radii the ease with which the lens forms depends on the beam radius. Therefore, for a converging beam, electrostriction might be expected to be less effective as the external focusing becomes sharper. In a sense, then, one again enters a region corresponding to transient behavior. Here damage threshold would be expected to occur at a constant power density independent of lens focal length. For very sharply converging beams, damage is expected to occur before electrostrictive self-focusing has a chance to develop. The tailing off of the curves at small radii (i.e., sharp focusing) in Fig. I-2 could be explained in terms of the behavior described above.

The power densities for bulk damage for very short focal length lasers where the incident power is too low for self-focusing to take place should give the intrinsic breakdown intensity for the material of

interest. A knowledge of the intrinsic damage threshold intensity coupled with self-focusing threshold powers can yield information as to the limiting size of the self-focused spot. The plots in Fig. 1-2 give lower limits for the intrinsic threshold intensities for sapphire and ruby of about 50 and 150 GW/cm², respectively. Since the curves have not really leveled off at these values, the intrinsic thresholds must be higher. If one takes typical self-focusing powers of 0.5 to 1 MW and imposes the constraint that at threshold the intensity must be at least 200 GW/cm², values of from 7 to 14 μ m for a limiting self-focus spot radius is obtained, which is reasonable when one considers that the transverse dimensions of the damage tracks for sapphire are about 6 μ m in diameter near the tip of the tail.

6. Bulk Damage and Self-Focusing for Noncircular Beams

In Semiannual Reports 4 and 5, some results of experiments in which an attempt was made to generate internal damage in sapphire using cylindrical lenses for focusing inside the sample were discussed. Experiments failed to obtain damage at power densities ten times higher than that previously obtained with circular spots of the same area. This led us to suspect that self-focusing might be sensitive to beam shape. The following simple ideas were first employed in an attempt to understand self-focusing with noncircular beams. This non-rigorous treatment predicts that the threshold for self-focusing of elliptical beams should be higher than that for circular beams, and the quantitative result is not far from that predicted using a more correct approach as discussed later.

If one considers an elliptically shaped beam of constant intensity entering a medium having an index nonlinearity Δn proportional to power density and define the critical power P_c to be that for which the angle for total internal reflection at the boundary equals the far-field diffraction angle characteristic of the smaller beam dimension, we find that the critical power increases linearly with the beam aspect ratio a/b , where a and b are the long and short dimensions of the

elliptical beam. The critical angle for total internal reflection is given by

$$\cos \theta_c = \frac{1}{1 + \Delta n/n} . \quad (I-1)$$

If we expand the cosine for small angles and the right-hand side of eq. (I-1) for small $\Delta n/n$, we obtain

$$1 - \frac{\theta_c^2}{2} = 1 - \Delta n/n \quad (I-2)$$

and

$$\theta_c^2 = \frac{2\Delta n}{n} = \frac{KP_c}{\pi ab} , \quad (I-3)$$

where K is a product of constants whose value depends on the choice of units.

The diffraction angle characteristic of the smaller dimension b is

$$\theta_{\text{diff}}^2 \sim \frac{\lambda^2}{b^2} \quad (I-4)$$

When the two angles are set equal,

$$P_c = K'\lambda^2 \left(\frac{ab}{b^2} \right) = P_c^* \left(\frac{a}{b} \right) \quad (I-5)$$

results, where P_c^* is the critical power for a circular beam ($a = b$). The diffraction criterion for the small beam dimension was chosen because it assured that the turning in of the rays would be accomplished for the whole beam under those conditions. It can be seen that at a

lower power $P'_c = P_c^*(b/a)$, there will be a sufficient nonlinearity for overcoming diffraction in the direction of the long dimension but the remainder of the beam will continue to diffract.

After our initial experimental results were obtained, A. Yariv of California Institute of Technology and J. H. Marburger of the University of Southern California became interested in offering more rigorous theoretical treatments of the phenomenon. As a result of this interest, a joint paper was written, presented at the Seventh International Quantum Electronics Conference in Montreal, Canada, and accepted for publication in Applied Physics Letters. A reprint of the manuscript follows.

Enhancement of self-focusing threshold in sapphire with elliptical beams*

C.R. Giuliano

Hughes Research Laboratories, Malibu, California 90265

J.H. Marburger

University of Southern California, Los Angeles, California 90007

A. Yariv

California Institute of Technology, Pasadena, California 91101

(Received 30 March 1972)

The power threshold for optically induced bulk damage in sapphire is a sensitive function of the ellipticity of the incident beam shape. Experimental results are consistent with a simple self-focusing theory.

We wish to report observations of the strong influence of departures from circularity of an optical beam on the power threshold for optically induced bulk damage in sapphire. This threshold, which is known to arise from the formation of a catastrophic self-focus in the medium,¹ is found to increase appreciably when the beam cross section is distorted from a circle to an ellipse, and when vertical and horizontal confocal parameters differ (leading to ellipsoidal phase fronts). These observations are consistent with the theoretical predictions of Vorob'yev² and Shvartsburg,³ which are extended slightly here to apply to our experiment.

Our experiments were performed using the output of a single-mode Q-switched ruby laser and amplifier focused inside sapphire samples with different lenses. The laser and associated monitoring apparatus are described in detail elsewhere.⁴ The far-field beam profile was measured to be Gaussian down to 8% of the peak, using a modified multiple-lens camera technique. Typical pulse lengths are 20 nsec. The sapphire samples are typically 3-in.-long by $\frac{1}{4}$ -in.-square bars.

Damage threshold powers for circular beams of different sizes are shown in Table I and compared with results for elliptical beams. The first three entries in Table I show the increased threshold power with beam size indicating the influence of electrostriction.¹ The dimensions listed in Table I are those at the beam waist, near which the self-focus first forms at threshold for circular beams. The remaining entries in Table I show the effect of noncircular beam shapes. The fourth entry gives the threshold power for an elliptical beam

whose short dimension is the same as the first entry, whose long dimension is the same as the third entry, and whose area is the same as the second entry. We see that the threshold power is appreciably higher for the elliptical beam compared with any of the circular beams. The last two entries in Table I show data for more elongated elliptical beams where we were unable to reach threshold at the maximum power available from our system.

Each power threshold in Table I was determined from a series of eight laser shots of differing peak powers. When damage occurred, the damaged region was found to possess a circular rather than an elliptical cross section. In fact, the appearance of the damage tracks formed above threshold was indistinguishable from those caused by circular beams. The tracks themselves were confined to the region between the two line foci of our astigmatic optical system, but there is no evidence that they would not extend beyond the upstream focus at higher powers.

To correlate these observations with theory, we have found it necessary to resort to the "paraxial-ray-constant-shape" analysis of self-focusing outlined in Ref. 5. More accurate numerical solutions of the nonlinear wave equation, such as those employed in Ref. 1, are extremely difficult to obtain in this case, because the noncircular beam shape requires an additional degree of freedom in the computer code. Nevertheless, the approximate analysis has had some qualitative success,⁶ and leads to simple expressions.

TABLE I. Comparison of damage threshold powers for circular and elliptical beams of different sizes.

Type of beam	Radius ^a (μm)	Area (μm ²)	Damage threshold power (MW)	Astigmatic focal length ^b in medium (cm)
Circular beams (dimensions at low-intensity waist)	14	6.3 × 10 ²	0.51 ± 0.04	...
	37	44 × 10 ²	0.74 ± 0.07	...
	100	308 × 10 ²	1.23 ± 0.10	...
Elliptical beams (dimensions at upstream low-intensity waist)	14 × 100	44 × 10 ²	6.0 ± 0.50	2.99
	14 × 1200	535 × 10 ²	> 17 ^c	∞
	7 × 1200	270 × 10 ²	> 17 ^c	∞

^aThe beam radius is defined as the 1/e radius for the intensity.

^bThis is the distance between the two line foci [see M. Born and E. Wolf, *Principles of Optics*, 3rd Ed. (Pergamon,

London, 1965), p. 171].

^cUnable to reach threshold at this power.

Assuming an optical field of the form

$$E = \frac{1}{2} E_0 \exp(i\varphi) \exp[i(kz - \omega t)] + \text{c. c.},$$

$$E_0 = E_m(z) \exp[-\frac{1}{2}(x^2/a^2 + y^2/b^2)],$$

we find by the method of Ref. 5 the following equations for the horizontal and vertical beam parameters a and b :

$$k^2 \frac{d^2 a}{dz^2} = \frac{1}{a^3} - \frac{\eta}{a^2 b}, \quad (1)$$

$$k^2 \frac{d^2 b}{dz^2} = \frac{1}{b^3} - \frac{\eta}{ab^2}. \quad (2)$$

Here $\eta = P/P_1$, where P is the total power and $P_1 = n^3 c / 4\epsilon_2 k^2$ in Gaussian units. The first terms on the right-hand sides of Eqs. (1) and (2) represent the effect of diffraction, while the second terms arise from the nonlinear contribution $\frac{1}{2}\epsilon_2 E_0^2$ to the dielectric constant. n is the linear refractive index. Vorob'yev,² who derived Eqs. (1) and (2) in a different way, has shown that they imply

$$\frac{d^3}{dz^3} (a^2 + b^2) = 0, \quad (3)$$

which can be integrated to give

$$k^2(a^2 + b^2) = [k^2(\dot{a}_0^2 + \dot{b}_0^2) + (2/a_0 b_0)(\eta_c - \eta)]z^2 + 2k^2(a_0 \dot{a}_0 + b_0 \dot{b}_0)z + k^2(a_0^2 + b_0^2). \quad (4)$$

Here a_0 and b_0 are the axes of the ellipse formed by the e^{-1} points of the transverse intensity profile at $z=0$, and $\eta_c = a_0/2b_0 + b_0/2a_0$. The initial rates of change \dot{a}_0 and \dot{b}_0 are simply related to the principal radii of curvature R_a and R_b of the phase fronts at $z=0$:

$$R_a = a_0/\dot{a}_0, \quad R_b = b_0/\dot{b}_0.$$

Using Eq. (4), the reader may easily find that the on-axis intensity, which is inversely proportional to $2ab \leq a^2 + b^2$, becomes infinite at the point

$$z_f = ka_0 b_0 (\eta/\eta_c - 1)^{-1/2}, \quad (5)$$

for plane incident phase fronts and $\eta > \eta_c$. It is therefore clear that the critical power for self-focusing is

$$P_c = \eta_c P_1 \quad (R_a = R_b = \infty), \quad (6)$$

which equals P_1 for circular beams. For finite values of R_a and R_b , a real solution for z of the condition $a^2 + b^2$

= 0 occurs only if P/P_1 exceeds

$$\eta_{cc} = \eta_c + \frac{(ka_0 b_0)^2}{4\eta_c} \left(\frac{1}{R_b} - \frac{1}{R_a} \right)^2. \quad (7)$$

For $P = \eta_{cc} P_1$, the self-focus occurs at $z = z_0$, where

$$-(a_0^2 + b_0^2)/z_0 = a_0^2/R_a + b_0^2/R_b. \quad (8)$$

For higher powers the self-focus will be found at

$$z_f = \frac{z_0}{1 + (z_0/k a_0 b_0)(\eta - \eta_{cc})/\eta_c}^{1/2}. \quad (9)$$

For the fourth entry in Table I, the beam parameters are $a_0 = 0.179$ mm, $b_0 = 0.232$ mm, $R_a = 4.05$ cm, and $R_b = 7.04$ cm. The measured power threshold for the onset of bulk damage was from five to twelve times higher than that for circular beams of comparable dimensions, and the damage first appeared at $z = 5.8$ cm from the entrance face. Assuming that the damage should first appear when a catastrophic self-focus forms at $P = \eta_{cc} P_1$, we expect from Eqs. (7) and (8) that the threshold power should be increased by $\eta_{cc} = 12.7$ and that the damage at threshold should appear at $z_0 = 5.51$ cm. The latter figure agrees well with the measured value, and the change in critical power is certainly of the right order. Unfortunately, our knowledge of the influence of the transient electrostrictive contribution to ϵ_2 is too poor to allow us to know which of the first three entries in Table I we should choose as P_1 . The first entry ($P_1 = 0.51$ MW) gives excellent agreement with theory, but the electrostrictive response for an elliptical beam can hardly be as large as that for a circular beam whose diameter equals the small radius of the ellipse. Nevertheless, the agreement with theory is sufficiently good to allow us to conclude that the damage morphology and threshold are well understood in terms of the self-focusing theory.

The theory outlined above gives simple formulas for the powers and distances at which the quantity $a^2 + b^2$ vanishes, but the intensity can become infinite only if the area πab of the beam vanishes. A closer examination of the solutions of Eqs. (1) and (2) shows that a and b both vanish at the same point. Prior to this point, the ratio a/b approaches unity. This is consistent with the observation that the cross sections of the damaged region have a circular shape along the entire length of the damage track. We remind the reader that at some point

between the astigmatic line foci the low-intensity-beam cross section must be circular, but elsewhere it is elliptical

These results imply that difficulties which arise from bulk damage due to self-focusing in high-power optical systems can be avoided or ameliorated by the proper choice of beam parameters.

The authors are grateful to V. Evtuhov for helpful discussions and for providing English translations of Refs. 2 and 3.

*Work supported in part by the Advanced Research Projects Agency under ARPA Order No. 1434 with Air Force

Cambridge Research Laboratories.

¹C. Giuliano and J. Marburger, *Phys. Rev. Letters* **27**, 905 (1971).

²V. V. Vorob'yev, *Izv. Vysshikh Uchebn. Zavedeni Radiofiz.* **13**, 1905 (1970).

³A. B. Shvartsburg in Ref. 2, p. 1775.

⁴C. R. Giuliano and L. D. Hess in *Damage in Laser Materials*, Nat. Bur. Std. Special Publication No. 341, edited by A. J. Glass and A. H. Guenther (U. S. GPO, Washington, D. C., 1970), p. 76.

⁵W. G. Wagner, H. A. Haus, and J. Marburger, *Phys. Rev.* **175**, 256 (1968).

⁶E. Dawes and J. Marburger, *Phys. Rev.* **179**, 862 (1969). This paper contains a detailed comparison of results of the paraxial-ray-constant-shape approximation with exact numerical solutions.

7. Further Comments on Elliptical Beams

The results of the self-focusing theory for gaussian elliptic beams compared with circular beams are summarized in Table I-1. Table I-2 is a comparison of experimental results with theory for both critical power and self-focusing distance. As mentioned in the preceding manuscript, the comparison between theory and experiment is of the right order for the critical power and is very good for the self-focusing distance. In view of the fact that the theory is approximate and that the effects of noninstantaneous response are ignored completely, we are confident that the treatment is satisfactory.

Certainly a great deal of work must be carried out in this area before a complete appreciation of the phenomenon can be realized. However, we feel that these results point to a very promising solution of bulk damage problems which arise from self-focusing. Their applicability for providing solutions to this problem in a number of high power laser and amplifier systems is evident and should be pursued.

8. Use of Elliptical Beams for Determining Intrinsic Damage Threshold Power Densities

As mentioned in Section I-B-5, the measurement of damage threshold for short focal length lenses can yield information on intrinsic breakdown power densities if such damage can be initiated in the absence of self-focusing. However, for this type of experiment, when threshold is reached the damage always occurs at the low power lens focus whether or not self-focusing occurs. Hence it is difficult to know whether in such experiments self-focusing can be avoided completely.

With focused elliptical beams, however, one can more easily distinguish between the two possibilities. The location of the first self-focus for externally focused elliptical beams occurs at a point between the two line foci as given by eq. (8) in the preceding manuscript or in Table I-1. This point, however, does not in general

TABLE I-1

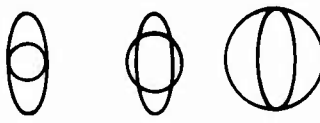
Theoretical Comparisons of P_c and z_f
for Circular and Elliptical Beams

Type of Beam		Critical Power for Self-Focusing, P_c	Self-Focusing Distance, z_f at $P = P_c$
Collimated	Circular	$P_c = P_1 = n^3 c / 4 \epsilon_2 k^2$	∞
	Elliptical	$P_c = \eta_c P_1$ $\eta_c = 1/2 \left(\frac{a_o}{b_o} + \frac{b_o}{a_o} \right)$	∞
Externally Focused	Circular	$P_c = P_1$	$z_f = -R$
	Elliptical	$P_c = \eta_{cc} P_1$ $\eta_{cc} = \eta_c + \frac{(ka_o b_o)^2}{4\eta_c} \left(\frac{1}{R_a} - \frac{1}{R_b} \right)^2$	$z_f = \frac{-(a_o^2 + b_o^2)}{a_o^2/R_a + b_o^2/R_b}$
a_o, b_o = beam radii at entrance to medium R_a, R_b = radii of curvature of phase fronts at entrance to medium.			

T628

TABLE I-2

Comparison of Theory with Experiment

	Ratio of Critical Power of Elliptical Beam to Circular Beam, P_c/P_1	Self-Focusing Distance at Threshold, z_f
Calculated	12.7	5.51 cm
Observed	 12.0 8.1 5.0	5.8 cm
Experimental beam parameters at entrance to medium: $a_o = 0.179$ mm $R_a = -4.05$ cm $b_o = 0.232$ mm $R_b = -7.04$ cm		

T629

correspond to the point of highest intensity for linear propagation. The experimental conditions can be chosen so that the location of the first self-focus and the location of the maximum intensity point for a linearly propagating beam can be made to differ arbitrarily. Hence one can tell whether the damage near threshold arises from self-focusing or by intrinsic breakdown depending on where it is located in the medium. If damage occurs at the high intensity point predicted on the basis of linear propagation, then the intrinsic breakdown intensity can be determined from a knowledge of the power and spot size.

9. Optical Pumping Experiments

Early in the program we presented the results of a number of experiments where we optically pumped the sample while performing damage threshold measurements. (Details of this experimental setup and procedure were given in Semiannual Report 2.) We observed a large amount of scatter in the data because of interference from plasma formation at the entrance surface and were not able to state clearly whether or not the threshold is affected by optical pumping. At a later time, we repeated the pumping experiments with better precision and found a slight decrease in threshold with optical pumping. This is shown in Fig. I-3. The upper graph shows the later more precise data for C_z ruby L107. The lower three graphs are earlier data presented for comparison. We see about 20% decrease in relative threshold for the most extreme pumping case compared with the unpumped case.

We also discussed in Semiannual Report 2 an interesting effect concerning the location of damage in the sample as a function of optical pumping of ruby. We noted that the beginning of the damage track (i. e., the upstream end) is shifted downstream with optical pumping. (We know now from the streak photographs that the upstream end of the damage track is really the last part formed.) From this shift in the damage track in ruby, we inferred that the optical focus was shifting, but we now know from our beam profile measurements that the focus

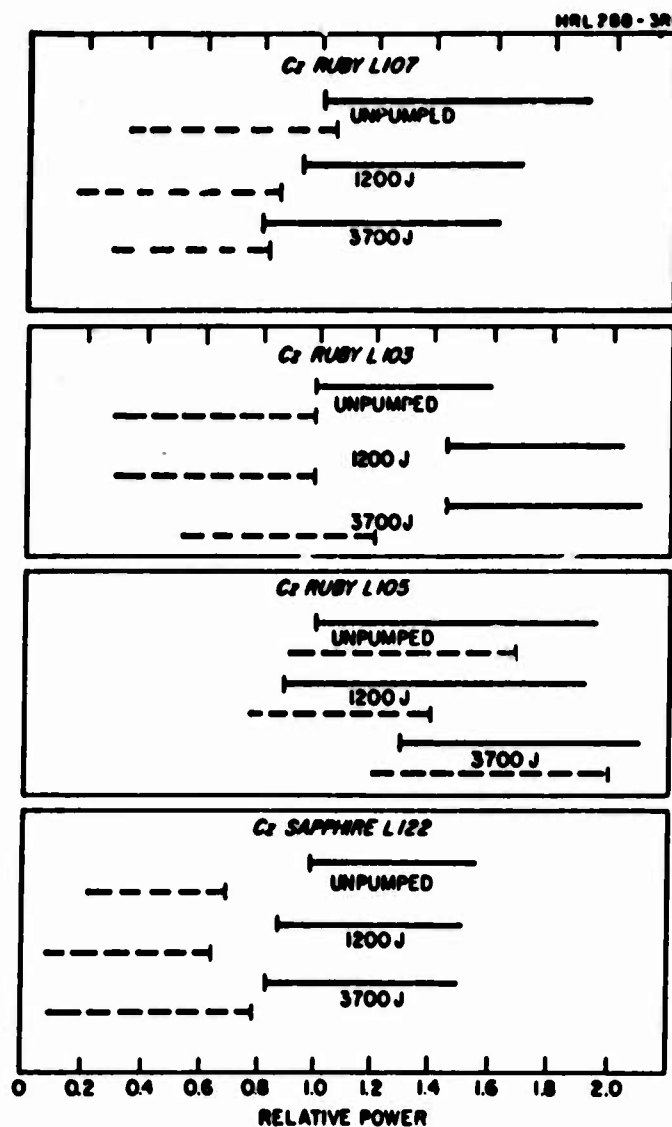


Fig. I-3.
Relative Bulk Damage Threshold as a Function of Optical Pumping for Different Samples. The Thresholds are Normalized to Unity for the Unpumped Sample. Dashed Line - No Damage; Solid Line - Damage. The Three Lower Graphs are Reproduced from the Last Report; the Upper Graph shows Results of more Reproducible measurements taken during this Reporting Period.

is located downstream from where we thought it was. In fact, from our streak camera measurements, we know that the damage track lies between the natural focus and the entrance surface. In sapphire, the track begins at or very close to the natural focus and progresses upstream; in ruby the points of beginning and end of the track occur substantially upstream from the natural (i. e., low power) focus. Optical pumping in ruby shifts the track toward downstream locations as well as making it longer. That is, it approaches the behavior for sapphire.

Precise data on this point are not available at this time. However, we wish to point out that the shift in track location is not necessarily related to a defocusing due to pumping solely, but may be connected with the fact that pumped ruby behaves more like sapphire simply by virtue of its being pumped.

C. SURFACE DAMAGE STUDIES

1. Relation Between Surface Damage and Plasma Formation

During the latter one-third of this program more emphasis has been placed on the problem of surface damage rather than bulk damage. Our efforts in this area have been to measure the thresholds for ruby and sapphire under different conditions and to attempt to understand the connection, if any, between the damage and the surface plasmas which occur. A paper has been written describing this work; it has been accepted for publication in the IEEE Journal of Quantum Electronics. An expanded version of this work was presented at the Fourth ASTM-NBS Symposium on Damage in Laser Materials, Boulder, Colorado, June 1972 and will be published in the Proceedings. The manuscript is presented in the following pages.

The Relation between Surface Damage and Surface Plasma Formation*

Concetto R. Giuliano

Hughes Research Laboratories
Malibu, California 90265

A number of experiments are described in which entrance and exit surface laser-induced damage on sapphire samples are studied. Damage thresholds are measured as a function of beam size and divergence at the surfaces. Temporal evolution of surface plasmas is studied using a streaking camera, and spatial differentiation of surface plasmas is accomplished by allowing the light to strike the surfaces away from normal incidence. It is found that the entrance surface has two plasma components, an air plasma which is directed along the light beam and an "explosion" plasma which is directed normal to the surface. The exit surface has only the explosion plasma. It is concluded that surface plasmas are a result of, rather than a cause of surface damage.

Key Words: Entrance and exit surface damage, sapphire, spatial and temporal plasma resolution, streak camera experiments, surface plasmas.

1. Introduction

It has been known for some time that laser-induced surface damage has distinctly different physical characteristics, depending on whether the entrance or exit surface is damaged. [1-4]¹ To a certain extent the conditions under which the damage is generated (e.g., focusing, surface finish) are important in determining some of the details of the appearance of the damage, but as a general rule entrance surface damage is less extensive and more difficult to detect visually than exit surface damage, especially when generated under conditions of gentle focusing. Under such conditions for sapphire the distinguishing features are that exit surface damage can be most easily described as relatively deep fractured areas, while entrance surface damage is relatively shallow crazed areas. Scanning electron micrographs of both types of damage are presented in Figures 1 and 2.

The occurrence of laser-induced surface damage is known to be accompanied by a bright flash of light which comes from a spark or plasma at the surface. [1-5] (See Figure 3) In fact, the occurrence of a visible spark has been held to be a criterion for surface damage. [4] Spectra taken of exit surface plasmas show that the light contains spectral lines characteristic of the material being irradiated. [1] The connection between the surface plasma and the damage was not established in the early work. Whether or not the plasma is a result of or a cause of the surface damage or whether it is an independently occurring phenomenon that simply accompanies the damage phenomenon was not determined.

* Work supported by the Advanced Research Projects Agency under ARPA Order No. 1434 with Air Force Cambridge Research Laboratories.

¹ Figures in brackets indicate the literature references at the end of this paper.

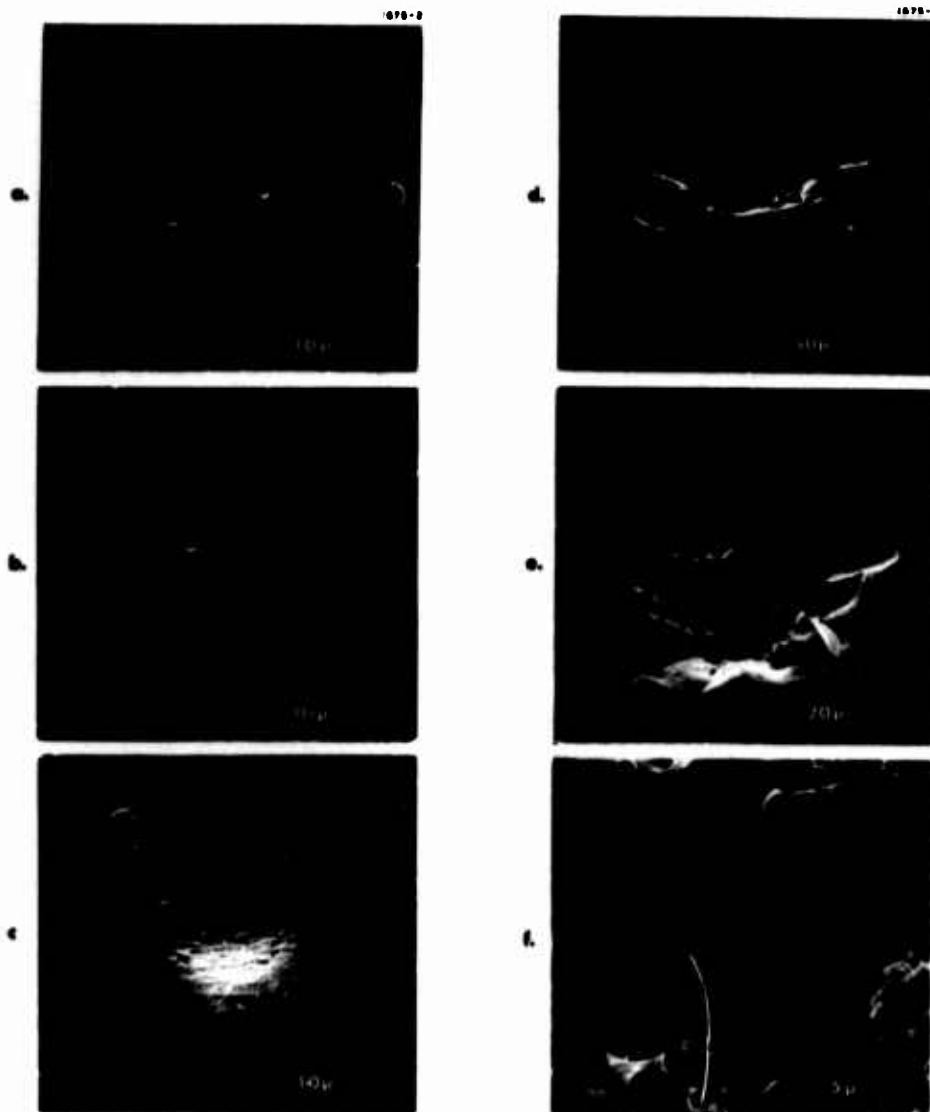


Fig. 1. Scanning Electron Micrographs of Exit Damage Sites for Sapphire. Pulse Energy Increases from a through d; e and f are Magnified Views of Site Shown in d.



Fig. 2.
Scanning Electron Micrographs
of Entrance Damage for Sapphire.
Pulse Energy Increases from a-c.

M7251

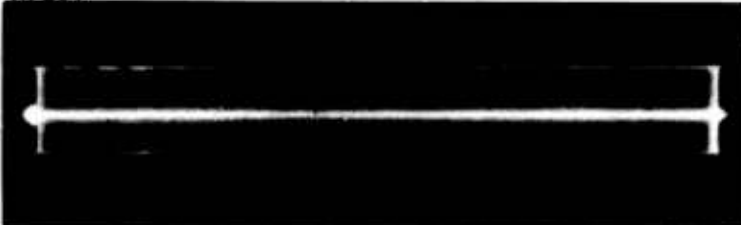


Fig. 3. Example of Entrance and Exit Surface
Plasmas Formed When Light From a Q-
Switched Ruby Laser Passes Through a
Sample. Sample Length - 3 in. Light
is Traveling from Left to Right.

Fersman and Khazov [3] have suggested that the surface damage is caused by a plasma-surface interaction and have explained the difference between entrance and exit surface damage using a model in which both the plasmas grow in an upstream direction as they develop in time, an extension of the observations for air breakdown plasmas. [6] The exit damage would then be expected to be more extensive than entrance damage because the exit plasma grows into the surface, while the entrance plasma grows away from the surface. Fersman and Khazov observe a compressional wave which propagates inwardly from the exit surface. Compressional waves arising from damage sites in solids have been observed by others using both schlieren and holographic techniques. [7,8] While the above picture can predict a difference between the entrance and exit damage, it was not experimentally confirmed.

Another possible explanation for the difference between exit and entrance damage is that exit damage might be somehow influenced by self-focusing of the beam in the material, while the beam at the entrance would not be so affected.

We have carried out a number of experiments in an attempt to determine more explicitly the connection between the surface damage and the plasmas and to clarify the nature of the damage mechanism or mechanisms.

All the experiments described in this paper were carried out using a single longitudinal and transverse (TEM₀₀) mode Q-switched ruby laser. The laser and associated monitoring apparatus are described in detail elsewhere. [2] Typical laser pulse width and peak power are 20 nsec (FWHM) and 1 MW, respectively.

2. Damage Threshold as a Function of Beam Size and Divergence

One of the questions which arises in the consideration of exit surface damage is concerned with the possibility that the damage at the exit surface might be influenced by what the beam does in the bulk of the material. For example, if some self-focusing or other nonlinear phenomenon takes place, it might affect the beam so that the intensity at the exit face will be different from that expected on the basis of linear propagation theory. Also, some phenomenon which might cause the generation of acoustic waves directed toward the exit surface would be affected by how the beam propagates inside the sample before reaching the exit surface. A series of experiments on sapphire was carried out in which the sample was moved relative to the focusing lens, so that the spot size at the surface would vary over a wide range and also so that the beam could be either converging or diverging at the surface, depending on whether the beam waist lay downstream or upstream from the surface.

The result of these experiments is shown in Figure 4. In these experiments a 19 cm lens for focusing the light from the mode-controlled ruby laser was used. The sapphire samples were moved in 5 mm increments relative to the lens, and surface damage threshold was measured for each location. The data on the left half of the figure correspond to the case of rays converging at the exit surface and the data on the right half to diverging rays. The beam area at the surface is also plotted as a function of distance in the figure.

Figure 4 shows that the results for exit surface damage threshold power in sapphire sample L134 fall very close to the beam area curve. The fact that they fall so closely is a coincidence of the scale and the units chosen, but the fact that they have the same functional dependence on distance is significant in that it strongly indicates that the damage threshold is a power density phenomenon. Also, the fact that the threshold is independent of whether the beam is converging or diverging at the exit surface indicates that the damage seems to be strictly a surface or near-surface phenomenon. The exit surface damage threshold for this sample is about 1 GW/cm². The data for entrance surface damage for sapphire sample C129 are shown in Figure 5. A similar dependence on lens-to-sample distance is seen in the plot but in this case the scatter in the points is somewhat greater. Here the beam area curve is plotted on a different scale than in Fig. 4 to show that the dependence of threshold power with distance is essentially the same as the dependence of beam area with distance, again indicating that damage threshold is a power density phenomenon. The entrance damage threshold for this case is about 1.5 GW/cm².

3. Surface Damage without Plasma Formation

We have carried out a few experiments in which surface damage was generated without observing an accompanying plasma. These experiments were conducted on sapphire samples and the observations apply only to the exit surface (entrance damage was not pursued in

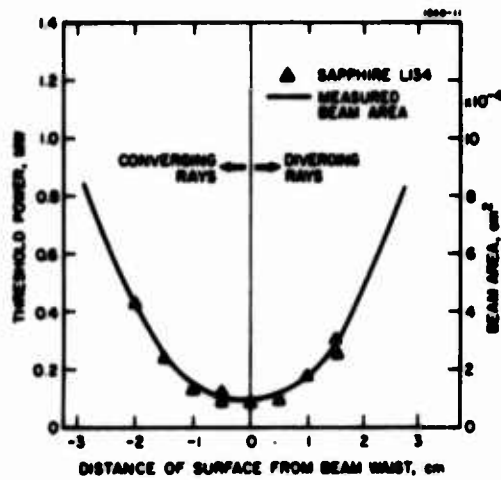


Fig. 4. Exit Surface Damage Threshold Power for Sapphire Sample as a Function of Surface Distance from Beam Waist for 19 cm Lens. Beam Area is also Plotted.

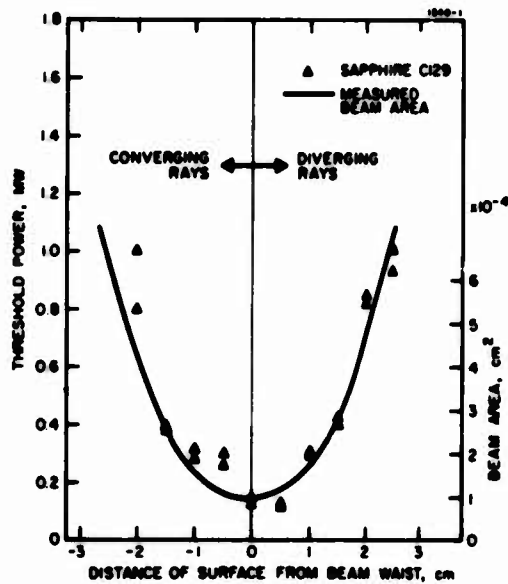


Fig. 5. Beam Area and Entrance Surface Damage Threshold as a Function of Surface Distance from Beam Waist for 19 cm Lens.

this series of experiments). In these experiments we observed the exit surface during laser irradiation both visually and photographically under different conditions of optical filtering and exposure. It was found that when the sample was exposed to focused radiation very close to the threshold, damage could be generated in the form of a series of micropits without the simultaneous accompaniment of a detectable plasma or spark.

A series of experiments was initiated in which the sample was irradiated well above damage threshold, and the plasma observed as the power was gradually reduced, each time exposing a fresh area of the surface. During this series, the accompanying plasma was seen to decrease in size and brightness as the laser power was reduced, until a power point was reached at which the spark was no longer visible. On a number of occasions after laser irradiation at a level just below that for generating a visible plasma, it was possible to detect damage in the form of a number of micropits when the sample was carefully examined through a microscope with properly chosen illumination. This micropitting, which is seen only very close to threshold, is less extensive than the single fracture crater that occurs more often at slightly higher powers when the plasma is clearly visible. It should be noted that at the times when no plasma is visible, it is possible to see small amounts of laser light scattered from the tiny surface pits which are being formed.

The results of these observations suggest that it is possible to obtain exit surface damage without plasma formation. Of course, the nonobservability of a plasma does not necessarily imply that it is not present, and these results alone do not allow us to form any definite conclusions regarding the connection between the damage and the plasma.

4. Time Evolution of Surface Plasmas

One reason for the interest in studying the temporal evolution of the surface plasmas has been to determine the direction of growth of the plasmas relative to the crystal surface, which would lead to a possible explanation of the differences between exit and entrance damage and to test the mechanism proposed by Fersman and Khazov.

We have employed an STL image converter camera operating in the streaking mode for observing the growth of the entrance and exit surface plasmas (see Figure 6). For these experiments, the output from our single-mode ruby laser was focused with a 19 cm lens on the desired surface of the sapphire sample being examined. Typical laser output is about 20 mJ in a 20 nsec pulse, which gives a power density at the focus of approximately 10 GW/cm², about 10 times above damage threshold. For the streak camera experiments, a portion of the incident laser light was allowed to enter the camera directly to serve as a marker streak for synchronization purposes.

Streak photographs showing the temporal development of the surface plasmas are shown in Figures 7 and 8. Because the photographic setup is such that the camera views the surface at an angle less than 90° to the normal (see Figure 6), both the plasma and its reflection in the surface are often seen. The fact that there are indeed reflections was confirmed by placing an appropriately oriented Polaroid filter in front of the camera, in which case the reflection from the dielectric surface disappears as expected.

Essential features of these streak photographs to be noted are

- The plasmas grow away from the surfaces in both cases, the entrance plasma growing in the upstream direction and the exit plasma in the downstream direction.
- The entrance plasma has two temporal components, whereas the exit plasma has one temporal component.
- The extent of growth and luminosity of the faster growing component of the entrance plasma depends on the incident laser pulse in that it ceases to expand and to emit light when the laser terminates.
- The slower growing, longer lived component of the entrance plasma expands at about the same rate as the exit plasma. These plasmas continue to expand outward and emit light long after the laser has terminated.
- Typical velocities of expansion of the luminous plasma fronts are $\sim 2 \times 10^6$ cm/sec for the short-lived entrance component and $\sim 1 \times 10^6$ cm/sec for the long-lived entrance component and for the exit plasma.

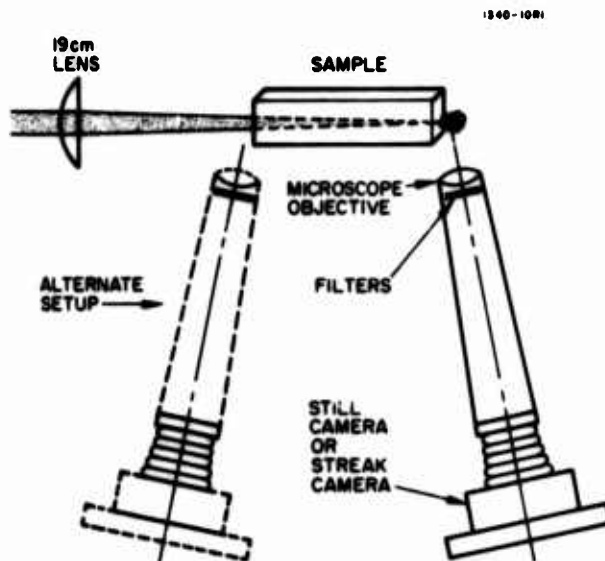


Fig. 6. Schematic Diagram Showing Setup used for Photographing Surface Plasmas both for Still and Streak Photography.

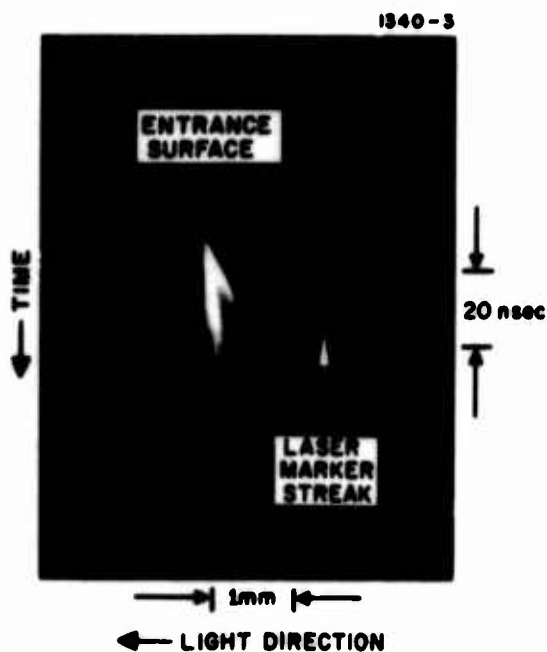


Fig. 7. Streak Photograph of Entrance Plasma on Sapphire Surface Showing Two Temporal Components.

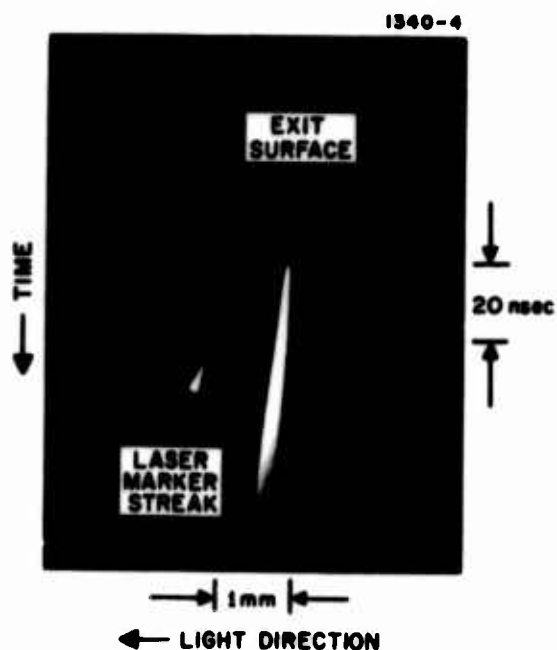


Fig. 8. Streak Photograph of Exit Plasma on Sapphire Surface.

Several ideas are suggested by these observations. First, the fact that both entrance and exit plasmas grow away from the surfaces suggests that the mechanism proposed by Fersman and Khazov is incorrect. From the time dependences of the plasmas relative to the incident laser pulse it can be inferred that the short-lived entrance component is a plasma supported in the ambient atmosphere and sustained directly by the laser beam itself, while the longer-lived components at both surfaces result from a kind of micro-explosion caused by the deposition and subsequent release of energy at or near the surface.

5. Spatial Differentiation of Surface Plasmas

To test these hypotheses, further, we devised additional experiments that were designed to allow a spatial differentiation of the plasmas. The reasoning behind these experiments is as follows. A plasma sustained directly by the light beam would be expected to exist only where the light is present and to be directed along the light beam independent of the angle at which the light enters the material. A plasma which results from a surface explosion caused by a deposition of energy at the surface would be expected to extend in a direction normal to the surface no matter at what angle the light should enter the material.

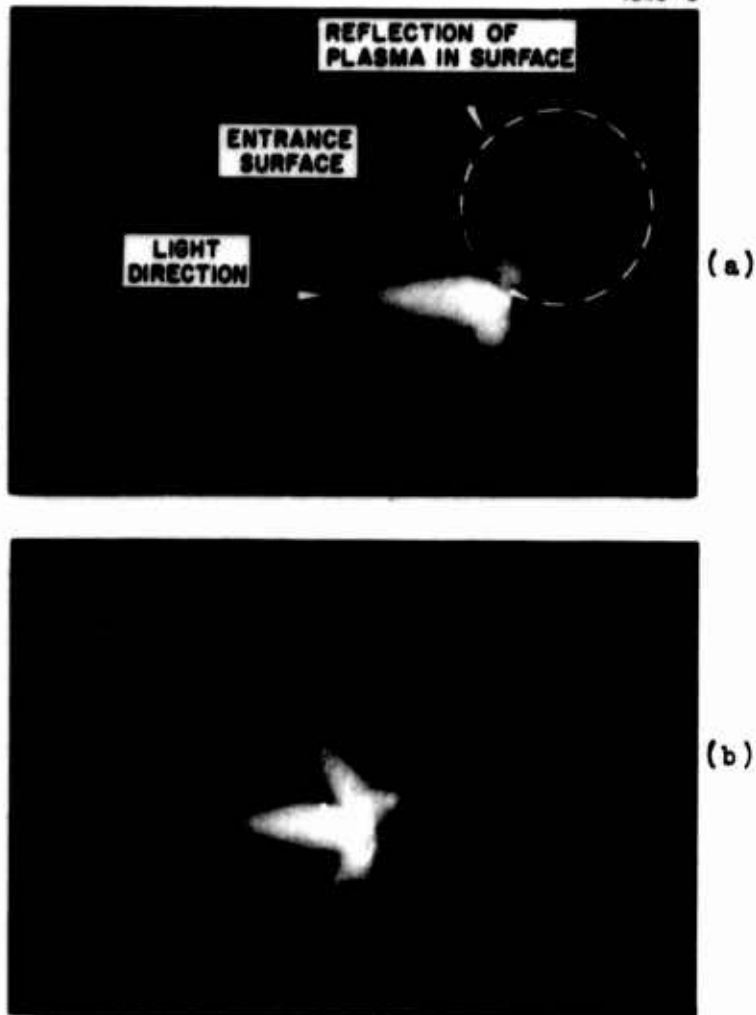
Figure 9 shows time-integrated photographs of the entrance plasma formed when the light is allowed to strike the surface at angles other than normal incidence. The photographs show the separation of the plasma into different spatial components. One component extends along the direction of the light beam; this apparently is the short-lived air plasma. Another component that extends normal to the surface can be seen; this is the component resulting from the surface explosion. A third more diffusely defined plasma component can be seen, extending in the direction of the light reflected from the surface and is presumably additional air plasma sustained by the reflected light. Figure 10 shows a time-integrated photograph of the exit plasma formed when the light leaves at an angle of 45° to the surface. This photograph shows a single plasma component directed normal to the surface, as expected if a surface explosion were taking place.

As a final confirmation of assignments for the different plasma components, we looked at the entrance plasma in a vacuum. Figure 11 shows photographs of the entrance plasma for a sample tilted 26° from the incident light both at 1 atm pressure and at about 1 Torr pressure. Because of the shape and size of the container, it was impossible to perform the experiment at angles larger than 26° . As a result, the two spatial components are not distinguishable in Figure 11(a) and (b). However, note that when the air is removed from the system (Figure 11(c) and (d)), the plasma component which extends along the light beam is no longer seen; the plasma visible in vacuum is directed normal to the surface, i.e., only the explosion plasma remains.

6. Conclusions

As a result of these experiments, the following conclusions are reached. First, the surface plasmas are a result rather than a cause of the surface damage. Second, two kinds of plasmas occur at the entrance surface, one which is sustained by the light beam in the ambient atmosphere and another which arises from a micro-explosion at or near the surface. The exit surface plasma is of the explosion type. While it may be true that some of the features seen on the surface of a material that has been subjected to damaging laser radiation might be caused by the interaction of the plasma with the surface, the primary cause of the damage is not the plasma. Rather, the surface plasmas are a result of the process or processes, whatever they may be, that give rise to the surface damage.

It is still not clear why the exit damage is physically so different in appearance than entrance damage. If the mechanism of energy deposition were simply one of surface absorption, it would be expected that the damage would be very similar on both surfaces. For some reason, there seems to be a distinct directionality to the surface damage mechanism. Since the exit surface damage threshold appears to be power density phenomenon and since it is not apparently dependent on whether the beam is converging or diverging before it reaches the surface, one would be inclined to conclude that the damage mechanism does not depend strongly, if at all, on phenomena which take place in the bulk of the material. It appears to be strictly a surface or near-surface phenomenon. The possibility that a directed intense acoustic wave [1] is involved in the damage mechanism is still open, although Stimulated Brillouin Scattering (SBS) is not likely since there seems to be no correlation between SBS thresholds and damage thresholds for a number of different solids. A mechanism of the type proposed by Hellwarth for bulk damage [9] might be a valid surface damage mechanism. The end result of this mechanism is the generation of intense acoustic phonons, but whether one would expect the acoustic wave to be directed in any particular way is not known at this time.



Reproduced from
best available copy.

Fig. 9.
Time Integrated Photographs of Entrance
Plasma at Sapphire Surface Tilted With
Respect to Incident Beam Direction.
Angle Between Light Direction and Sur-
face Normal (a) 45° , (b) 60° .



Fig. 10.
Time Integrated Photograph of Exit
Plasma at Sapphire Surface Tilted
 45° With Respect to Light Propaga-
tion Direction.

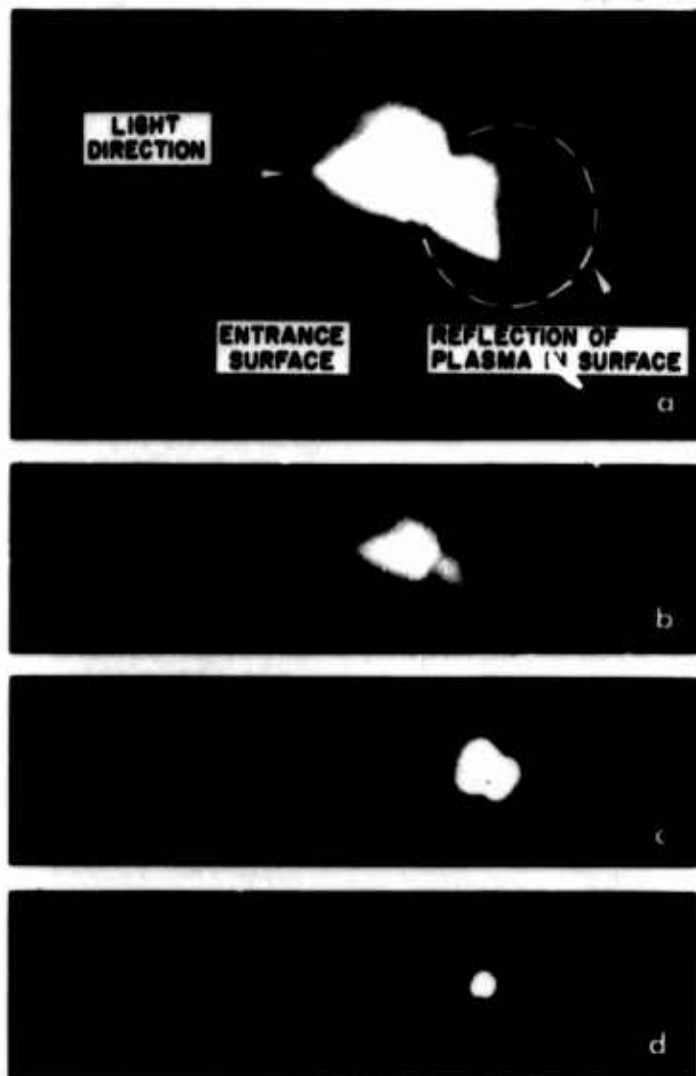


Fig. 11.
Time Integrated Photographs of Entrance Plasma at
Sapphire Surface Tilted 26° From Beam Direction
for Different Optical Attenuations at Camera.
(a) and (b) Taken at 1 atm in Air, (c) and (d)
Taken at 1 Torr Pressure. Optical Attenuation
(a) N.D. 1.0, (b) N.D. 1.7, (c) N.D. 0.7,
(d) N.D. 1.7.

7. Acknowledgment

The author wishes to acknowledge the skilled technical assistance of G. R. Rickel.

8. References

- [1] Concetto R. Giuliano, "Laser-induced damage to transparent dielectric materials," *Appl. Phys. Letters* **5**, 137-139 (1964).
- [2] C. R. Giuliano and L. D. Hess, "Damage threshold studies in ruby and sapphire," in Damage in Laser Materials, edited by A. J. Glass and A. H. Guenther, U. S. National Bureau of Standards Special Publication No. 341 (U. S. GPO, Washington, D. C. 1970), pp. 76-89.
- [3] I. A. Fersman and L. D. Khazov, "Damage of transparent dielectric surfaces by a laser beam," *Sov. Phys. -Tech. Phys.* **15**, 834-838 (1970).
- [4] Michael Bass, "Nd:YAG laser-irradiation-induced damage to LiNbO_3 and KDP," *IEEE J. Quantum Electron.* **QE-7**, 350-359 (1971).
- [5] L. D. Khazov, A. N. Shestov, and G. P. Tikhomirov, "Luminous discharge on non-absorbing surfaces produced by a single pulse laser," *Sov. Phys.-Tech. Phys.* **13**, 1112-1114 (1969).
- [6] S. A. Ramsden and W. E. R. Davies, "Radiation scattered from the plasma produced by a focused ruby laser beam," *Phys. Rev. Letters* **13**, 227-229 (1964).
- [7] T. P. Belikova, A. N. Savchenko, and E. A. Sviridenkov, "Optic breakdown in ruby and related effects," *Sov. Phys.-JETP* **27**, 19-23 (1968).
- [8] N. L. Boling and R. W. Beck, "Laser glass damage threshold studies at Owens-Illinois," in Damage in Laser Materials, edited by A. J. Glass and A. H. Guenther, U. S. National Bureau of Standards Special Publication No. 356 (U. S. GPO, Washington, D. C., 1971), pp. 15-23.
- [9] R. W. Hellwarth, "Role of photo-electrons in optical damage," in Damage in Laser Materials, edited by A. J. Glass and A. H. Guenther, U. S. National Bureau of Standards Special Publication No. 341 (U. S. GPO, Washington, D. C., 1970), pp. 67-75.

2. Surface Damage Threshold for Ruby as a Function of Beam Size and Divergence

A series of experiments similar to those performed for sapphire and described in the preceding manuscript were carried out on a ruby sample. Both entrance and exit surface damage thresholds were measured as a function of lens-to-sample distance. While the entrance damage threshold power shows a similar dependence on distance as that for the sapphire sample (see Fig. I-4), the exit threshold shows a marked difference (Fig. I-5). This phenomenon is not understood, but we strongly suspect that it is related to the intensity dependent beam distortion observed in ruby. The latter phenomenon is discussed in Semiannual Report 3 and summarized in Section I-D-2. Since the beam distortion was observed to occur at powers well below the surface damage threshold power, it is reasonable to suspect that the intensity at the exit surface of a ruby sample would not be easy to predict. The fact that the beam profile in ruby changes with incident power and position indicates that the power density at a given location (e.g., the exit surface) cannot be easily determined.

3. Morphology of Entrance and Exit Damage

Figures 1 and 2 of the preceding manuscript show scanning electron micrographs of entrance and exit damage sites which illustrate the striking difference in the morphology of the two types of damage. At the time the paper was written it was not clear why the two kinds of damage have such a different appearance. The crazing, which is the distinguishing characteristic of entrance damage, is not seen at the exit except at very high powers, and the crater type damage that occurs at exit surfaces is not seen at the entrance surface. Additional pictures of the different features of surface damage are shown in a paper which we published early in this program.² Recently we have examined the morphology of entrance surface damage that was formed when the sample was placed in a vacuum chamber at

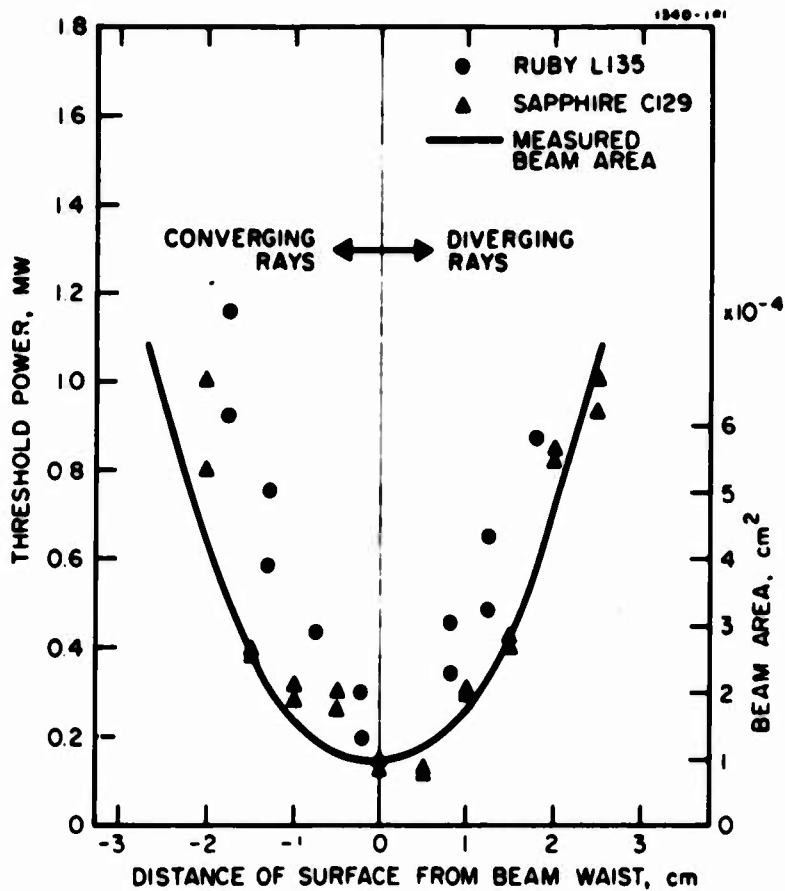


Fig. I-4. Beam Area and Entrance Surface Damage Threshold as a Function of Surface Distance from Beam Waist for 19 cm Lens.

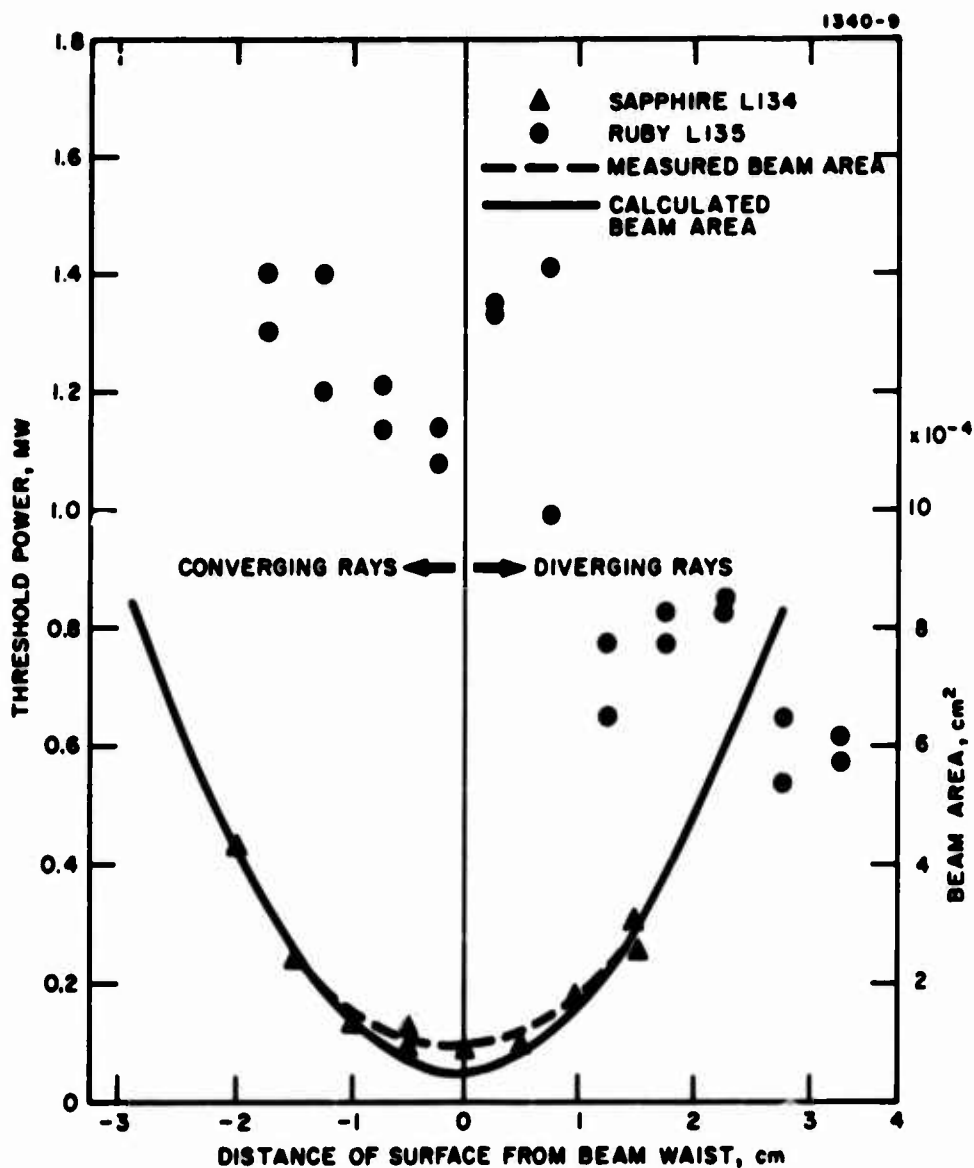


Fig. 1-5. Exit surface damage threshold power for sapphire and ruby samples as a function of surface distance from beam waist for 19 cm lens. Beam area is also plotted. The left half of the figure corresponds to a converging beam; the right half to a diverging beam.

~1 Torr pressure. Recall that the entrance surface plasma was seen to have two components, an air plasma and an explosion plasma. The air plasma is absent when the sample is damaged in a vacuum. Figure I-6 shows optical and scanning electron micrographs of entrance surface damage generated in a vacuum. Note that no crazing exists in these pictures. The distinguishing feature is now a slight rippling of the surface. Figure I-7 shows an optical micrograph of vacuum entrance surface damage for a sample tilted 45° with respect to the incident light beam. Here we see what appears to be only a slight darkening of the surface with little or no change in surface topography. Attempts to obtain scanning electron micrographs of this damage site have so far failed, perhaps because there is too small a change in surface features to be detected.

From these observations we conclude that the crazing which characterizes entrance surface damage arises from an interaction of the air plasma with the surface.

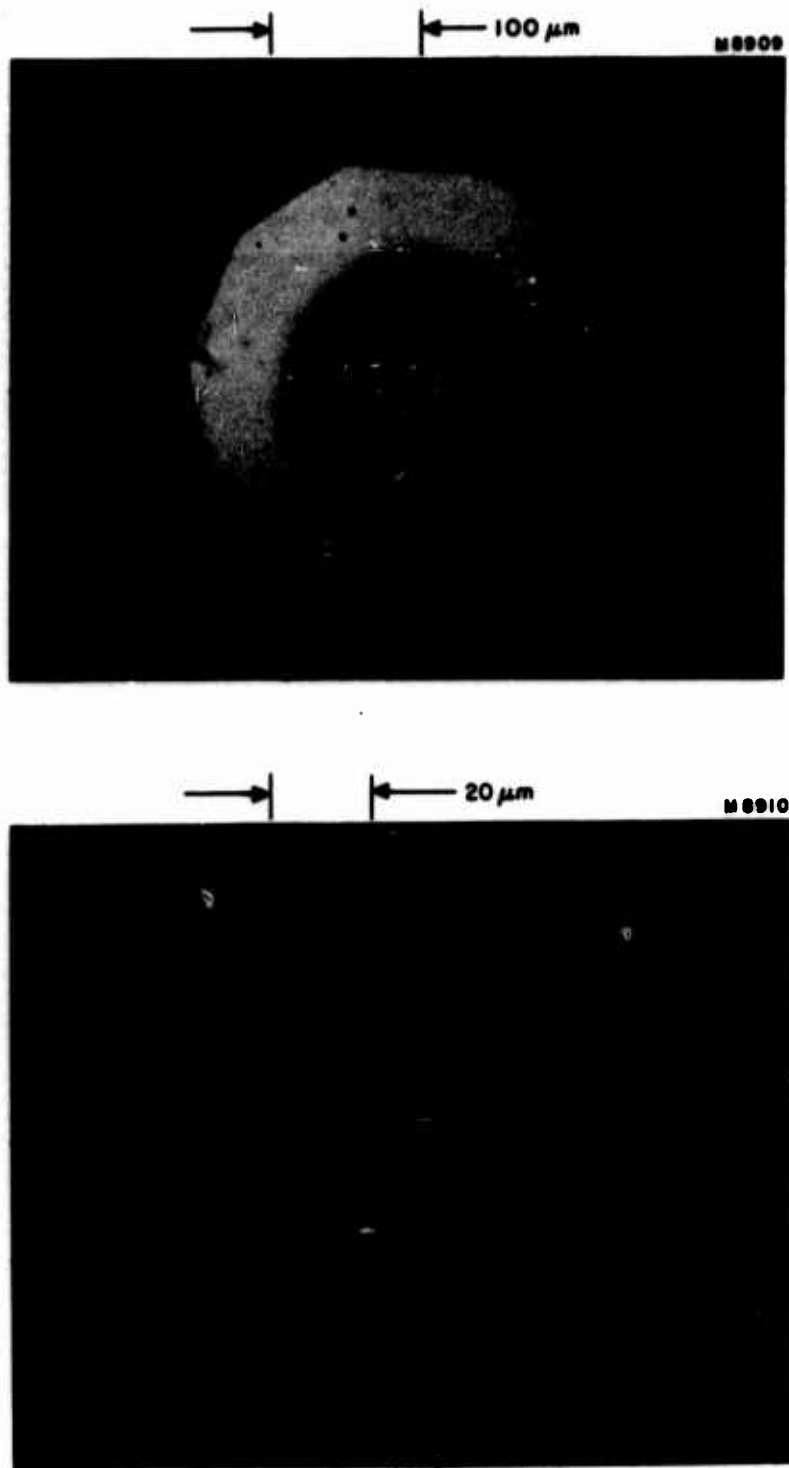


Fig. I-6. Optical and Scanning Electron Micrographs of Vacuum Entrance Surface Damage for Beam at Normal Incidence.

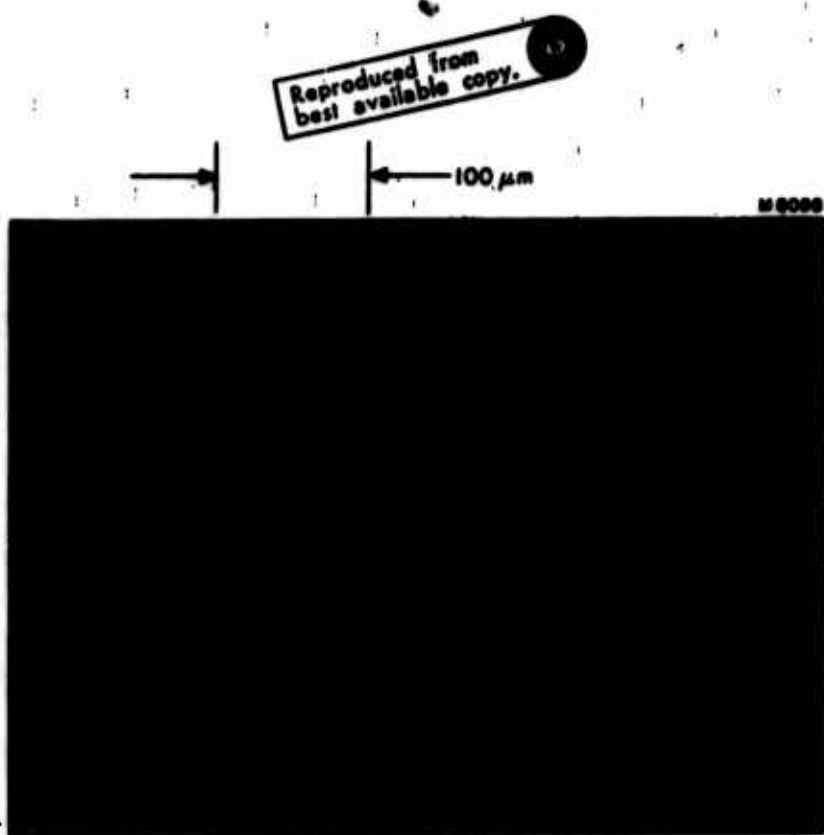


Fig. I-7. Optical Micrograph of Vacuum Entrance Surface Damage for Beam Incident at 45°.

4. Attempts to Increase Surface Damage Threshold by Ion Beam Polishing

During the latter stages of this program we have obtained some very encouraging results which indicate that surface damage thresholds can be substantially improved. We carried out a few experiments in which sapphire samples were polished using an energetic argon ion beam and found that the surface damage threshold for both entrance and exit were increased substantially (up to ten times depending on the particular points compared). This work led to a publication in *Applied Physics Letters* (1 July 1972) and a presentation at the Fourth ASTM: NBS Conference on Damage in Laser Materials, Boulder, Colorado, June 1972. A reprint of this manuscript, which gives the essential features of this work, follows.

Laser-induced damage in transparent dielectrics: ion beam polishing as a means of increasing surface damage thresholds*

Concetto R. Giuliano

Hughes Research Laboratories, Malibu, California 90265

(Received 14 April 1972)

Polishing of sapphire surfaces with energetic Ar^+ ion beams is shown to result in a substantial increase in laser damage threshold over that for conventionally polished surfaces. Data for both entrance and exit damage are presented. The results are interpreted in terms of an increase in surface strength with ion beam polishing.

It is a generally accepted fact that the threshold for laser-induced surface damage of transparent dielectrics is a function of the condition of the surface being irradi-

ated. Any foreign material on a surface subjected to high optical fluxes can cause catastrophic damage to occur at levels well below those which can be sustained

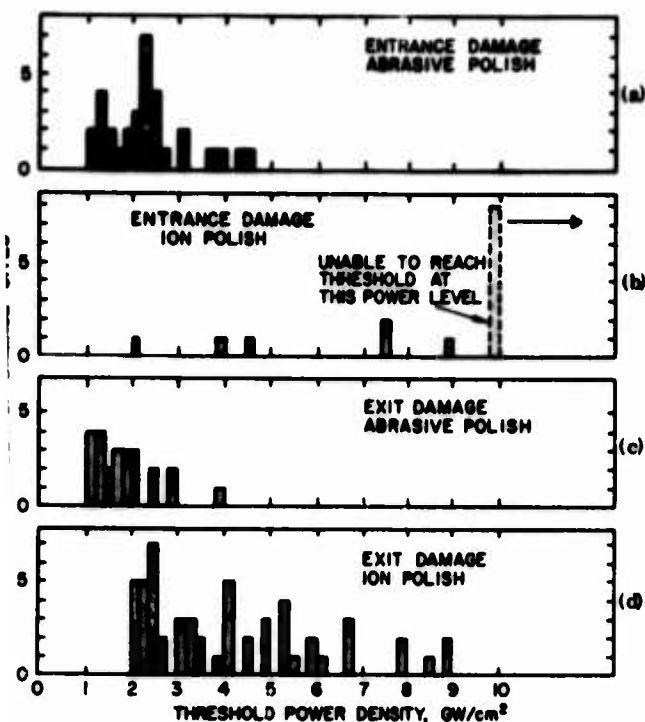


FIG. 1. Number of damage sites as a function of threshold power density at entrance and exit surfaces of sapphire crystals for abrasively polished and ion-beam-polished samples.

age is observed the incident power is increased (by ~10–20%) and again the sample is examined. The procedure continues until damage is observed; then the sample is moved and the process repeated on an undamaged spot. Typically 10–20 damage thresholds are measured in this way for a given surface.

Abrasively polished samples were used as obtained from the manufacturer (Union Carbide). They were fabricated with the "laser finish" specifications typical for ruby laser rods. Ion-polished samples were exposed after mechanical processing to an Ar^+ beam (7 kV, $300 \mu\text{A}/\text{cm}^2$) for periods from 2 to 4 h. The beam strikes the surface at an angle of 20° from the surface plane. An estimated $200 \text{ \AA}/\text{min}$ is removed from the sapphire surface under these conditions, giving a total of from about 2.5 to 5μ of material removed in a given exposure.

The results of a series of measurements on abrasively polished and ion-beam-polished samples are shown in

clean surfaces. The quality of surface fabrication has so been recognized as being important in influencing the damage resistance of materials. For example, it is now known that a frosted surface damages more easily than a surface with a good optical polish.¹ Various chemical surface treatments have been tried on different materials,^{2,3} some of which have shown improvement, but the effect is only temporary.

We have found that polishing of sapphire surfaces with ion beams results in a marked increase of surface damage threshold compared with that for abrasively polished samples.

Experiments were carried out using a single transverse-longitudinal-mode ruby laser whose output is focused on either the entrance or exit surface of a sapphire sample. The samples are sapphire bars 3 in. long by 0.25-in.-square cross section. The laser and associated monitoring apparatus are described in detail elsewhere.⁴ Typical laser pulse width and peak power are 20 nsec (FWHM) and 1 MW, respectively. The area of the focused spot has been measured using a modified knife-edge-camera technique⁵ to be 10^{-4} cm^2 at the 1/2 intensity points. The beam profile was measured to be Gaussian down to 8% of the peak. The power incident on the sample is varied by rotating the first of a pair of spaced polarizers, the second being held at a fixed orientation.

A typical series of measurements is carried out as follows. The laser is fired at a particular spot on the entrance surface at a power below damage threshold. The sample is then examined through a traveling microscope without disturbing the sample between shots. If no dam-

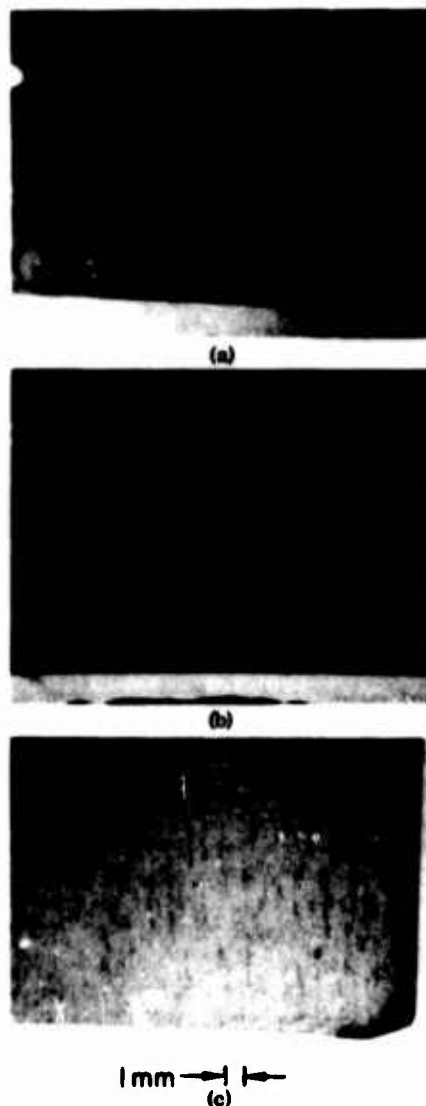


FIG. 2. Examples of x-ray diffraction topographs taken for (a) abrasively polished sample, (b) Ar^+ ion polished for 2 h (7 kV, $300 \mu\text{A}/\text{cm}^2$), (c) same conditions as (b), but for 4 h.

Reproduced from
best available copy.

Fig. 1. In Figs. 1(a) and 1(b) the results for entrance surface damage are shown. For the abrasively polished sample most of the damage thresholds occur between 1 and 2.5 GW/cm² with a few higher values occurring. For the ion-polished case [Fig. 1(b)] we see a few damage thresholds ranging from 2 to 9 GW/cm² with a large fraction (>50%) above 10 GW/cm². [The dashed portion of Fig. 1(b) indicates that we were unable to reach damage threshold with the maximum output from our laser under the focusing conditions of our experiment.] Figure 1(c) shows the exit damage thresholds for the abrasively polished sample. Here the bulk of the points are clustered between 1 and 2 GW/cm². For the ion-polished case [Fig. 1(d)] the values are again spread over a wide range (up to 9 GW/cm²), but for this case no damage thresholds lower than 2 GW/cm² are observed. The data in Fig. 1(d) were obtained from samples which were ion polished for 2 and 4 h. No noticeable change in the distribution was observed between the 2- and 4-h cases, and the data are presented together in the figure.

Figure 2 shows examples of x-ray reflection topographs for sapphire samples which were abrasively polished [Fig. 2(a)] and ion beam polished [Figs. 2(b) and 2(c)]. The depth of the region being probed in these topographs depends on the angle of incidence and energy of the x rays as well as other experimental conditions and sample properties. An estimated region 10–20 μ thick is being probed in the above topographs. We see in Fig. 2(a) a number of deviations from crystallinity which appear to follow scratch lines from the mechanical polishing process. In Fig. 2(b) the topograph for a different sample shows that some of the mechanical damage appears to have been "erased" after 2 h of ion beam polishing. Figure 2(c) shows a topograph taken after 4 h of exposure to the ion beam, and, although evidence of damage still is seen, there is a marked difference between this and the previous topographs. We present these topographs to point out that a distinct change in surface topography is brought about by ion beam polishing. A detailed correlation between the changes in the topographs and the damage thresholds is not possible at this time.

The main conclusion reached by these preliminary results is that a distinct increase (~2–6 times) in surface damage threshold can be realized by ion beam polishing. Although there is a wide scatter of results in measured thresholds for ion-polished samples, we see that even the low values for the ion-polished samples are generally higher than those for the abrasively polished samples. We interpret the scatter in the threshold data for the ion-polished samples to indicate a variation of surface strength from place to place over the sample. It is very likely that the influence of mechanical damage due to abrasive polishing, although somewhat lessened, has not been completely removed under the conditions of

our experiments. This is suggested by the x-ray topographs, although as yet no definite correlation between topograph details and threshold variations has been established. We choose to interpret the data as reflecting a variation of threshold from spot to spot on the surface rather than in a probabilistic manner as described by Bass and Barrett.⁶ It is apparent from the topographs that the surface crystallinity varies considerably from place to place over the sample and that the surface is not uniform all over. A possible interpretation of the difference between the abrasive-polish and ion-polish results is that in the former case the surface is "uniformly weak" and the damage thresholds are found to have a relatively narrow range of values, whereas in the latter case a distinct toughening of the surface has taken place, but the influence of mechanical damage from the abrasive polishing still exists.

A final point worthy of mention is that the damage, when it occurs at a high threshold, is generally much more extensive than when it occurs at a low threshold. For example, exit surface damage in abrasively polished samples is generally characterized by a small fractured crater or pit about 10 μ in diameter when it occurs near threshold. On the other hand, the high-threshold damage seen in the ion-polished samples is more severe; the damage craters are usually several times larger and more extensively fractured. This fact suggests that the effect of ion polishing is to toughen or strengthen the surface in some way rather than to change the basic damage mechanism, whatever it may be. It seems that the surface is able to sustain a larger deposition of energy before catastrophic breakdown occurs, but, when the surface does let go, it goes with a bigger bang.

The author wishes to acknowledge critical suggestions by V. Evtuhov, as well as the aid of H. L. Garvin, who performed the ion beam polishing, and K. T. Miller, who provided the x-ray topographs.

*Work supported by the Advanced Research Projects Agency under ARPA Order No. 1434 with Air Force Cambridge Research Laboratories.

¹L. D. Khazov, A. N. Shestov, and G. P. Tikhomirov, *Sov. Phys. Tech. Phys.* 13, 1112 (1969).

²J. E. Swain, *IEEE J. Quantum Electron.* QE-4, 362 (1968).

³J. Davit in *Damage in Laser Glass*, American Society for Testing and Materials Technical Publication No. 469, edited by A. Glass, A. Guenther, C. Stickely, and J. Myers (American Society for Testing and Materials, Philadelphia, Pa., 1969), p. 100.

⁴C. R. Giuliano and L. D. Hess in *Damage in Laser Materials*, Natl. Bur. Std. Special Publication No. 341, edited by A. J. Glass and A. H. Guenther (U.S. GPO, Washington, D.C., 1970), p. 76.

⁵I. M. Winer, *Appl. Opt.* 5, 1437 (1966).

⁶M. Bass and H. H. Barrett, *IEEE J. Quantum Electron.* QE-8, 338 (1972).

5. Comments on Fluctuations of Surface Damage Threshold Values

We commented in the preceding manuscript that we chose to interpret the large scatter in our threshold results as reflecting a real variation in damage resistance from spot-to-spot on the surface rather than reflecting an intrinsic damage probability. To support this point further, we will describe the experimental technique employed in obtaining the threshold values.

The site of interest on the sample surface is first irradiated with the laser at a level well below that believed necessary to cause damage, and then the sample is examined carefully for the presence of damage. If no damage is observed the power is increased (by 10 to 20%) and another shot is fired at the same spot. The sample is then reexamined and the process continues until damage is finally observed (or until, as in some cases of entrance damage, the maximum power available from our laser is reached). In a number of cases when the spot of interest was not damaged at a relatively high power (say twice the value for some of the lower thresholds observed for other sites), we held the power essentially constant and fired the laser for as many as fifteen times before continuing to increase the power further. Hence, a number of sites were subjected to up to 20 nondamaging shots whose peak powers lay in the range from 70 to 90% of the power at which damage was finally seen to occur. This type of behavior strongly supports the conclusion that a marked variation in damage resistance exists from spot-to-spot on the surface and that the surface cannot be considered to be uniform. The smaller degree of scatter for the abrasively polished samples suggests that the surface is more uniform (in this case, uniformly bad) than in the ion polished samples, in which the effects of mechanical damage due to the influence of the abrasive seem to have been removed in some spots but not in others.

D. BEAM PROFILE AND SPOT SIZE MEASUREMENTS

1. Summary of Early Work

In the early stages of this program the damage threshold power densities quoted were based on beam sizes calculated according to the following assumptions:

- The spatial beam profile at the laser output mirror is gaussian with a 1 mm radius (1/e radius for the electric field).
- The beam diffracts according to the well-known expressions for gaussian beam propagation.
- The beam suffers no distortion, focusing, or defocusing on passing through the ruby amplifier; hence, the diffraction-limited beam waist occurs at the location calculated according to the propagation equations.

During the period discussed in Semiannual Report 3, we looked more carefully into the validity of these assumptions; these results will be summarized in this report.

We undertook a series of measurements to determine the spatial beam profile at different locations and under a number of different conditions. Early experiments employed the measurement of a pair of spots with a known relative attenuation for both near and far-field spot sizes. As mentioned in the previous report, we obtained a near-field spot size of 1 mm (~15% accuracy) by photographing a pair of spots on a ground glass screen and also by measuring beam patterns on exposed Polaroid film with the relative energies of successive shots known. Far-field divergence measurements of the unamplified oscillator using the two spot technique gave a divergence of 0.3 ± 0.05 mrad (half-angle). These results are based on the assumption that the beam profile is gaussian.

For the more detailed studies, we attempted to determine how close to gaussian the beam profile actually is. To accomplish this we have used a multiple lens camera and the technique described by

Winer³. The setup is illustrated in Fig. I-8. We image a particular plane (plane A) onto a MgO block with the imaging lens choosing the object and image distances to get convenient magnification, and photograph the spot on the MgO block with the multiple lens camera. (This is accomplished by placing a pinhole of known size at plane A, imaging it on the MgO block with appropriate magnification, and photographing it.) The camera has nine lenses ($f = \sim 11$ cm, 12 mm diameter), each of which is backed by a different calibrated neutral density (N. D.) filter. Thus we obtain nine spots on the focal plane of the camera with known relative exposures.

The principle of the multiple lens camera technique for measuring intensity profiles is that the film response need not be known. Densitometer scans of the different spots are made, and the widths of the scans are measured at a constant density determined by the peak of the curve with the least transmission.

Beam profiles and spot sizes were photographed using the multiple exposure camera at different places and under different conditions of amplifier pumping. For example, we measured the beam size at the laser output resonant reflector, at the entrance and exit of the amplifier, at the focusing lens position, and at a number of locations beyond the focusing lens, including the focal plane.

The details and results of these measurements are presented in Semiannual Report 3. The following summarizes the highlights.

- Although the beam profile is very close to a gaussian distribution, the far-field divergence is substantially larger than that calculated for a gaussian beam (0.35 mrad half-angle compared with a calculated value of 0.20 mrad).
- The measured beam waist spot size is also substantially larger than that calculated using the gaussian mode propagation equations. The discrepancy between measured and calculated values depends on the focal length of the lens. Because of these two observations, it is clear that calculated spot sizes are suspect even for beams which are very close to gaussian.

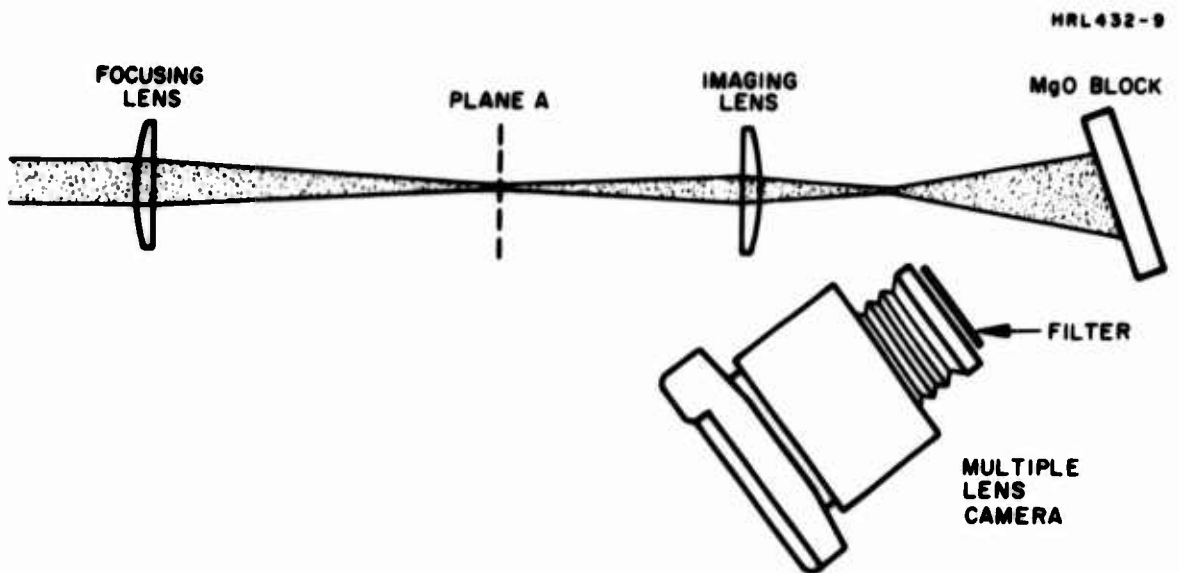


Fig. I-8. Schematic Representation of Setup Used in Beam Profile Measurements.

- The ruby amplifier acts as a negative lens whose focal length depends on optical pumping. As a result, the position of the beam focus varies as the amplifier pumping varies. After having discovered this fact, a particular set of pumping conditions were chosen, and all subsequent experiments were carried out with those conditions fixed.

2. Spot Size Measurements Inside Samples

In this section we discuss the results of experiments where we measured the spot size inside both ruby and sapphire samples by the same techniques as that described in Section I-D-1. The obvious extension of the previous spot size measurements in air would be to continuously monitor from shot-to-shot the beam width inside a sample while performing the damage experiments. In this way we would have a direct measure of energy density rather than having to infer it from previous measurements. All the experiments described here were carried out using the 19 cm lens focused inside the particular sample. The pumping conditions in the amplifier were fixed at 150 μ F and 7.5 kV, and the light intensity incident on the sample was varied by a pair of Glan-Kappa prisms, the first of which was rotated to the desired angle and the second of which was fixed so that the polarization was always the same inside the sample (\vec{E} perpendicular to the C-axis).

The lenses and samples were placed so that the waist of the focused light beam would occur about 2 cm inside the exit surface of the sample. The plane being imaged in the photographs lies 0.5 cm upstream from the beam waist.

A number of photographs taken with the multiple lens camera are shown in Figs. I-9 and I-10. The interesting result of this probing is that the beam profile begins to change radically in ruby at powers well below the damage threshold; whereas for sapphire, the beam profile is essentially smooth all the way to and beyond the threshold for bulk damage.

We wish to emphasize here that all the photographs were taken in the same plane in the sample, and the only parameter that was

M 7692



(a) 0.33 mJ

M 7691



(b) 3.0 mJ

M 7690



(c) 5.1 mJ

M 7684



(d) 10.5 mJ

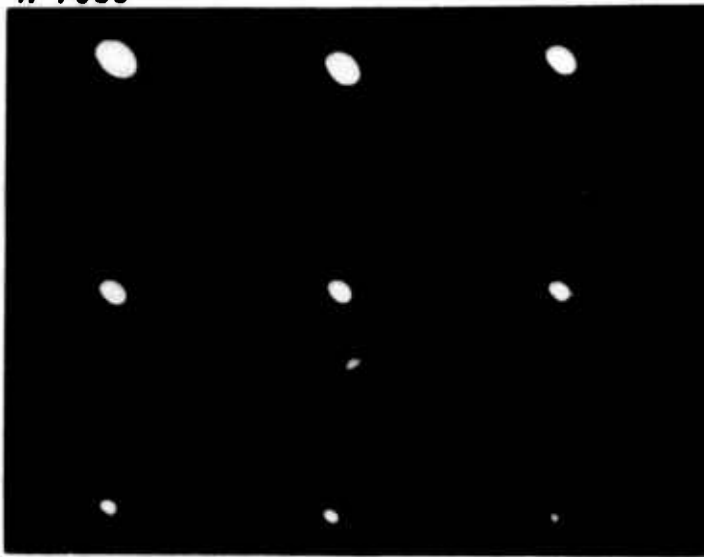
M 7685



(e) 10.8 mJ

Fig. I-9.
Multiple Lens Camera Photo-
graphs of Beam Profile Inside
Ruby Sample for Different
Incident Energies and Arbitrary
Relative Exposures.
(Constant amplifier pumping -
150 μ F, 7.5 kV.)

M 7688



(a) 0.3 mJ

M 7687



(b) 25 mJ

Fig. 1-10.
Multiple Lens Camera Photographs of Beam
Profile Inside Sapphire Sample for Dif-
ferent Incident Energies and Arbitrary
Relative Exposures.

varied was the amount of energy incident on the 19 cm focusing lens. We see from Fig. I-9(a) that at low incident energy (0.33 mJ) the beam profile is smooth, but that by the time we reach 3 mJ (Fig. I-9(b)) we begin to see what appears to be a bright central spot with a less bright peripheral halo. (In these experiments, the laser pulse width was about 30 nsec, FWHM.) At higher incident energies we see a variety of patterns in the beam profile. We note also that the threshold for internal damage in this particular sample measured under the same conditions is 30 mJ incident on the focusing lens, and that the threshold for exit surface damage is about 10 mJ. Thus we see these effects of beam distortion well below the threshold for any catastrophic phenomena.*

The whole question of measurement of energy density inside ruby samples by measuring spot sizes assumes a completely different aspect in the light of these drastic changes in the beam profile. Obviously, it would be extremely difficult to determine energy densities in these peculiar spatial distributions.

When we examine sapphire under the same conditions as those described for ruby, we see no such behavior. Figure I-10 shows photographs taken under two extreme conditions. Figure I-10(a) was taken at low incident energy (~ 0.3 mJ) and Fig. I-10(b) at an energy higher than the bulk damage threshold, which was 20 mJ for this sample. For a large number of shots over this range of energies we saw no irregularities in the beam profile. After reaching threshold for internal damage, we saw a general decrease in light reaching the imaging optics presumably because of scattering from the damage sites and increased beam spreading due to self-focusing.

Again we see an interesting difference in the behavior of ruby as compared with sapphire when subjected to intensive illumination at 6943 \AA . It is reasonable to suspect that the beam distortion seen in ruby arises from its absorption at 6943 \AA .

* We do not have sufficient data to locate the threshold for this beam distortion effect. We only know it lies between 0.3 and 3 mJ for the conditions described above.

Because the obvious difference between sapphire and ruby at 6943 Å is the optical absorption, we decided to look at the beam profile inside pumped ruby samples to see whether the same distortion is seen under these circumstances. We chose an incident power level where the distortion is pronounced in an unpumped sample and optically pumped the sample at different levels. The results were inconclusive, because while the beam profile definitely changed with optical pumping, there was no marked improvement or lessening of the distortion that could be directly attributed to the pumping. At the time these experiments were carried out, we were having difficulty with oscillator and amplifier alignment fluctuations, which also gave rise to distinct beam profile irregularities. It was not possible at the time to separate effects arising from a possible misalignment variation from shot-to-shot. This lack of reproducibility of results from shot-to-shot and from day-to-day made it impossible to reach any definitive conclusion concerning the effects of optical pumping on the beam distortion in ruby. At this time the question still remains unanswered.

3. Ring Structure in the Focused Single Mode Laser Beam Beyond Beam Waist

Our plans to examine in more detail the beam distortion effect in optically pumped ruby samples were preceded by preliminary experiments in which the ruby sample was absent from the beam. During these experiments we obtained an unexpected result which diverted us from our original objective and which we pursued further to understand its origin. We will describe the results of these observations in this section.

We wish to point out that these phenomena were observed with only the light from the laser. No other elements are placed in the beam between the oscillator output mirror and the lenses except for beam splitters and polarizer attenuators; the removal of these does not change what was observed. Also, the presence or absence of the amplifier does not affect what is observed.

The essential result of the observations is shown in Fig. I-11, in which we see the following features. The beam profile is smooth and approximately gaussian in the back focal plane of the lens and also at the beam waist.

At a point somewhat beyond the beam minimum, the beam begins to show a marked deviation from a smooth profile. This first shows up as a bright spot in the center of the beam. A short distance farther down we encounter a minimum on-axis with a bright ring around it. As we progress farther downstream we see more rings developing in the beam profile.

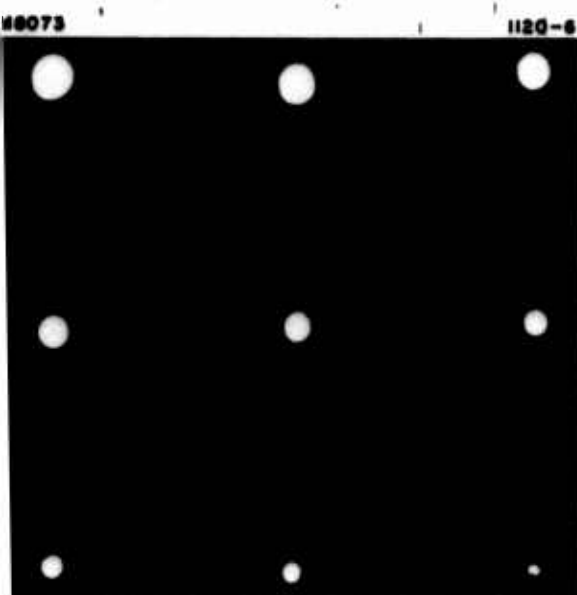
At first we suspected that these peculiar beam profiles might be an artifact of some sort, and attempted to examine more closely the conditions under which they are observed (i. e., we wanted to determine if the phenomenon was real).

We found that the same kind of behavior was observed for different focusing lenses and different imaging lenses, showing that our observation was not a peculiarity of a particular lens. The pattern of rings, etc., is reminiscent of what might be expected if spherical aberration were present. To check whether the phenomenon was a property of the lenses or the ruby laser itself, we passed the light from the He-Ne alignment laser through the same setup. A number of regions along the beam were imaged onto the MgO block and photographed. We saw no evidence of rings or other irregularities over the entire range of positions on both sides of the beam focus. This led us to conclude that what we observed was a property of the ruby laser itself and not of the lenses.

Further evidence supporting the contention that the structure is a property, at least in part, of the ruby laser itself and not an artifact of the system of observation is as follows.

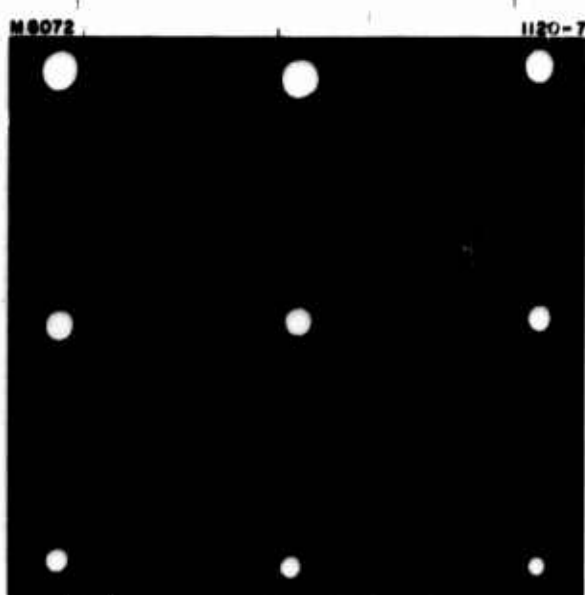
- The structure is observed with different focusing and imaging lenses.
- The structure is not simply a propagation phenomenon.

To verify the latter point, we imaged the same plane with lenses of different focal length. Therefore the distance between focusing and



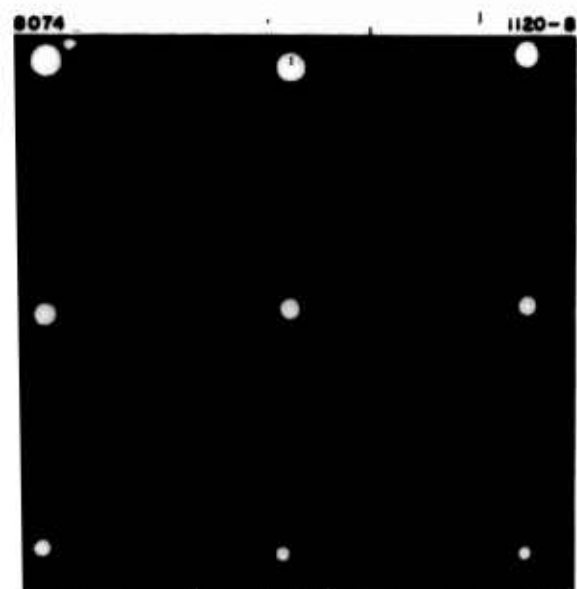
29.0 cm

(a)



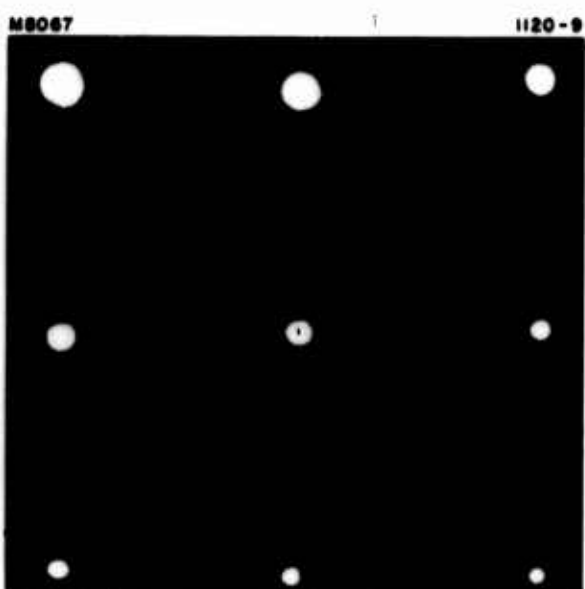
30.0 cm

(b)



31.0 cm

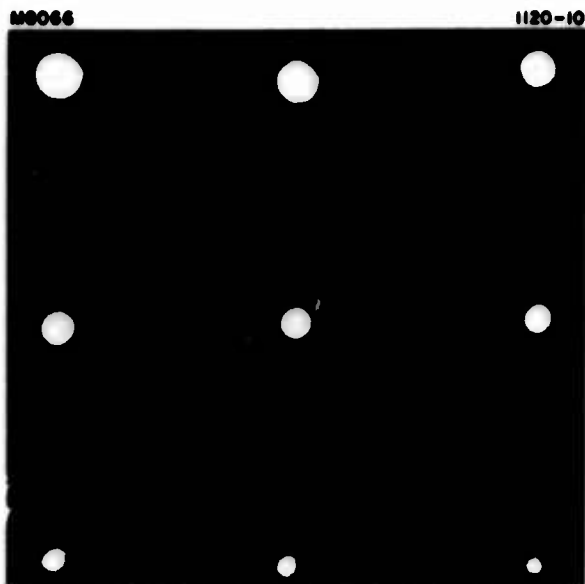
(c)



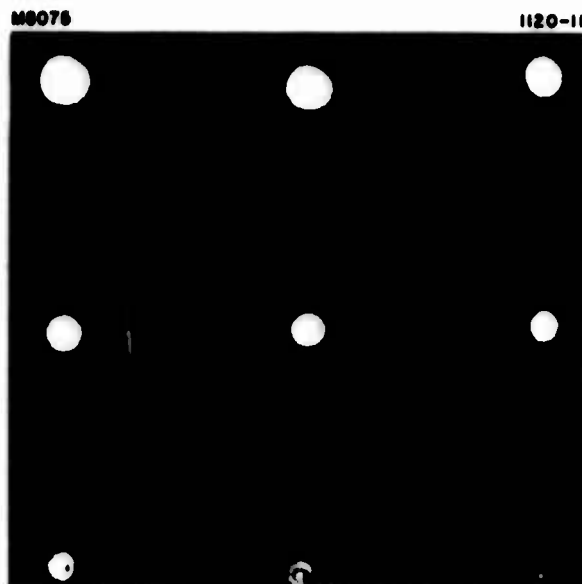
32.0 cm

(d)

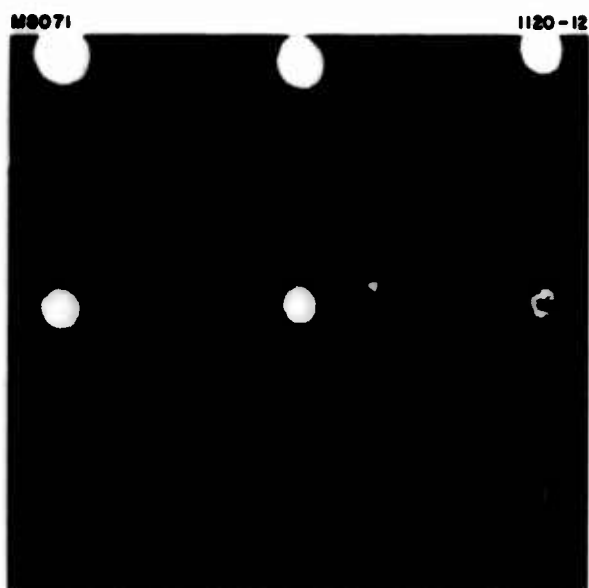
Fig. I-11. Beam profile at different distances from 30.5 cm lens. Beam waist is at approximately 31.5 cm.



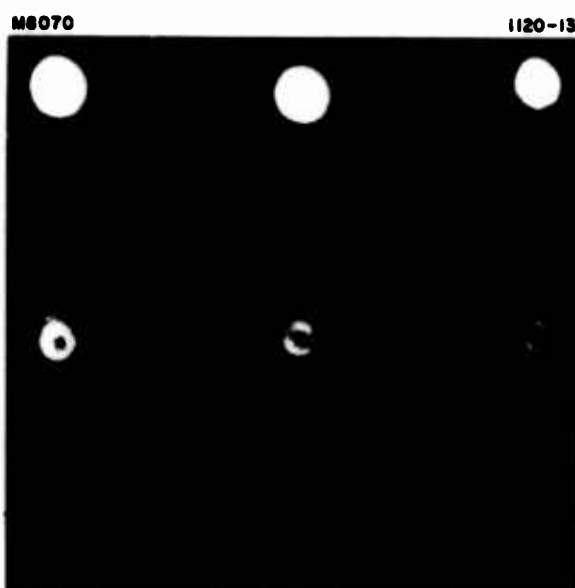
33.0 cm
(e)



33.5 cm
(f)



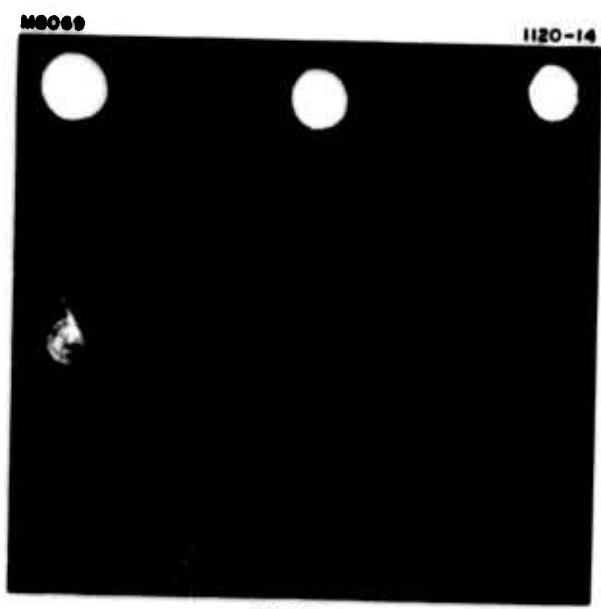
34.0 cm
(g)



34.5 cm
(h)

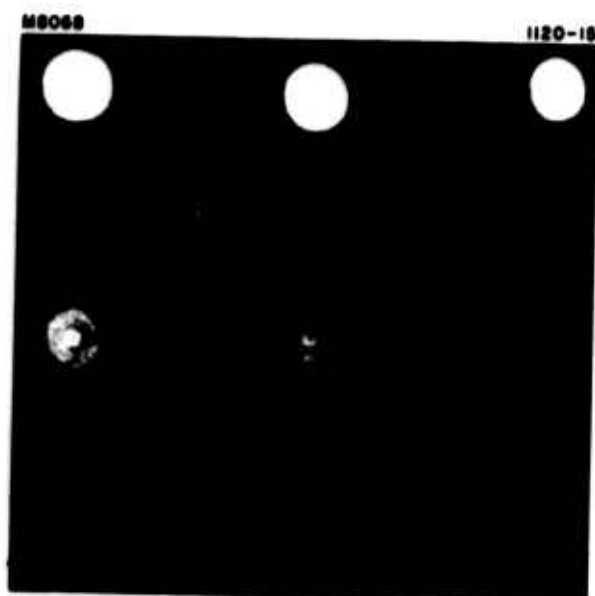
Reproduced from
best available copy.

Fig. I-11. (Cont'd).



35.0 cm

(i)



35.5 cm

(j)

Fig. I-11. (Cont'd).

imaging lenses is different in each case. The pattern observed is the same in the two experiments, indicating that the imaging lenses are indeed imaging information from the plane of interest. Another similar experiment was performed in which the distance between the two lenses was kept constant and the MgO block was moved to different positions. Here we were imaging different object planes at different magnifications. Patterns characteristic of the planes of interest when viewed at the same magnification were observed. The pattern changed when the MgO block was moved from one position to the other, and the corresponding change was the same as if the new plane was imaged by moving the imaging lens rather than moving the MgO block alone and keeping the lens-to-lens distance fixed.

With this result and others discussed in Semiannual Report 4, we were convinced that the phenomenon is real and a property of the ruby laser or perhaps a combined property of the laser and the lenses. We took a few beam profile pictures of the laser output with no lenses in the beam at a number of distances from the laser from 2 to 55 m; no evidence of ring structure in the beam profile was seen.

The behavior described above is reminiscent of the description given by Innes and Bloom⁴ who discuss beam profiles for focused gaussian beams for different amounts of truncation and spherical aberration. However, the effects they predict become significant only for large spherical aberration ($\lambda/2$) and relatively severe truncation of the gaussian beam. Of course, we have no assurance that the phase fronts of our beam are uniform at the output mirror of the oscillator. Nonuniform phase across the beam could certainly give rise to irregularities in the beam profile such as that observed. It is interesting to note that this behavior could well be a general characteristic of all single mode, solid state lasers. Further pursuit of this phenomenon would certainly be valuable but is probably outside the realm of the present program.

We have recently become aware of a similar observation by workers⁵ at the University of Southern California who observed fluctuations in the on-axis intensity of a focused ruby laser beam at points

downstream from the beam waist. They also pointed out that computer solutions for focused truncated gaussian beams showed that such fluctuations are to be expected and result from the truncation. Since the phenomenon occurs much closer to the beam waist for short focal length lenses than for long focal length lenses, it is important that the precise location of the beam waist be known for experiments where the beam is focused on a surface, because small fluctuations in sample-to-lens distance could give rise to a large variation in beam properties and damage thresholds.

E. EXPERIMENTAL APPARATUS USED IN DAMAGE THRESHOLD STUDIES

The early stages of the experimental phase of this program were devoted to improving and refining the performance of the laser source used in the program. The setup showing the laser, amplifier and other experimental apparatus is shown in Fig. 1-12. The single longitudinal and transverse mode oscillator employs a 4 in. long by 1/4 in. diameter ruby pumped by two linear lamps in a double elliptical pump cavity. The ruby crystal is water cooled by a closed cycle refrigeration system maintained at 0°C. The high reflectivity mirror is coated with a 99+% reflectivity high field damage coating from Perkin Elmer Corporation. The original Q-switch, a rotating Brewster angle prism, was replaced by a solution of cryptocyanine in methanol in a 1 mm path length cell whose transmission is ~30% at 6943 Å. The 2 mm diameter aperture allows oscillation in the TEM₀₀ mode.

The temperature controlled (34°C) resonant reflector that was designed to optimize longitudinal mode control consists of two quartz etalons and a quartz spacer whose combined effect is to enhance cavity modes separated by 2 cm⁻¹ and to discriminate against intermediate modes.

Portions of the laser beam are split off in various ways (see Fig. 1-12), so that the power output, near and far-field patterns, and Fabry-Perot patterns can be monitored for each shot. This is accomplished in the following way. Light reflecting from wedged beamsplitter

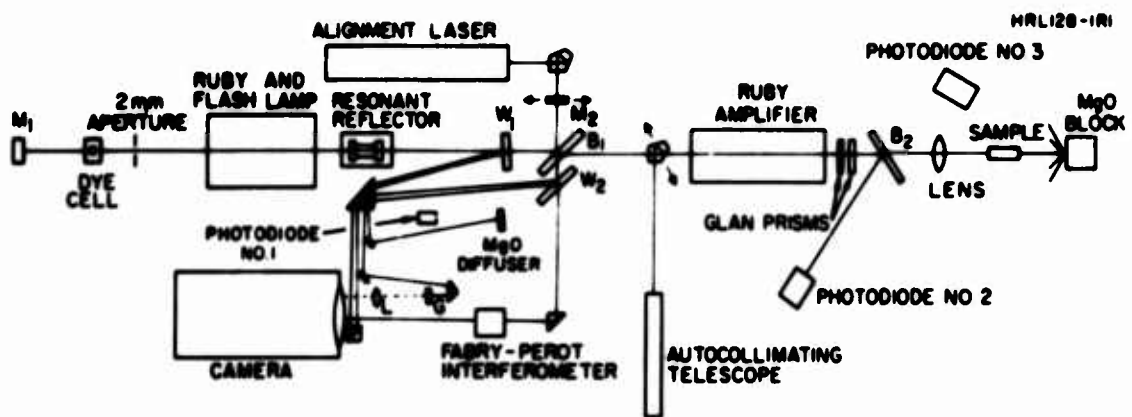


Fig. I-12. Schematic Representation of Experimental Apparatus.

W_1 gives two diverging beams; one of them hits the magnesium oxide diffuser, where the scattered light is monitored by a biplanar photodiode used as our power monitor. The second beam from W_1 hits ground glass screen G , where it is photographed through lens L and the 1 m focal length camera focused at infinity. This gives a magnified ($\sim 5\times$) near-field picture. Another portion of the light is removed by beam-splitter B_1 and hits mirror M_2 , which can be placed in or out of position depending on the use of the alignment laser. From M_2 the light either goes to the Fabry-Perot interferometer or can be partially reflected from wedged beamsplitter W_2 , where it results in a pair of far-field patterns. A 0.6 neutral density filter is placed near the focal plane of the camera so that the far-field pattern and the Fabry-Perot pattern can be seen at two different exposures. The two Glan prisms are used as a variable attenuator after the amplifier. Beamsplitter B_2 samples the light to photodiode No. 2, which monitors the power incident upon the focusing lens which was designed for minimum spherical aberration (Special Optics). The signal from the detector is integrated and displayed on an oscilloscope.

The water cooled amplifier ruby is 6 in. long by 0.5 in. diameter, with one end wedged relative to the other by about 0.5° . The input end of the amplifier rod is antireflection coated to minimize the chances of oscillation within the amplifier itself. The ruby rod is closely coupled to a helical flashlamp, which is pumped with a power supply capable of delivering 8 kJ in a 3 msec pulse. The power supply employs a pulse shaping network of 20 sections, each section pumping for 150 μ sec. The maximum gain obtained with the amplifier is about 10 dB.

Figure I-13 shows an example of what we see with our monitoring camera, and Fig. I-14 shows a time trace of the laser output taken with photodiode No. 1 and displayed on the Tektronix 519 oscilloscope. Figure I-14(a) shows the smooth temporal shape seen over 95% of the time, while Fig. I-14(b) is an extreme example of multimode oscillation. In this case two modes are oscillating with a frequency separation of 750 MHz. This frequency corresponds to the spacing between the end of the ruby and the resonant reflector. The overlapping spectral ranges

HRL 265-7

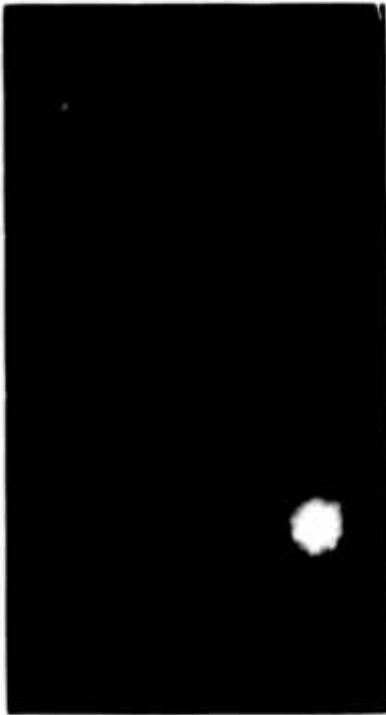


Fig. I-13.
Typical Photo Monitoring Fabry-Perot Interferogram, Near-Field and Far Field Beam Patterns. The Difference in Optical Density Between the Two Halves of the Picture is N.D. 0.6. The Free Spectral Range of the Interferometer is 1.6 cm^{-1} .

Reproduced from
best available copy.

HRL 265-5

(a)



(b)



Fig. I-14. Tektronix 519 Oscilloscope Traces of Laser Output with 20 nsec/Division Sweep Rate. (a) Smooth Pulse Observed $\sim 95\%$ of the Time. (b) Modulated Pulse ($\sim 750 \text{ MHz}$).

of the Fabry-Perot interferometer and the 519 oscilloscope insure that the oscillation of anything other than a single longitudinal mode will be detected.

The characteristics of the laser are summarized in Table I-3.

TABLE I-3
Characteristics of Ruby Laser

Energy Output ^a	12 to 15 mJ ($\pm 15\%$)
Pulse Length	~ 20 nsec
Peak Power	0.6 - 0.8 MW
Beam Radius (1/e for E field)	1 mm ($\pm 10\%$)
Beam Divergence	0.6 ± 0.1 mrad (full-angle)
Calculated Beam Divergence	0.44 mrad (full-angle)
^a Our energy monitor was checked against three different "calibrated" detectors; the error quoted ($\pm 15\%$) reflects the disagreement of the standards.	

T627

A typical set of experiments involves setting up the sample relative to the focusing lens for either surface or bulk damage. The location of the beam in the sample is determined by the use of a He-Ne laser which is colinear with the ruby laser. The sample is mounted in such a way that it can be translated either vertically or horizontally in a known way. After damage is observed in a given location the sample is translated usually 0.5 mm to a new site. During the experiments the sample is examined for damage between shots using a traveling microscope mounted on the optical bench. In this way the sample is not disturbed in relation to the laser beam, and a given spot can be illuminated many times if desired. The amplifier lamp is always

pumped with a constant voltage monitored with a digital voltmeter and the energy incident on the sample is varied by rotating the first of a pair of polarizing prisms. For each shot of the laser, we monitor the temporal profile, the total energy incident on the sample, near-field and far-field profiles, and Fabry-Perot spectrum. Hence, any deviation from the desired conditions is noted and the data handled accordingly.

SECTION II

THEORETICAL STUDIES: OPTICAL DAMAGE

The results of our theoretical studies of optical damage during the period of this project are summarized in this section. In line with the experimental study breakdown of Section I, this review will be divided into a discussion of bulk damage and surface damage.

A. BULK DAMAGE

1. Breakdown Mechanisms

At the time this project began, the existing theories of optical breakdown in ideal crystals all hypothesized the creation by the high optical electrical fields of enough hot electrons (of ionizing energy) to create an ionizing avalanche. (For a review of these theories, see Appendix A, reproduced here from the second semiannual report.) In the first semiannual report of this project, it was shown (using the same Frölich model for a conduction electron in a polar lattice from which other theories had started) that the average kinetic energy of such an electron would not be significantly above kT (the lattice temperature times Boltzmann's constant) in the optical fields at which breakdown was believed to occur. However, as was stated there: "A possible complication that we will study further is that a very few electrons might be created in the high energy wings of the electron distribution."

In our fourth semiannual report, the equations were developed which determine the electron energy distribution and, after several simplifying assumptions, it proved possible to cast them in a form that might be solved on a computer. However, we have not expended the considerable effort that would be required to do this; efforts to see by analytical methods whether a high energy tail would be predicted in the electron distribution have not proved fruitful.

Recently, speculation has been rekindled by Bass and Barrett about the plausibility of the existence of such a high energy tail in connection with their experimental results on surface damage.⁶ They call this tail "lucky electrons" as they have undergone just the right kinds of collisions at the right phase in the optical field to be continuously accelerated by it. However, in order to appreciate the kind of theoretical effort required to make even a semiquantitative estimate of the electron velocity distribution, we refer the reader to Appendix B of this report which reviews our development of truncated, but still complicated, equations for the electron distribution from the Frölich model that is universally used in these problems.

In conclusion, we are certain that potentially damaging amounts of heat ($\sim 10^2$ J/cm³) will be transmitted from the optical beam to the lattice by cold electrons at optical intensities around 10^{10} to 10^{11} W/cm² if the light has created at least 10^{16} photoelectrons/cm³. This was demonstrated in Semiannual Report 2 and reproduced in Appendix A here (and reported at the Second Annual Symposium on Laser Damage, Boulder, Colorado, June 1970). Whether other damaging processes occur first is not clear. However, it is now known that sapphire resists bulk damage until self-focusing produces high enough intensities to produce any of a number of nonlinear effects.

Semiannual Report 4 documented the first conclusive experimental evidence that self-focusing had actually been occurring whenever bulk damage was produced in ruby or sapphire. These results are reviewed in Section I-B of this report. Whenever self-focusing sets the threshold for damage, it is less interesting to know the actual mechanism of rupture than the mechanism and threshold for self-focusing. Consequently, after the first demonstration by this project that bulk optical damage in sapphire and ruby always follows self-focusing for pulses in the 10 to 20 nsec region, we have sought and found correlations between the tendency of a material to self-focus and its other material properties. In this report we hypothesize and give arguments that the tendency of crystals to self-focus increases with their ordinary Raman scattering strength, provided the pulses are

short enough to freeze out electrostriction. This rule is in contradiction to an anharmonic oscillator model, which scales the nonlinear refractive indices to the linear, and which in some instances predicts tendencies for self-focusing opposite to those predicted by the Raman effect. We have also considered the use of optical beams of elliptical cross-section in order to prevent self-focusing. The experimental results obtained in this project which show the reduced self-focusing tendencies of elliptical beams and the reason for this effect are discussed in Section I-B. However the detailed behavior of elliptical beam propagation at high optical powers is not understood completely, and it is possible that objectionable beam distortions may occur even if self-focusing is prevented. Some hope for reducing optical damage and distortion thresholds in bulk lies in finding and employing crystals with a smaller nonlinear refractive index; our findings on this are reviewed here. We have also continued the efforts begun in previous years to understand the actual mechanisms of crystal breakdown and destruction. The most important of these mechanisms are linear and nonlinear heating and electron avalanche ionization. Because surface damage seems to be initiated by these mechanisms rather than by self-focusing, these latter studies are probably more pertinent to the surface damage problem and therefore will be discussed in Section II-B on surface breakdown.

2. Mechanisms Governing Self-Focusing

From our own self-focusing measurements in ruby and sapphire, it is now evident that sapphire has a nonlinear refractive index n_2 (in the absence of electrostriction) that is an order of magnitude smaller than that of laser glasses. It also appears that this index is significantly smaller still in YAG laser crystals. One cannot understand this trend by the philosophy of the well-known "Miller's rule," which predicts that the material with the higher linear refractive index will have the higher nonlinear refractive index n_2 insofar as the latter arises from the nonlinear polarizability of the electronic orbits. The nonlinear index

for self-focusing of linearly polarized light is defined in terms of the power dependent change δn in the refractive index by

$$\delta n = n_2 E^2, \quad (\text{II-1})$$

where E is the rms electric field. A rudimentary model of anharmonically bound electrons predicts that n_2 scales like

$$n_2 \propto (n^2 - 1)^3. \quad (\text{II-2})$$

The linear indices of laser glass, ruby, and YAG are about 1.53, 1.76, and 1.82, respectively from which eq. (II-2) would predict n_2 (glass): n_2 (sapphire): n_2 (YAG) $\sim 2.4: 9: 12$. It does not matter that (II-2) is crude; any anharmonic model would predict that n_2 increases with n , the opposite of what is observed. This suggests that the fast self-focusing indices are not entirely due to nonlinear electronic distortions, but also to nuclear nonlinearities, i. e., the field-induced alterations in local nuclear arrangements which give a lowering of the crystal-field energy via the linear electronic response about the altered nuclear positions. This nuclear contribution to n_2 is much slower responding in time to field amplitude changes than are electronic nonlinearities, but much faster responding than electrostrictive changes that arise from a macroscopic density change. The nuclear response time is of the order of an inverse nuclear vibration frequency, typically $10^{-12} - 10^{-13}$ sec. Therefore, even picosecond pulses would experience self-focusing from this nuclear mechanism; it is presently difficult to distinguish nuclear from electronic nonlinearities by time dependence.

If nuclear motions are mainly responsible for n_2 in laser crystals, then one might roughly and arbitrarily guess how n_2 scales by replacing n^2 , the electronic dielectric constant, by $\epsilon_0 - n^2$, the nuclear contribution to the dc dielectric constant in (II-2). The values of ϵ_0 for laser glass, ruby, and YAG are about 6, 10, and 12,

respectively; the relation (II-2) thus revised would predict n_2 (glass) : n_2 (sapphire) : n_2 (YAG) $\sim 1 : 5 : 10$, in even worse disagreement with experiment. As an alternative hypothesis, with much more physical basis, we propose here that the size of n_2 is proportional to the tendency of the crystal to scatter (low intensity) light, at least insofar as electronic nonlinearities can be neglected. We have demonstrated that such a relation is true within the linear dipole approximation (LDA) for isotropic materials (glasses and fluids),⁷ i.e.,

$$n_2 \text{ (nuclear)} = \frac{\pi \lambda^4 S}{n \kappa T}, \quad (\text{II-3})$$

where S is the total scattering cross-section per unit solid angle per unit volume of material to scatter plane polarized light into parallel polarized light at 90° , $\lambda = \omega_0/c$, κ is Boltzmann's constant, and T the absolute temperature. If Brillouin scattering is included in S , then n_2 includes the contribution of electrostriction as well as the nuclear redistribution; if the Brillouin scattering contribution to S is omitted, then (II-3) gives the fast nuclear contribution only. We have recently shown that (II-3) is also true under more general assumptions than the LDA.

Unfortunately, a comparison of the inelastic light scattering strengths S for laser glasses, sapphire, and YAG are not yet available. However, it appears that most glasses have a broad Raman band from 50 to 500 cm^{-1} shift that is about as intense as that of liquids like benzene which exhibit large Rayleigh wing scattering.⁸ It is also known that Raman scattering intensities are not correlated with the refractive indices or dielectric constants of materials; our hypothesis is not unreasonable on physical grounds.

If (II-3) is valid for predicting self-focusing in crystals, then crystals like the alkali halides, which have no allowed first-order Raman scattering, and hence a small scattering cross-section S , should have uncommonly high thresholds for self-focusing of short pulses. Measurements on alkali halides to test this hypothesis

are currently underway at other laboratories. As part of this project, we have estimated n_2 for the alkali halide crystals, using eq. (15a) of Ref. 7 for S in (II-3) above and the known ionic polarizabilities, masses, and restrahl frequencies. In this model the change $\delta n_{//}$ in refractive index results essentially from the field-induced change in the local field factor at an ion due to the slight statistical anisotropy induced in the neighborhood of the ion by the lattice-field interactions. The results of these calculations for some typical alkali-halide crystals are given in Table II-1 along with a recently measured estimate of n_2 for fused quartz for comparison. Here the nuclear contributions to n_2 are so small that one suspects that the electronic contribution must dominate.

TABLE II-1

Calculated Nuclear Contribution to the Fast Nonlinear Index n_2 for Optical Self-Focusing of Certain Alkali Halide Crystals.^a

Material	n_2 (esu) $\times 10^{17}$
RbI	20
KI	10
KCl	6
LiF	0.4
NaCl	0.3
Fused SiO ₂	10,000 ^b
^a No electrostriction or electronic hyperpolarizability effects are included. Total fast index for fused quartz is given for comparison. ^b From Ref. 9.	

T637

Whether the nuclear contribution dominates n_2 or not in any given material can be determined directly by comparing the Kerr effect and the intensity dependent change in polarization in the material.⁹ Attempts to do this in glass, sapphire, and YAG are currently in progress elsewhere. We feel that with the knowledge gained in such studies, there is a real possibility of finding materials for which bulk damage thresholds for short laser pulses are much higher, and non-linear optical distortions of the beam are much smaller, than in existing laser glass and sapphire.

B. SURFACE DAMAGE

Damage by an unfocused optical pulse in sapphire, as in most materials, appears first at its surfaces and at about the same flux local optical field densities for the entrance as for the exit surfaces. Our investigations described in Section I-C show that, for a given pulse length, the damage threshold of sapphire is reached when the peak power per unit area exceeds a certain value at the surface, and the threshold does not depend on the characteristics of the beam inside the crystal. Mainly from these facts, we have narrowed the possible mechanisms for the surface damage to three types. In order of descending likelihood, these are (1) heating by normal linear absorption in a surface layer, (2) heating from nonlinear absorption by photoexcited electrons in a surface layer, and (3) electron avalanche ionization of the surface material. We discuss what each of these mechanisms predicts and various experimental ways of verifying or discounting them below.

1. Heating from Linear Absorption

Suppose a thin uniform surface layer of thickness l and absorption coefficient α is irradiated by an optical pulse of $U \text{ J/cm}^2$ energy

density. If the pulse length τ is less than $\ell +$ (the velocity of sound), then the temperature rise ΔT in the layer is

$$\Delta T \sim \alpha \frac{U}{C_V} \quad (\text{II-4})$$

where C_V is the average specific heat ($\text{J cm}^{-3} \text{ }^\circ\text{K}^{-1}$) at constant volume in the given temperature range. For sapphire at room temperature, $C_V \sim 3$ and a potentially damaging surface temperature rise of $10^3 \text{ }^\circ\text{K}$ would result at $U \sim 30 \text{ J cm}^{-2}$ (a typical observed threshold value for $\tau \sim 10^{-8}$ sec) if the layer absorption coefficient satisfied

$$\alpha > 100 \text{ cm}^{-1}. \quad (\text{II-5})$$

For a layer thickness $\ell \sim 10^{-6}$ cm, a fractional linear absorption of only 10^{-4} at a surface could therefore be strongly suspected to give rise to surface damage at typically observed thresholds.

Layers of such fractional absorptivities $F \sim 10^{-3}$ to 10^{-5} may well exist on even the most carefully prepared surfaces. Suppose, for example, that a certain surface density N/cm^2 of absorbing centers (e. g., dangling bonds, oxygen impurities, etc.) having optical absorption cross-sections $\sim 10^{-18} \text{ cm}^2$ were present in a surface layer. Then only 10^{13} to 10^{15} such impurities per cm^2 would give rise to dangerous absorption, a not unreasonable number.

This mechanism can be distinguished from the other two leading candidates by the dependence of the threshold power density on the pulse time τ for a carefully controlled single mode beam. This study is difficult and has not yet been done. Therefore, we have considered various methods for detecting and measuring the α and ℓ of a surface layer nondestructively. The most promising methods seem to be the following.

a. Calorimetry

For a thin sample of material (≤ 1 mm), more of the optical power would be absorbed in the surface layer than in bulk, if surface absorption is important in surface damage. The surface absorption in this case could be measured by monitoring the temperature rise (after thermal equilibration) produced in such a thin sample by a laser pulse. For a fractional surface absorption $F \sim 10^{-4}$, a temperature rise of $1/300^\circ\text{C}$ would be produced by each J/cm^2 incident over a sapphire slab 0.1 mm thick. Thermal decay times could be made such that, for example, a 1 W cw Nd:YAG laser might easily deposit $1000 \text{ J}/\text{cm}^2$ during a thermal decay time and produce a measureable temperature rise that would then give the fractional absorption $F = \alpha \ell$ for the surface layers.

b. Measurement of a Dielectric Reflection and/or Transmission Anomaly

It is a straightforward matter to derive the fractions of power reflected R_ℓ and transmitted T_ℓ from a plane wave incident, through a lossless medium (of dielectric constant $\epsilon = n^2$), upon a uniform absorbing layer of complex dielectric constant ϵ_ℓ and thickness ℓ , that is followed by a lossless semi-infinite crystal medium having a real dielectric constant ϵ_c . The results show, for example, that for normal incidence on a thin layer, the power reflectivity R_ℓ will deviate from the reflectivity R_o for the case of no absorbing layer by a fraction

$$D_\ell = \frac{(R_\ell - R_o)}{R_o} = -4 \left(\frac{\omega \ell}{nc} \right) \left(1 - \frac{\epsilon_c}{\epsilon} \right)^{-1} \text{Im } \epsilon_\ell + O(\ell^2), \quad (\text{II-6})$$

where ω is the optical (angular) frequency. The fraction F_ℓ of the incident beam absorbed in the layer is (for $D_\ell \ll 1$)

$$F_\ell = D_\ell \frac{1 - \epsilon_c/\epsilon}{1 + \epsilon_c/\epsilon} \quad (\text{II-7})$$

and is seen to be of order $1/2 D_l$ for sapphire. It is difficult, though possible, to see a deviation in reflectivity from nominal D_l of the order of a percent. Therefore, reflectivity measurements are a feasible way to measure layer absorptions of the order of a percent or greater. (The fractional change in transmission is generally much smaller and more difficult to interpret because it must involve two surfaces.)

c. Reflection at Nominal Index Matching

One might vary the index of the incident medium (by placing the crystal in a liquid of variable composition) in contact with the surface of the crystal. As the nominal reflection passed through zero ($\epsilon = \epsilon_c$), the actual residual reflection due to the layer would be (at $\theta = 0$)

$$\frac{1}{4} \left(\frac{\omega l}{nc} \right)^2 \left| \epsilon_l - \epsilon \right|^2 \quad (\text{II-8})$$

which is roughly the square of the fraction absorbed. Though small, this reflection might be measurable from a layer absorbing as little as 10^{-2} to 10^{-3} (depending on complications from birefringence) because there is no normal background reflection.

d. Residual Reflection at Brewster's Angle

Rather than vary the incident medium index, one could observe and plot the reflection versus angle of incidence and polarization near Brewster's angle to discern the small residual reflection, which again would be of the order the square of the fraction absorbed in the beam. Therefore, fractional layer absorptions less than 10^{-2} could be observed by this method.

Reflection measurements, unlike calorimetric measurements, offer the possibility of determining the layer thickness as well as absorption. Comparing reflectivities at enough different angles and polarizations would determine each of $\text{Re } \epsilon_l$, $\text{Im } \epsilon_l$, and l . The fact that an absorbing layer might not be uniform with depth, or laterally,

would complicate the interpretation, though reasonable estimates of an effective F and ℓ could still be made for a given angle of incidence.

e. Measurement of Reflectivity Change Due to Predamage Heating of Surface Layer

If a layer is being damaged by linear-absorption heating, then a very short lived but large temperature rise must take place in the surface layer at pulse-energy levels just below that required for damage. This large temperature rise should cause a large change in the complex optical index, in and near the layer, that should produce a marked change in reflectivity, calculable for example at normal incidence by (II-6). Perhaps easier to observe would be the heating by a polarized pulse, incident upon the surface at Brewster's angle. The light pulse itself should show an increase in reflection and scattering during its latter phase, as Brewster's angle will have changed with the heat-altered dielectric constant. This increase could be correlated with the layer absorption, and it would be at least as sensitive an indicator of a surface layer as the previous detection methods.

f. Interferometric Measurement of Heating: Induced Change in Surface Refractive Index

The increase in phase of a wave after it has traveled a distance z into a medium is (in the WKB approximation) $\int_0^z \omega n'(z') dz' / c$, where n' is the real part of the refractive index. The change $\delta n'$ in n' could well be of order unity in a layer that is heated to just below damage. An interferometric measurement of this phase shift (by Michelson, Mach-Zender, holographic, or other such interferometric technique) would probably allow detection of a hundredth of a wavelength fringe shift, which would occur if the absorbing layer were roughly a hundredth of a wavelength thick or of the order of 60 \AA .

g. Measurement of Layer Heating by Polarization Change of Reflected or Transmitted Light

If a beam of arbitrary elliptical polarization is incident at an arbitrary angle on a surface, upon which is a layer whose index has been changed by optical heating, then the reflected and transmitted

beams will experience a change in their polarizations. Polarization analyzers, which detect only the polarization orthogonal to that reflected from the preheated surface, would sense the changed index of refraction against a very low background. Straightforward calculation would reveal the incident polarization and angle that would give the largest effect for a given material. The polarization measurement would be sensitive to heat-induced changes in the birefringence of the material as well as to the changes in absolute index. The sensitivity of this method would depend critically on the degree to which the polarization analyzer can be made to reject the nominal reflected polarization.

h. Measurement of Optical Heating of Layer Through Change in Surface Resistance

The electrical resistivity of any small volume element at or near the surface of an insulator will decrease roughly as $A \exp (T_0/T)$ with increasing absolute temperature T . (For bulk sapphire $T_0 \sim 5 \times 10^4$ K and $A \sim 10^{7.5} \Omega \cdot \text{cm}$). If any observable resistance change could be induced by a beam falling between two closely spaced electrodes on a surface, one could correlate its initial value with (the absorbed fraction) \times (layer thickness affected). Uncertainties in space charge, contact resistance, and surface conductivity dependence on temperature would weaken the correlation. The time dependence of the resistance after a short optical heating pulse would shed much light on these uncertainties and on whether the nonlinear absorption of the type discussed next was present.

2. Heating from Nonlinear Absorption

The mechanism we have proposed in this project as responsible for bulk damage (see Appendix A and Ref. 10) is also likely to be operative at surfaces. This mechanism is the nonlinear absorption of the optical beam by electrons excited to the conduction band by the beam itself through various single or multistep excitation processes. (We refer to this mechanism as APE – absorption from photo electrons.) This absorption is expected to increase rapidly with beam power

density P by a relation that depends on the nature of the photoexcitation process. It must increase at least as rapidly as P ; we have argued that it ought to increase according to an avalanche type equation, once the photoelectron density is high enough.¹⁰

Shallow electron states may abound near material surfaces, and electron-lattice scattering is greater near a surface, both effects tending to make the absorption coefficient α from this process much greater near a surface than in bulk. We have calculated that for a free carrier density around 10^{17} cm^{-3} , α would be at least 10^{-1} cm^{-1} in a perfect sapphire crystal; it is therefore conceivably orders of magnitude greater at an irradiated surface.

To establish the existence of this mechanism independently of damage, one could measure the surface photoconductivity of a sample irradiated by a laser pulse so short that no space or electrode charges would have time to build up during the conductivity pulse. (Ordinary giant pulses would perform this function well.) Recombination times are expected to be much less than a nanosecond; therefore, this conductivity pulse would end with the optical pulse, unlike the thermal change in conductivity mentioned in the preceding subsection.

The dependence of damage threshold on pulse length would distinguish this effect from linear heating. In the nanosecond pulse region at least, APE would tend to have a power density threshold, whereas heating effects would cause an energy density threshold. The first published, and rather tentative, evidence on pulse length variation of ruby surface damage favors the latter.¹¹

3. Electron Avalanche Ionization

From their studies of optically induced surface damage of various crystals, Bass and Barrett have proposed that an ionizing electronavalanche is the responsible mechanism.⁶ We had previously argued in this project that their coupling to the optical phonons would cool conduction electrons too fast to allow any of them to achieve energies much above the ambient lattice temperature. We attempted to

verify this by examining the equations that govern the fraction of electrons that would have enough energy to ionize a lattice site in bulk, but did not pursue the extensive computer program that we found would have been required to solve them (see Semiannual Report 4 of this contract, July 1971 and Appendix B of this report); no other investigators have accomplished more. The surface problem is further complicated by lack of reliable physical parameters.

Like the APE mechanism, this effect would tend to have a constant power density threshold. Ionizing electrons, if they existed, might be detected as high energy photoelectrons ejected from the surface into a surrounding vacuum.

SECTION III

SUMMATION OF EXPERIMENTAL AND THEORETICAL STUDIES

The work carried out during this program has led to a number of fruitful results. Although the emphasis has been placed on damage in ruby and sapphire at 6943 Å, many of the phenomena studied are generally applicable to all transparent material for visible and infrared radiation. The highlights of our findings are summarized in the following.

- We have demonstrated the extreme importance of using a well-controlled and well-characterized laser source for performing studies of this type.
- The initiating mechanism for bulk damage in inclusion-free sapphire and ruby is self-focusing. Good semi-quantitative agreement has been obtained between our experimental results and the theory for a moving self-focused spot.
- We have shown experimentally and theoretically that the self-focusing threshold power is a function of beam shape, elliptical beams having a higher threshold than circular beams. A solution to the problem of self-focusing damage is suggested by proper choice of beam shape.
- Spatial and temporal studies have shown that the surface plasmas are a result of rather than a cause of surface damage. At power levels well above threshold, however, the surface damage morphology can be influenced by interaction with the plasma.
- The threshold for surface damage of sapphire can be considerably enhanced when the surfaces are polished with ion beams. Marked changes in both surface smoothness and crystallinity take place on ion polishing. It is not yet known to what extent these changes are responsible for the improvement in damage thresholds.
- We have developed a new model for the optical breakdown of a material based on estimates of the relative likelihood of many nonlinear photoelectron processes in polar crystals.

- A theoretical framework has been established for the study of the momentum distribution of conduction electrons in a polar lattice being driven by a strong optical field. Although we have not expended the considerable computational effort to obtain numerical estimates of numbers of high energy electrons, we have been able to show that many ad hoc hypotheses that have been put forward are without theoretical basis.
- We have developed models of the mechanisms responsible for the self-focusing that triggers bulk damage. We have found evidence that electronic hyperpolarizability is not the dominant mechanism in laser glass, sapphire, and YAG but probably is in the alkali halides. We have pointed out ways of establishing the mechanisms by standard, nondamaging, optical measurements.
- We have studied the three types of mechanisms most likely to be central in surface damage: heating by linear surface absorption, heating by photoelectron absorption, and avalanche ionization. We have isolated eight methods which we show can achieve nondamaging measurements of surface absorption and distinguish among the mechanisms.

SECTION IV

RECOMMENDATIONS FOR FUTURE WORK

As is typical in research programs of this type, more questions are raised during the course of the involvement than are answered. Because of the scope of the work, certain areas were pursued more actively than others. Also, termination of such programs occurs for a number of practical reasons according to a predetermined time interval and not necessarily when the pertinent questions have been satisfactorily answered. As a result, we will discuss briefly a number of areas which deserve further attention. Some of these have been pursued fairly actively on the present program and should be pursued further for additional clarification. Others are interesting areas, which were uncovered during the course of this work, but for which there were neither sufficient capacity nor immediate justification to pursue in detail.

The following pertinent comments, not necessarily in order of importance, evolved from our investigations and observations during the course of this program and are based on the results of these studies.

- Work of the type carried out on this program should be extended to other materials and wavelengths (as is being done already to some extent) with initial emphasis on whether the damage is intrinsic or extrinsic.
- Self-focusing experiments of the type explored in this program with the streak camera studies should be continued in more depth for both sapphire and ruby and for other laser materials as well. Pertinent results for pulses of different duration and for different focusing conditions will allow appropriate modification of the present theory to account for the relative contributions

of slow and fast response mechanisms to the nonlinear index of refraction.

- More experimental data should be taken on self-focusing with beams of noncircular spatial distributions, especially with elliptical beams. A comparison of the results with theory in more detail than was possible in this work is essential in determining the applicability of this phenomenon to avoiding self-focusing in high power lasers and amplifiers. Along this same line, experimental and theoretical work should be pursued in the area of optical resonators with elliptical modes of oscillation.
- Intrinsic breakdown thresholds in the absence of self-focusing should be studied for a variety of optical materials. (A good method for doing this type of experiment is described in Section I-B-8.) This type of measurement will yield information about the limiting size of self-foci as well as further insight into the nature of the ultimate breakdown mechanisms.
- A number of the differences between damage properties of ruby compared with sapphire pointed out in this report are suspected to arise from ruby's absorption at 6943\AA and possibly because the laser and sample are at different temperatures. Detailed exploration into the nature of the above differences should be carried out in order to clarify them.
- Further studies are needed in the area of surface preparation techniques such as ion beam polishing or related methods to surface damage resistance, not only in the materials studied on this program

but in laser materials in general. The reasons for threshold enhancement should be understood so that proper direction can be given for future work.

- As implied in the above comment, all the available surface diagnostic techniques should be brought to bear, where applicable, to studying the effects of various surface treatments.
- The question to be answered as far as surface damage is concerned is: How do surface finish, crystallinity, and material purity (e.g., presence of surface states) affect the surface damage threshold of a given material and what are the mechanisms?
- Some of the techniques outlined in Section II for measuring surface light absorption should be pursued in future work. This type of data will not only yield information as to the purity of the material but also will give some clues to the pertinent damage mechanisms.
- The equation derived in Appendix B on the theory of electron velocity distribution in a crystal irradiated by a strong optical beam should be solved numerically. Although considerable effort and computer time will be involved in accomplishing this, the results promise to be quite pertinent for exploring the contribution of avalanche breakdown to optical damage.

SECTION V

PRESENTATIONS AND PUBLICATIONS

HRL work on this program has resulted in a number of presentations and publications which are listed here.

A. PRESENTATIONS

- "Damage Threshold Studies in Ruby and Sapphire"
C. R. Giuliano and L. D. Hess, presented at the ASTM-NBS Symposium on Damage in Laser Materials, Boulder, Colorado, June 1970.
- "Role of Photo-Electrons in Optical Damage"
R. W. Hellwarth, presented at the ASTM-NBS Symposium on Damage in Laser Materials, Boulder, Colorado, June 1970.
- "Optical Damage in Polar Crystals"
R. W. Hellwarth, presented at the Gordon Conference on Nonlinear Optics, Issaquah, Washington, August 1970.
- "Damage Threshold Studies in Laser Crystals"
C. R. Giuliano, L. D. Hess, and E. S. Bliss, presented at the Sixth International Quantum Electronics Conference, Kyoto, Japan, September 1970.
- "Optical Damage"
R. W. Hellwarth, presented at the Physics Colloquium of the Clarendon Laboratory, Oxford, November 1970.
- "Time Evolution of Damage Tracks in Sapphire and Ruby"
C. R. Giuliano, presented at the ASTM-NBS Symposium on Damage in Laser Materials, Boulder, Colorado, May 1971.

- **"Self-Focusing of Gaussian-Elliptic Light Beams"**
C. R. Giuliano, J. H. Marburger, and A. Yariv,
presented at the Seventh International Quantum
Electronics Conference, Montreal, Canada,
May 1972.
- **"The Relation between Surface Damage and Surface
Plasmas"**
C. R. Giuliano, presented at the ASTM-NBS
Symposium on Damage in Laser Materials,
Boulder, Colorado, June 1972 (to be published
in the Proceedings).
- **"Ion Beam Polishing as a Means of Increasing Surface
Damage Thresholds in Sapphire"**
C. R. Giuliano, presented at the ASTM-NBS
Symposium on Damage in Laser Materials,
Boulder, Colorado, June 1972 (to be published
in the Proceedings).
- **"Fundamental Absorption Mechanisms in High-Power
Laser Window Materials"**
R. W. Hellwarth, presented at the ASTM-NBS
Symposium on Damage in Laser Materials,
Boulder, Colorado, June 1972 (to be published
in the Proceedings.)
- **"Laser-Induced Damage in Optical Materials"**
C. R. Giuliano, presented at the Gordon Confer-
ence on Nonlinear Optical Effects, Beaver Dam,
Wisconsin, July 1972.

B. PUBLICATIONS

- **"Damage Threshold Studies in Ruby and Sapphire"**
C. R. Giuliano and L. D. Hess, National Bureau
of Standards Special Publication 341, U.S. GPO,
Washington, D.C. (Dec. 1970) p. 76 (ed. by
A. J. Glass and A. H. Guenther).
- **"Role of Photo-Electrons in Optical Damage"**
R. W. Hellwarth, National Bureau of Standards
Special Publication 341, U.S. GPO, Washington,
D.C. (Dec. 1970) p. 67 (ed. by A. J. Glass and
A. H. Geunther).

- "Time Evolution of Damage Tracks in Sapphire and Ruby"
C.R. Giuliano, National Bureau of Standards Special Publication 356, U.S.GPO, Washington, D.C. (Nov. 1971) p.44 (ed. by A.J. Glass and A.H. Geunther).
- "Observations of Moving Self-Foci in Sapphire"
C.R. Giuliano and J.H. Marburger, Phys. Rev. Letters 27, 905 (1971).
- "Laser-Induced Damage in Transparent Dielectrics: Ion Beam Polishing as a Means of Increasing Surface Damage Thresholds"
C.R. Giuliano, Appl. Phys. Letters 21, 39 (1972).
- "Enhancement of Self-Focusing Threshold in Sapphire with Elliptical Beams"
C.R. Giuliano, J.H. Marburger, and A. Yariv, Appl. Phys. Letters 21, 58 (1972).
- "Laser-Induced Damage in Transparent Dielectrics: The Relationship between Surface Damage and Surface Plasmas"
C.R. Giuliano, to be published in IEEE-J. Quantum Electronics 8, 749 (1972).

REFERENCES

1. C. R. Giuliano and J. H. Marburger, "Observations of Moving Self-Foci in Sapphire," *Phys. Rev. Letters* 27, 905 (1971).
2. C. R. Giuliano and L. D. Hess, "Damage Threshold Studies in Ruby and Sapphire" (ed. by A. J. Glass and A. H. Geunther) National Bureau of Standards Special Publication 341, U. S. GPO, Washington, D. C. (Dec. 1970) p. 76.
3. I. M. Winer, *Applied Optics* 5, 1437 (1966).
4. D. J. Innes and A. L. Bloom, *Spectra Physics Laser Technical Bulletin No. 5*, Spectra Physics, Inc. (1966).
5. B. Newnam, private communication.
6. M. Bass and H. Barrett, *J. Quantum Electronics* 8, 338 (1972).
7. R. W. Hellwarth, *J. Chem. Phys.* 52, 2128 (1970).
8. S. P. S. Porto, private communication.
9. A. Owyong, R. W. Hellwarth, and N. George, *Phys. Rev.* B5, 628 (1972).
10. R. W. Hellwarth, "Damage in Laser Materials" (ed. by A. J. Glass and A. H. Geunther National Bureau of Standards Special Publication 341 (December 1970); HRL Semiannual Technical Report 2, AFCRL-70-0437 (July 1970).
11. Y. Danileiko, A. Manenkov, A. Prokhorov, and V. Y. Khaimov-Malkov, *Sov. Phys. -JETP* 31, 18 (1970).

APPENDIX A

Role of Photo-Electrons in Optical Damage¹

R. W. Hellwarth

Department of Electrical Engineering
University of Southern California
Los Angeles, California 90007
and
Hughes Research Laboratories
Malibu, California 90265

Previous workers have discussed the possibility that electrons photo-excited into the conduction band of a polar crystal by a high-intensity, short optical pulse may gain enough energy to damage the lattice by initiating an ionizing avalanche. We discuss here other processes by which these conduction electrons may damage the lattice even before they gain enough energy to ionize their surroundings, specializing our calculations to the case of sapphire and ruby. First, we show that the energy that the conduction electrons absorb linearly from the optical beam is deposited almost immediately in the lattice without significant heating of the electrons. At electron densities ($\sim 10^{16} \text{ cm}^{-3}$) and optical intensities ($\sim 10^{10} \text{ W/cm}^2$) likely to exist at sapphire damage thresholds, this deposited energy is found to be of the order of what one might expect would be required to form a rupturing shock wave. We also show that the photo-excitation of both bound and unbound impurity levels is enhanced by the presence of conduction electrons, so markedly so for the former that the promotion of electrons into the conduction band may be significantly "bootstrapped," thereby increasing the optical absorption. The presence of conduction electrons and excited impurities in the expected numbers is likely to alter the refractive index significantly and affect thereby the focusing (self- or external) of the beam in a complicated way. For the simplest model these nonlinear index contributions would tend to produce repeated focal regions along the beam. Implications of these results for raising damage thresholds are discussed.

Key words: Crystals, electrons, optical damage, photo-absorption, photo-conductivity, photo-electrons, polar crystals, ruby, sapphire, self-focusing.

1. Introduction

The physical processes responsible for the bulk damage caused in various transparent crystals by short optical pulses (causing negligible electrostriction) have not yet all been identified. Here we argue that several processes not considered previously are likely to be important in the optical damage of inclusion-free polar crystals, especially sapphire and ruby. For their initiation, these processes would all seem to require on the order of 10^{16} conduction electrons per cc to be present at the point of maximum optical intensity, a number widely suspected to be present in sapphire and ruby at peak intensities $\sim 10^{10} \text{ W/cm}^2$ just below damage threshold. We will argue here that such densities of cold electrons can a) transfer damaging amounts of heat from the beam to the lattice; b) accelerate the rates of photo-excitation of bound and free impurity electron states, thus significantly increasing the supply of conduction electrons, possibly even in "avalanche"; and c) significantly change the local refractive index, possibly in a way which, in conjunction with the normal nonlinear index, could cause repeated beam focusing along its axis. In none of these processes do the electrons become hot enough ($\sim 8 \text{ eV}$) to ionize the lattice, in contradistinction to the process suggested by previous workers [1-4]².

¹Work supported in part by the Joint Services Electronics Program (U. S. Army, Navy, and Air Force), under Grant No. AF-AFOSR-69-1622A, and in part by the Advanced Research Projects Agency through Air Force Cambridge Research Laboratories.

²Figures in brackets indicate the literature references at the end of this paper.

Hence, we will refer to them as "cold" conduction electrons. How the damage processes discussed here depend on crystal temperature, optical wavelength and pulse duration is a complex function of the energies and wavefunctions of the states of the impurities supplying and trapping conduction electrons, the electrons' effective mass(es), the longitudinal optical (LO) phonon structure, and the electron-phonon coupling. Although only the latter two are fairly well known for ruby and sapphire, plausible hypotheses about the former lead one to single out the processes we propose as potentially important to damage. It would appear that reducing donor concentrations or increasing their electron binding energies might produce more damage-resistant crystals. However, if the conduction electron density were proportional to optical intensity (which appears not to be the case at such high intensities), it would tend to reduce self-focusing (or produce a net defocusing) and thereby lower damage thresholds. Other conclusions and suggested experimental checks of electron processes are mentioned in the final Section. In the following Section 2 we summarize the parameters and physical regimes we encounter in ruby and sapphire and we outline our rough criteria for when damage is expected. In Section 3 we define the approach we take for evaluating the required parameters and discuss difficulties with previous calculations of the conditions under which hot ionizing electrons might be produced. The calculations of the enhancement by conduction electrons of lattice heating and photo-excitation follow in Sections 4 and 5. Before proceeding, we first summarize our assessment of often-conflicting reports on photoconductivity in ruby and sapphire.

Hochuli [5] has measured the low-frequency photoconductivity at various wavelengths and temperatures of ruby and sapphire at optical intensities $I \sim 0.2$ to 5 W/cm^2 and using applied voltages at frequencies zero Hz, 100 Hz, and 9.39 GHz. He found no essential differences in results for the two crystals. The observed conductivities (at 5 W/cm^2) were 4×10^{-13} , 10^{-11} , and $4.2 \times 10^{-8} (\Omega\text{cm})^{-1}$, respectively, at the above frequencies. Since all these frequencies are well below the electron collision frequency (which from the theory of Section 4 we estimate to be $\sim 10^{14}$ rps), the wide variations in results indicate the magnitude of experimental pitfalls in any attempt to measure such low bulk conductivities. Anomalies at the two lower frequencies probably arise from surface effects, from the inability of electric contacts to inject charges into the crystal, and from space charge buildup. Therefore, the 9.39 GHz value, obtained in a microwave cavity with a small electron drift excursion amplitude (of the order of an Angstrom), is probably the most reliable. This conductivity was linear in the optical intensity within the range of observations. Its wavelength dependence suggested that the electrons were supplied from donor levels between 0.6 and 1.2 eV below the conduction band, in agreement with what one would conclude by studying the normal bulk conductivity variation with temperature at higher temperatures. The wavelength dependence also suggested more donor levels appearing around 3 eV. Although Hochuli was able to observe a Hall voltage, it did not vary when the light was turned on or off. The nominal Hall mobility value $\mu = 0.052 \text{ cm}^2/\text{V sec}$, derived therefrom has nevertheless been used without question by other workers whenever a value was required in calculations. This value corresponds to a collision time τ of 4×10^{-17} sec., or an electron mean path of the order 10^{-10} cm, and must be considered unphysical, corroborating the difficulty of making electrodes on sapphire. Using the standard Frohlich theory of a conduction electron in a polar crystal adapted to the large coupling constant of sapphire [6], one estimates τ (at room temperature) to be between $10^{-14.4}$ and $10^{-13.4}$ sec, depending on where the effective band mass lies between $1/10$ and 10 electron masses. Assuming a free electron mass for which $\tau = 7 \times 10^{-15}$ sec (and $\mu = 12 \text{ cm}^2/\text{V sec}$), one would infer from Hochuli's microwave observations that he produced $\sim 2 \times 10^8$ photo-electrons per cc with 5 W/cm^2 of broadband Hg lamp exciting intensity. We see from this that 10^{16} electrons per cc would very likely be excited near damage thresholds of 10^{10} W/cm^2 provided that 10^{16} donor levels per cc were occupied, a provision which is unknown.

Except possibly for the experiments of Belikova, *et al.* [7,8], other reported observations of photoconductivity in ruby appear to be plagued by surface and contact effects. Belikova, *et al.*, observed the photoconductivity to be highly nonlinear with the (6943 Å) optical intensity I for intensities near 10^{10} W/cm^2 [7]. One can use our value of τ above with their data to estimate very crudely (since their beam geometry was unspecified) that they were observing well over 10^{16} electrons/cc at 10^{10} W/cm^2 (provided that the electron recombination time was short compared with the optical pulse length). Belikova, *et al.*, also observed optical emission bands near 2, 2.7, and 3 eV (they could not see below 2 eV) which are suggestive of some impurity level transitions. The foregoing is about all one can conclude about photo-electrons from existing data for ruby and sapphire.

2. Description of Electron Interactions

In studying the role of photo-excited electrons in crystal damage, we will constantly apply our formulae to the case of sapphire and ruby. The phonon structure of these two crystals are essentially identical, as are the low-intensity photoconductivities. Although distinct differences in damage behavior have been observed, the gross damage thresholds are statistically indistinguishable for sapphire and ruby. Therefore, most pertinent aspects of these two crystals can be studied together. For brevity, we shall refer hereafter only to sapphire, but shall intend our remarks to apply also to ruby unless stated otherwise. We shall also assume throughout that the optical beam wavelength is 6943 Å, that of the room temperature ruby laser.

A free electron gas of density 10^{16} cm^{-3} has a plasma frequency $\omega_p \sim 6 \times 10^{12} \text{ rps}$ that is much lower than a) the optical beam frequency of interest ν ($2.71 \times 10^{15} \text{ rps}$), b) the phonon frequencies ω_k ($\sim 10^{14} \text{ rps}$), and c) typical electronic excitation frequencies ($\sim 10^{16} \text{ rps}$).

We shall call a conduction electron "cold" when its energy is much less than interband energies and its wavelength is much longer than the scale of potential variations of the field lattice. Other electrons we will refer to as "hot." The time for cold electrons in the 1/40 to 3 volt range to equilibrate among each other by collisions at a density 10^{16} cm^{-3} is of the order of 10^{-10} to 10^{-13} sec [9], much longer than the inverse electron-lattice collision time ($\sim 10^{-14} \text{ sec}$ in ruby). Therefore, at least before any large ionizing avalanche occurs, the cold conduction electrons may be studied as independent particles, not interacting among themselves but interacting only with the fields and other particles in the crystal.

When a cold electron moves in a polar crystal such as ruby or sapphire, it is often called a "polaron." Its interactions with the crystal phonons are known to be well-described at room temperature and above by the Hamiltonian derived by Frohlich [10] and used by all previous workers in calculating electron motions leading to damage:

$$H_F = h_0 + v_F \quad (1)$$

where

$$h_0 = \frac{1}{2} [p - A(t)]^2 + \sum_k \omega_k a_k^\dagger a_k \quad (2a)$$

and

$$v_F = \sum_k C_k a_k e^{ik \cdot x} + \text{h. c.} \quad (2b)$$

Here p is the electron's momentum, and x the electron's position coordinates, a_k is the annihilation operation for a LO phonon of frequency ω_k . Optical wavelengths are long enough so that the vector potential $A(t)$ may be taken as a function of time only oscillating at a frequency ν . We use dimensionless "polaron" units in which the effective band mass of the electron m_b is unity as is Planck's constant \hbar . All energies are measured in units of an effective LO phonon energy $\hbar\omega_0$ (840 cm^{-1} or 1200° K for sapphire and ruby). Frequencies are measured in units of ω_0 ($= 1.6 \times 10^{14} \text{ rps}$) so that $\nu = 17$ for a 6943 \AA beam in sapphire. Lengths are measured in units of $(\hbar/m_b \omega_0)^{1/2}$ which is $8.5 \times 10^{-8} \text{ cm}$ for ruby if we take m_b to be the free electron mass m_0 . Frohlich showed that in these units the coupling coefficients C_k are well approximated by $V^{-1/2} \alpha_k^{1/2} k^{-1}$ where V is the crystal volume, α is the dimensionless polaron coupling constant $(\epsilon^{-1} - \epsilon_0^{-1}) (\text{Ryd}'/\hbar\omega_0)^{1/2}$. Here Ryd' is the Rydberg for an electron with mass m_0 , and ϵ and ϵ_0 are the optical and static dielectric constants (3.1 and 10). For $m_b = m_0$, $\alpha \sim 3$ for ruby. In ruby an electron is hot if k is of order 10 or more (in polaron units). Hot conduction electrons have neither the simple forms of kinetic energy or lattice interaction energies found in eq (1) but obey complex equations in which exchange must be accounted for and which have never satisfactorily been approximated in usable form for a dynamic lattice. There would seem to be no way at present to make a reliable estimate of how strong an optical field would be required to produce enough interband electronic transitions (i. e., lattice ionization) to cause damage.

From the discussion of the previous section, it is evident that the electrons photo-excited (below damage thresholds) in ruby and sapphire crystals come from donor impurities to which they are bound initially with much less energy than the valence-conduction band gap energy ($\sim 8 \text{ eV}$). The effects of these impurities on the supply and motions of conduction electrons, as well as on the excitation of the donors by conduction electrons, can be studied by considering the Coulomb interactions v_t between a conduction electron at x and the i th particle of the a th impurity having charge eq_i^a and located at x_i^a .

$$v_t = e^2 \epsilon_s^{-1} \sum_{i,a} q_i^a / |x - x_i^a| \quad (3)$$

where the electronic charge e is 4 in our polaron units, and is screened by the dielectric constant ϵ_s appropriate to the frequencies of motions under consideration.

To deal with the elastic scattering of the electrons, one needs only the matrix element of eq (3) diagonal in the impurity's ground state. This gives an effective classical scattering potential seen by the conduction electron. To study inelastic scattering, we will assume that the impurities may be described by an unperturbed Hamiltonian $h_i = \sum_a h_{ia}$ with "ionized" or unbound as well as bound electronic eigenstates. Calculations will therefore start from a total Hamiltonian H comprised of

Frohlich's Hamiltonian eq (1) (which describes cold electrons, phonons, and their interactions) plus the electron impurity interactions of eq (3) and with h_i determining impurity states:

$$H = h_0 + h_i + v_F + v_t. \quad (4)$$

We will assume that damage to the crystal occurs when the interactions v_F and v_t combined cause the conduction electrons to absorb an energy U per cubic centimeter with a short optical pulse that exceeds a threshold value U_0 . That is, we shall strive to determine at what optical beam intensity we may expect

$$U \geq U_0. \quad (5)$$

Present evidence indicates that U_0 is of order 10^2 to 10^3 J/cm³ for ruby and sapphire for 20 nsec pulses in a beam of order one mm diameter. A shock wave of this energy surrounding the beam would develop stresses on the order of the static yield stress [3]. Obviously a large part of understanding optical damage in crystals entails developing an accurate theory of the amount of energy deposition required to produce rupturing strains as a function of the amount and spatial and temporal distribution of this deposition. However, we shall content ourselves here with the above crude estimate for U_0 .

3. Approaches to the Calculation of Damage Thresholds

Previous treatments of the role of electrons in damage [1, 4] started from Frohlich's Hamiltonian eq (1) and sought to calculate the optical intensity at which electrons would gain enough energy u to excite an avalanche of interband transitions. The expected energy u of an electron in the optical field was estimated from the equation

$$\frac{du}{dt} = R_{fe} - R_{el} \quad (6)$$

where R_{fe} is the average rate at which the optical field does work on the electron and R_{el} is the average rate at which the excited electron "radiates" phonons, i. e., transfers its energy to the lattice. Previous treatments have all taken for R_{fe} the usual linear conductivity loss per electron with reasonable order of magnitude estimates from eq (1) for the optical conductivity (or "electron collision rate"). However, they have made approximations for, or statements about, R_{el} that are not directly based on a quantum average of the appropriate operator. Wasserman [1] took for R_{el} the rate at which an electron having a Maxwellian distribution would lose energy to a cooler lattice in the absence of the optical field ($A = 0$). He predicted breakdown intensities orders of magnitude above those actually observed. Sverev, et al. [4], used for R_{el} the approximate rate at which an electron would lose energy to the lattice starting from a momentum eigenstate $|p\rangle$ for which $\frac{1}{2}p^2 = u$ also in the absence of the optical field. His predicted thresholds also exceeded observed thresholds by over two orders of magnitude. We feel it is quite probable that a precise evaluation of the spectral energy distribution of an electron obeying eq (1) would show that the electrons do in fact remain too cool to ionize impurities or the lattice at optical fields below damage thresholds. In the next section we show that, indeed, collisions with phonons dominate an electron's motion. We have checked that it follows rigorously from eq (1) that, to lowest order in the optical intensity and coupling parameter α , an electron's expected kinetic energy is simply the sum of its coherently oscillating energy plus $3kT/2$ where T is the ambient lattice temperature. The coherent energy is very much smaller than kT for optical intensities of interest. Therefore, we now proceed to examine whether cold electrons may not mediate the deposition of damaging amounts of energy in a sapphire lattice.

As we mentioned in the previous section, our approach will be to calculate the beam intensity at which the energy U deposited per unit volume in the lattice from the optical field via the electrons exceeds a threshold value U_0 . If the maximum optical beam energy per unit area is S , then

$$U = \kappa_\nu S \quad (7)$$

where κ_ν is the absorption per unit length of an optical beam of frequency ν . Following FHIP [6], we write the quantum expectation value of the amplitude of an electron's coordinate at frequency ν as $\text{Re } E e^{i\nu t} / (-\nu^2 + \chi_\nu)$ when the electron is in an optical electric field $\text{Re } E e^{i\nu t}$. With this definition we have

$$\kappa_v \lambda = (\omega_p^2 / c) \text{Im}[v^2 - \chi_v]^{-1} \quad (8)$$

where λ is the wavelength of the light in the crystal $\div 2\pi$ and ω_p is the electron plasma frequency (in units of ω_0). In cgs units $\omega_p^2 = 4\pi n e^2 / m_b$ with n being the number density of electrons.

The evaluation of κ_v falls naturally into two parts: first, the determination of the rate at which a single conduction electron takes energy from the field (and delivers it to the lattice) by a calculation of χ_v , and second, the estimation of the number density n of these electrons. We consider these two questions, respectively, in the following two sections.

4. Optical Response of Single Electron

We examine first an electron's optical response in the case that it is affected only by electron-phonon interactions as described by Frohlich's Hamiltonian eq (1) with coupling parameters appropriate to sapphire. We then find that, at least at room temperatures and above, collisions with impurities are relatively less important. When the electron response is linear in the applied field for a given lattice temperature, we may use the determination of χ_v by FHIP who calculated the quantum expected value of the electron position to first order in the optical field. Their expression is exact for all temperatures at small coupling ($a < 1$) and gives an accurate solution even when $a \sim 3$ as for ruby. In this case it shows that, for $\gamma = 17$, both the real and imaginary parts of χ_v are much less than v^2 so that we need only calculate $\text{Im}\chi_v$ to estimate the absorption constant. (The $\text{Re}\chi_v$ can of course be determined from $\text{Im}\chi_v$ by Kramers-Kronig relations.)

$$\text{Im}\chi_v = \frac{2\pi^{-\frac{1}{2}} \beta^{3/2} \sinh(\beta v/2)}{3 \sinh(\beta/2)} \left(\frac{v}{w}\right)^3 \int_0^\infty \frac{\cos(vu) \cos u \, du}{[u^2 + a^2 - b \cos(vu)]^{3/2}} \quad (9)$$

Here v and w are parameters to be chosen from a variational principle. $a^2 \equiv \beta^2/4 + R\beta \coth(\beta v/2)$; $R \equiv (v^2 - w^2) / (w^2 v)$; and $b \equiv R\beta \sinh(\beta v/2)$.

In the weak coupling limit $v = w = 3$, $R = b = 0$ and $a = \beta/2$. Then the integral can be evaluated exactly in terms of modified Bessel functions. At temperatures much lower than the Debye temperature (β large) this result reduces to

$$\text{Im}\chi_v \rightarrow 2a(v - 1)^{3/2}/3 : a < 1, \beta \gg 1, v > 1. \quad (10)$$

For $a = 3$ and $\gamma = 17$, this is 8. The leading correction to eq (10) for finite temperatures multiplies it by $(1 + \beta^{-1})$, increasing it by 30% at room temperature ($\beta = 3.3$).

When $a = 3$, the variational principle gives $v = 3.4$ and $w = 2.55$ in the zero temperature limit [6]. Using these parameters with $\beta = 3.3$ gives $R = 0.229$, $a = 1.866$ and $b = 5.53 \times 10^{-3}$. We have evaluated eq (9) numerically for these parameters and have obtained $\text{Im}\chi_v = 15$. We have also evaluated eq (9) at frequencies in the neighborhood of $v = 17$ and found that, as in eq (8), $\text{Im}\chi_v$ varies slowly with v . Therefore, electron transients associated with the rise and fall of even picosecond optical pulses are very small, and it is a good approximation in practice to assume that at any instant the electron's motion is the same as for a purely sinusoidal field of amplitude appropriate to the intensity at that instant. The fast response of the electron's motion, as evidenced by the nonresonant character of χ_v , together with the knowledge that, at intensities of interest, the electron is gaining negligible energy (staying "cold"), implies that the absorbed energy is being passed on essentially instantaneously to the phonons via the coupling eq (2b). Therefore, it is valid to obtain the rate of deposition of energy in the lattice by determining the rate at which the electrons absorb energy from the optical beam, and we return to this problem.

When a room temperature correction is made to v and w , we guess that, as for small a , the result is raised by around 30% so that the Frohlich model may be taken to yield

$$\text{Im}\chi_v \sim 20 \quad (11)$$

for a ruby laser beam driving an electron of band mass equal to a free electron mass in ruby or sapphire at room temperature. The main uncertainty in eq (11) comes from the uncertainty in the effective band mass m_b . $\text{Im}\chi_v$ varies roughly as $m_b^{1/2}$.

If the temperature goes higher than the phonon energy but is still small compared with ν , then eq (9) yields

$$\text{Im } \chi_y \sim 4\alpha \nu^{1/2} / (3\beta) \quad ; \quad \alpha \ll 1, \quad 1 \ll \beta^{-1} \ll \nu, \quad (12)$$

showing that the heated lattice causes the electrons to absorb even more light. Note that the "Q" of the electron's oscillation, $\nu^2 / (2 \text{Im } \chi_y)$, is of order 7 for our estimate eq (11), showing that indeed the optical frequency is much larger than the effective electron collision frequency as we assumed.

One can see at this point that absorption by conduction electrons may cause damage, for, if the electron density were 10^{16} cm^{-3} at an optical intensity of 10^{10} W/cm^2 (which the evidence outlined in Section 1 suggests as a conservative estimate), and if eq (11) were valid, then $\omega_p^2 \sim 10^{-3}$ and eq (8) gives $\chi_y \sim 0.012 \text{ cm}^{-1}$. For a 30 nsec pulse this absorption would deposit 40 J per cc in the lattice, somewhat less than the value U_0 expected to cause damage. However, Belikova, et al. [7], gave convincing evidence that the electron density is increasing very rapidly with optical intensity at these levels, an occurrence which we expect for reasons given in the following section. Before considering factors which affect the electron density, however, we consider contributions other than those of the linear response eq (9) to electron damping.

First, the question arises as to whether there are significant intensity-dependent corrections to the electron response at the optical frequency as represented by eq (9). (Responses at harmonic frequency multiples do not contribute to the average work done by the optical field on the electrons and so we need not consider these here.) There are two types of nonlinear corrections to eq (9): first, those arising from the nonlinear reactions of the phonons on the electron, and, second, those arising from the intensity-dependent deviations of the momentum distribution of electrons from a thermal distribution. We have estimated both effects by expanding the quantum expression for the expected electron position (and velocity) to the third order in the electric field. We have found that both effects tend to diminish the optical absorption from its linear response value, a result expected on the physical grounds that electrons of high energy interact less with the optical phonons than do low-energy electrons. For both corrections the natural dimensionless expansion parameter is $(k_0 r_0)^2$ where k_0 is the wavevector of an electron having energy $\hbar\nu$ and r_0 is the classical amplitude of a free electron oscillating in the applied optical field. In our case this parameter is $\sim [(W/\text{cm}^2) \times 10^{-13}]^{1/2}$. Since optical intensities have not yet been observed to approach even 10^{11} W/cm^2 before damage, we conclude that the nonlinear corrections to eq (9) are too small to be of importance in present considerations.

Next, we see why, under conditions of interest here, phonon scattering of conduction electrons dominates scattering by ionized and un-ionized lattice impurities. For each conduction electron there is in the lattice a heavy positive ion whose charge is shielded roughly by the static dielectric constant of the lattice ($\epsilon_0 \sim 10$). The linear absorption by 10^{16} electrons per cc in such a two-component plasma at room temperature is $\sim 10^{-6}$ per cm^2 [11]. This is so small compared with phonon effects that one can readily appreciate that even if 10^{19} per cm^3 of electrically neutral scattering centers were added to the lattice, one would not expect them to scatter electrons as effectively as do phonons at room temperature and above. This predominance of phonon scattering at or above room temperature has been observed in various ways even in crystals whose electron-phonon coupling is much smaller than in ruby and sapphire [12]. Having estimated the optical response of a single conduction electron, we now proceed to consider how their numbers are affected by their interactions with lattice impurities.

5. Conduction Electron Interactions with Impurities

From incomplete existing absorption [13] and luminescence [8] data, it is evident that sapphire has a complex impurity level structure with energy differences ranging up to at least 3 eV. Light of any single optical wavelength, such as 6943 \AA , will not be resonant with a significant fraction of the bound-bound transitions and, of course, will only excite transitions to the conduction band from bound levels within 1.8 eV of the band edge. If, however, the light became effective in exciting a large fraction of the bound-bound transitions, then cascade transitions of electrons into the conduction band from levels lying more than 1.8 eV below the band edge might dominate direct photo-excitation. We shall now show that, at conduction electron densities $\sim 10^{16} \text{ cm}^{-3}$, the light does become so effective in exciting bound-bound transitions with which it is not resonant that cascade photo-excitation may become important in increasing the conduction electron density near optical damage intensities. These non-resonant transitions are possible because the conduction electrons readily absorb the difference in energy $\nu - \omega_{ba}$ between an absorbed photon and the energy of transition between the upper and lower states $|b\rangle$ and $|a\rangle$. We now show that the rate R_{ab} for a typical impurity to make such a transition, multiplied by a reasonable impurity density ($\sim 10^{19} \text{ cm}^{-3}$), may exceed the total direct photo-excitation rate, and thereby initiate cascade ionization of impurities.

To calculate the rates R_{ab} it is convenient to re-express the interaction of eq (3) as a Fourier transform (the impurity index a is now omitted since we are considering only one impurity):

$$v_i = \sum_{\mathbf{k}} v_{\mathbf{k}} e^{i\mathbf{k} \cdot \mathbf{x}} \quad (13)$$

where $v_{\mathbf{k}}$ is the impurity operator $4\pi e^2 V^{-1} \epsilon_s^{-1} k^{-2} \sum_j \exp i\mathbf{k} \cdot \mathbf{r}_j$ and V is a fiducial interaction volume. The sum is confined to the bound impurity electrons as only electronic transitions will be considered. For the transitions of interest we may take ϵ_s to be the optical dielectric constant ϵ . With the form eq (13) it is a straightforward matter to re-derive the quantum "Golden Rule" for calculating transition rates but with an unperturbed Hamiltonian $h_0 = \frac{1}{2}(\mathbf{p} - \mathbf{A}_0 \cos \nu t)^2$ instead of $\frac{1}{2}p^2$. To lowest order in the electron-impurity interaction, the rate for an electron to scatter from momentum state $|\mathbf{p}\rangle$ to $|\mathbf{p} + \mathbf{k}\rangle$ while the impurity goes from $|a\rangle$ to $|b\rangle$ is

$$\Gamma(\mathbf{p} \rightarrow \mathbf{p} + \mathbf{k}; a \rightarrow b) = 2\pi |\langle b | v_{\mathbf{k}} | a \rangle|^2 \sum_{n=-\infty}^{\infty} \delta(k^2/2 + \mathbf{p} \cdot \mathbf{k} + \omega_{ba} + n\nu) \cdot [J_n(\mathbf{k} \cdot \mathbf{r}_0)]^2 \quad (14)$$

where we have retained the terms for n -photon emission and absorption for future comparison with the $n = 1$ term that we are now considering. In the polaron units used here the classical electron oscillation amplitude r_0 equals E/ν^2 , where the real amplitude E of the optical electric field equals the amplitude in esu divided by $E_0 = (\omega_0^2/e)(\hbar m_0/\omega_0)^{1/2}$. For our parameters E equals (the field in V/cm) $\div (1.24 \times 10^6)$. The Bessel function coefficients J_n in eq (14) are the exact amplitudes for absorbing (or emitting) n optical photons in the process. Their arguments squared are of order $10^{-13} \text{ I(W/cm}^2\text{)}$ and so the approximation $J_n(x) \sim (x/2)^n/n!$ is accurate here. Consider now the rate r_{ab} for the impurity interacting with one electron in the optical field to make a transition from a state $|a\rangle$ to a state $|b\rangle$, for which $\omega_{ba} < \nu$. In terms of the rate eq (14)

$$r_{ab} = \sum_{\mathbf{p}, \mathbf{k}} f(\mathbf{p}) \Gamma(\mathbf{p} \rightarrow \mathbf{p} + \mathbf{k}; a \rightarrow b) \quad (15)$$

where $f(\mathbf{p})$ is the initial conduction electron distribution and only the $n = 1$ term in Γ is needed. To evaluate r_{ab} it remains to estimate the dependence of the matrix elements of $v_{\mathbf{k}}$ on \mathbf{k} . We shall use the "dipole approximation" in which $\langle b | \exp i\mathbf{k} \cdot \mathbf{r}_j | a \rangle \sim i\mathbf{k} \cdot \langle b | \mathbf{r}_j | a \rangle$. For definiteness we will assume that the impurity is spherically symmetric so that $|\sum_j \mathbf{k} \cdot \langle b | \mathbf{r}_j | a \rangle|^2 = k^2 X_{ba}^2$ where X_{ba} is the dipole matrix element of the impurity transition. Finally, before evaluating eq (15), we average over all directions of \mathbf{E} so that the J_1^2 terms becomes $(kE/2\nu^2)^2/3$. The $n = 1$ contribution to the sum over \mathbf{k} in eq (15) is then

$$r_{ab} = V^{-1} 8\pi e^4 (r_0^2/12) \epsilon^{-2} X_{ab}^2 \sum_{\mathbf{p}} L(\mathbf{p}) f(\mathbf{p}) \quad (16a)$$

where

$$L(\mathbf{p}) = \int_{K_m - \mathbf{p}}^{K_m + \mathbf{p}} d\mathbf{k} k^{2n-1}/p. \quad (16b)$$

Generally $K_m = [p^2 + 2(\nu - \omega_{ba})]^{\frac{1}{2}}$ is much larger than the magnitude of \mathbf{p} allowed in $f(\mathbf{p})$. In this case, it is sufficiently accurate to approximate eq (16b) by

$$L \sim 2[2(\nu - \omega_{ba})]^{\frac{1}{2}} \quad (17)$$

and we see that the impurity excitation rate is essentially independent of the initial small conduction electron momentum \mathbf{p} . Since $\sum_{\mathbf{p}} f(\mathbf{p}) = 1$, this fact makes the sum in eq (16a) trivial. The total rate R_{ab} for an impurity to absorb a photon is r_{ab} times the number of conduction electrons in the interaction volume V . It is convenient to express R_{ab} in terms of a photon absorption cross-section σ_{ab} which equals $R_{ab} \div$ (the incident photon flux). Recalling that $2\nu r_0^2$ is numerically $10^{-13} \text{ I(W/cm}^2\text{)}$, we have from eq (15) for sapphire

$$\sigma_{ab} \sim 7.5 \times 10^{-11} \text{ I} X_{ab}^2 \epsilon^{-2} \nu^{-1} (\nu - \omega_{ba})^{\frac{1}{2}} \rho_e \quad (18)$$

in polaron units where the electron density ρ_e is 6.15×10^{-22} times the number of electrons per cc ρ .

To see the importance of the transition cross-section eq (18) relative to direct photo-excitation, we estimate the density of impurities $N_i \text{ cm}^{-3}$ that would be required to attenuate the optical beam more than does the direct photo-excitation process. Of course, the latter attenuation is not known, but it must be less than the total attenuation in sapphire, and that is less than 10^{-2} per cm. For argument, suppose that direct photo-excitation causes less than 10^{-3} per cm optical attenuation (it probably causes much less). For our estimate, let us assume in eq (18) that $X_{ab}^2 \sim 1/\psi_{ab}$, $\omega_{ab} \sim 8$, and $I = 10^{10} \text{ W/cm}^2$ and $\theta = 10^{16}$ as in previous examples. This gives $\tau_{ab} \sim 10^{22} \text{ cm}^2$, so that $N_i \sim 10^{19}$ impurities per cc would be required to make these conduction-electron-mediated impurity transitions attenuate the optical beam by 10^{-3} per cm. Considering all the kinds of dislocations and foreign ions which might take part as impurities in this process, we feel that it is not unreasonable that such an impurity density could exist. Of course, there are so many order-of-magnitude estimates of unknown quantities in the foregoing that the result can only be considered as suggestive of a kind of process that must be considered as competitive with other possibilities at this time. However, the experimental observation of a rapidly increasing dc photoconductivity near damage thresholds [7] does suggest a "bootstrap" process such as the above by which conduction electrons can create more of their kind, even before they become so energetic as to ionize the lattice.

We have examined the enhancement of the single-photon bound-free photo-excitation transitions that arise from eq (14), and have estimated that excitation cross-section also to be of order 10^{-22} cm^2 under the same conditions. This is probably less than the cross-section for direct photo-excitation. If multi-photon excitation is important in producing electrons, then the higher n terms of eq (14) probably dominate direct absorption near damage levels. The expansion parameter in eq (14) is of order $10^{-13} \text{ I(W/cm}^2\text{)}$, whereas it is $\sim 10^{-17} \text{ I}$ for direct multi-photon absorption.

6. Focusing Effects

In a region of the crystal in which conduction electrons have been excited there is a change in the refractive index δn given by

$$\delta n = -\omega_p^2/v^2. \quad (19)$$

At a density 10^{16} cm^{-3} , electrons (with free electron band mass) have a plasma frequency of 10^{12} Hz , which gives $\omega_p/v \sim 0.0023$ and $\delta n \sim 5.3 \times 10^{-6}$. This index change is comparable to that required to self-focus a one milliradian gaussian beam. If the electron density were proportional to the optical intensity I , and this index change were produced when $I = 10^{10} \text{ W/cm}^2$, then the index change would constitute a second order nonlinear index (often written $n_2 E^2$) whose nonlinear coefficient n_2 would be $-2 \times 10^{-13} \text{ esu}$. This is negative and an order of magnitude larger than what one would guess is the intrinsic nonlinear index of the bound electrons in sapphire. However, we suspect that the electron density is increasing much more rapidly than I at high intensities [7] and so the effect of the index of eq (19) is not simple. Furthermore, impurity electrons which are excited to bound states more than v below the band edge, such as by the process discussed in the previous section, have an increased polarizability and would tend to cancel the effect eq (19) of conduction electrons.

Suppose the net effect of impurity transitions were to produce a negative and highly nonlinear refractive index change, as would be the case if the conduction electron effect eq (19) dominated. Then there would be strong self-defocusing of a beam in regions of very high intensity, but only the intrinsic self-focusing index would be operative in regions of smaller intensity. This would evidently result in successive regions of high intensity along the beam as each effect produces in turn a focusing tendency that brings the other effect into dominance. Damage tracks in sapphire and other materials consist of a sequence of damage bubbles that are suggestive of such a process. However, we have not calculated the spacing of the successive high-intensity regions on the basis of some reasonable model to see whether there is any possible correspondence between these speculations and observation.

7. Discussion

Although there are alternate explanations for the behavior of damage tracks observed in sapphire [14], it seems likely that self-focusing is occurring and playing a role in the damage. (It is curious that the appearance, lengths, and positions of damage tracks differ between ruby and sapphire [14].) If self-focusing is occurring, it makes especially difficult the determination of the actual optical intensities at which the material ruptures, and this in turn lends an extra uncertainty to the parameters we have used in discussing the role of conduction electrons in damage. Probably the most promising way to determine more precisely what the electrons' role may be is to determine the parameters of these conduction electrons below damage intensities. It would be especially desirable to have reliable dc photoconductivity measurements between the intensities 5 W/cm^2 , the highest used by Hochuli [5], and 10^{10} W/cm^2 , the lowest used by Delikova, et al. [7], in their measurements. With the high light intensities available with lasers, it may now be possible to excite enough electrons to obtain a

meaningful Hall effect. Perhaps the time decay of photoconductivity and luminescence after an exciting pulse could be observed and yield information on carrier lifetimes, trapping times, etc. Unfortunately, the important and pervading parameter — the effective mass in the conduction band (and its anisotropy) — appears to be extremely difficult to determine experimentally.

Should the photo-excited electrons be found to play significant roles in damage, such as those we have discussed, then it may be possible to fabricate more damage-resistant sapphire and ruby. For example, if self-focusing is presently instrumental in damage, then it might be reduced by adding donor impurities that produce a linear photoconductivity at high intensities and thus reduce the total nonlinear index via the index change of eq (19). On the other hand, those donors that give a highly nonlinear photoconductivity and a sudden production of high electron densities that result in rupture by photo-absorption may perhaps be eliminated from the crystals or compensated by other additives. In any case, it is evident that the availability of high-intensity laser sources will greatly facilitate the study of the conduction bands and impurity levels in very weakly photoconducting materials such as sapphire and ruby.

8. References

- [1] A. Wasserman, "A mechanism for damage in solids by intense light," *Appl. Phys. Letters* 10, 132-133 (1967).
- [2] Y. A. Pashkov and G. M. Zverev, "Destruction of ruby and leucosapphire crystals by strong laser radiation," *Soviet Phys. -JETP* 24, 516-518 (1967).
- [3] E. A. Sviridenkov, "Mechanism of damage of ruby by laser radiation," *Soviet Phys. -Solid State* 9, 1917-1918 (1968).
- [4] G. M. Sverev, T. N. Mikhailova, V. A. Pashkov, and N. M. Solov'eva, "Mechanisms of destruction of ruby and leucosapphire crystals by powerful laser radiation," *Soviet Phys. -JETP* 26, 1053-1057 (1968).
- [5] Urs E. Hochuli, "Photoconductivity in ruby and sapphire," *Phys. Rev.* 133A, 468-471 (1964).
- [6] R. P. Feynman, R. W. Hellwarth, C. K. Iddings, and P. M. Platzman, "Mobility of slow electrons in a polar crystal," *Phys. Rev.* 127, 1004-1017 (1962). Hereinafter referred to as FHIP.
- [7] T. P. Belikova and E. A. Sviridenkov, "Photoconductivity of ruby when strongly irradiated by a ruby laser," *JETP Letters* 3, 257-259 (1966).
- [8] T. P. Belikova, A. N. Savchenko, and E. A. Sviridenkov, "Optic breakdown in ruby and related effects," *Soviet Phys. -JETP* 27, 19-23 (1968).
- [9] L. Spitzer, Jr., *Physics of Fully Ionized Gases* (Interscience Publishers, New York, 1956).
- [10] H. Frohlich, "Theory of electrical breakdown in ionic crystals," *Proc. Phys. Soc. (London)* A160, 230-241 (1937).
- [11] V. I. Perel and G. M. Eliashberg, "Absorption of electromagnetic waves in plasma," *Soviet Phys. -JETP* 14, 633-637 (1962).
- [12] R. H. Bube, *Photoconductivity of Solids* (John Wiley and Sons, New York, 1960).
- [13] N. V. Beardsley, *Proceedings of the Infrared Information Symposia*, Volume 1, No. 2, 47-53 (1956).
- [14] C. R. Giuliano and L. D. Hess, "Laser-induced damage in ruby and sapphire," in these *Proceedings*.

COMMENTS ON PAPER BY ROBERT HELLWARTH

The model employed in this paper was specifically developed for crystalline solids containing impurities. This model, involving definite impurity levels imposed on a well-defined band structure, does not apply to glasses in its present form.

APPENDIX B

THEORY OF ELECTRON VELOCITY DISTRIBUTION IN CRYSTAL IRRADIATED BY A STRONG OPTICAL BEAM

A. INTRODUCTION

Described here is the theoretical effort during the project period that was devoted to an attempt to understand in a fundamental way the heating of electrons in polar crystals by intense optical fields. Several theories have been proposed^{1, 2} in which the electrons gain enough energy from the laser radiation to overcome the energy loss due to the radiation of optical phonons and are "heated" to energies exceeding the valence-conduction band energy gap. These hot electrons ionize the lattice, each hot electron producing two slow electrons and a hole, which in turn are heated by the optical field. This results in an avalanche of carrier multiplication which results in a rapid increase in the absorption of laser energy. The absorption of a large energy in a small volume of the crystal is assumed to be the primary cause of the observed damage.

The theories of Zverev, et al.,² and Wasserman¹ were of the type described above. While appearing reasonable at first glance, they suffer from the weakness of being based on rather heuristic arguments. Both theories predict an avalanche threshold about an order of magnitude greater than that observed in sapphire. Recent experiments at Massachusetts Institute of Technology using CO₂ laser radiation in alkali halide crystals seem to agree with the estimates of Zverev's theory.³ Hellwarth⁴ conducted a study in which he found, on the basis of a more fundamental approach, that electrons could not be heated sufficiently by an optical field in ruby or sapphire to trigger an avalanche process. He suggested some alternate absorption mechanisms.

Because of the apparent controversy concerning the possibility of electron heating and avalanche in an intense optical field in ruby or

sapphire, we have begun an independent study. We have succeeded in deriving a kinetic equation describing the time evolution of the electron momentum (i. e. , lattice momentum) distribution function. The Frölich model of electrons interacting with longitudinal optic phonons in a polar crystal is used as in all the previous studies. The electron-phonon interaction is treated in lowest order perturbation theory. This not a good approximation for ruby or sapphire for which the polar coupling is strong and real polaron effects must be taken into account.⁴ However, it is the basis for the work of Zverev² and Wasserman¹ and is hoped to be of qualitative value for determining the feasibility of electron heating. In the kinetic theory, which we are developing, the interaction of the electromagnetic field of the laser with the electron is treated exactly to all orders.

Unfortunately, at the time of this report, the research is not complete. The detailed consequences of this kinetic theory are still not understood. Nevertheless, we believe the kinetic equation to be described here offers a fundamental basis to settle the questions of electron heating and work will continue on this problem.

B. KINETIC EQUATION

We will present a detailed derivation of the kinetic equation for electrons interacting with phonons in an intense ac electric field in another publication. This derivation is based on the Green's function formulation of nonequilibrium quantum statistical mechanics which has been used by the author in several previous studies.⁵ Here, we will start from this kinetic equation, carry out some simplifications and discuss its physical content and conditions for validity. Let $n_p(t) dp_x dp_y dp_z$ be the average number of electrons with lattice momenta in the range p_x to $p_x + dp_x$, etc. Then the equation for the time rate of change for this momentum distribution function is shown to be

$$\frac{dn_p(t)}{dt} = \frac{-eE_c}{2\pi m^*} \int \frac{d^3k}{k^2} \int_{-\infty}^{\infty} d\omega \int_0^{\infty} dt' \cos\left(\int_{t-t'}^t \frac{d\tau}{\hbar}\right) \left[h_{p+k}(\tau) - h_p(\tau) - \omega \right]$$

$$\left\{ \left[1 + n_{p+k} \left(t - \frac{t'}{2} \right) \right] n_p \left(t - \frac{t'}{2} \right) D_k^<(\omega) - n_{p+k} \left(t - \frac{t'}{2} \right) \left[1 + n_p \left(t - \frac{t'}{2} \right) \right] D_k^>(\omega) \right\} . \quad (4)$$

Here, E_c is a constant with the dimensions of an electric field intensity which measures the strength of the electron-phonon coupling in the Frölich theory

$$E_c = e\omega_{LO} \left(\frac{1}{\epsilon_{\infty}} - \frac{1}{\epsilon_0} \right) \frac{m^*}{\hbar} \quad (5)$$

where ω_{LO} is the LO phonon frequency (assumed independent of k), ϵ_{∞} and ϵ_0 are the high frequency and static dielectric constants, respectively, and m^* is the electron effective mass.

Approximation 1. We emphasize again that this equation is valid only to lowest order in the electron-phonon coupling. The LO phonon spectrum is contained in the functions

$$D_k^<(\omega) = \left[N_0 \delta(\omega - \omega_{LO}) + (N_0 + 1) \delta(\omega + \omega_{LO}) \right] \quad (6)$$

$$D_k^>(\omega) = e^{\beta\hbar\omega} D_k^<(\omega) . \quad (7)$$

where N_0 is the thermal equilibrium phonon occupation number

$$N_0 = \frac{1}{e^{\beta \hbar \omega_{LO}} + 1} \quad (8)$$

Approximation 2. The phonons are assumed to remain in equilibrium at the lattice temperature $T = \beta^{-1} k_B^{-1}$ (k_B = Boltzmann's constant). This approximation will fail once a considerable amount of heating occurs but should be sufficient for the calculation of avalanche thresholds.

The function $h_p(\tau)$ is the kinetic energy part of the Hamiltonian for an electron in a spatially uniform time-dependent electric field represented by the vector potential $A(t)$

$$h_p(\tau) = \frac{1}{2m^*} \left(p - \frac{e}{c} A(\tau) \right)^2 \quad (9)$$

The factors

$$\exp \pm i \int_{t-t'}^t \frac{d\tau}{\hbar} h_p(\tau)$$

which make up the cosine term in eq. (4) arise from the exact solution of the time-dependent Schrodinger equation in a spatially uniform ac field

$$i\hbar \frac{\partial}{\partial t} \psi_p(t) = h_p(t) \psi_p(t) \quad (10)$$

Thus, the kinetic equation treats the motion of free electrons in the ac field exactly.

Approximation 3. We have assumed a parabolic energy-momentum relation for electrons in the conduction band. This

approximation is easily relaxed to take into account nonparabolicity which is undoubtedly important for electrons excited high in the band.

For the ac field represented by the laser, the vector potential $A(\tau)$ can be taken to be

$$A(\tau) = \frac{-c E_0}{\omega_0} \sin \omega_0 \tau . \quad (11)$$

Approximation 4. The electromagnetic field is taken to be spatially uniform. This is not bad so long as the magnitude of the classical excursion

$$d = \frac{e E_0}{m^* \omega_0^2} \quad (12)$$

of an electron in the field is small compared with a wavelength of the actual physical field. This requirement is always well satisfied.

Using this form for the vector potential we obtain

$$\begin{aligned} \frac{1}{\hbar} \int_{t-t'}^t d\tau \left[h_{p+k}(\tau) - h_p(\tau) \right] &= (e_{p+k} - e_p) \frac{t}{\hbar} \\ &- \frac{k \cdot d}{\hbar} \left[\cos \omega_0 t - \cos \omega_0 (t-t') \right] , \end{aligned} \quad (13)$$

where d is given by eq. (12) and $e_p = p^2/2m^*$.

Approximation 5. We assume the electron density remains low enough that degeneracy can be neglected, i. e., $n_p(t) \ll 1$. Then the

expression in curly brackets in eq. (4) can be written as

$$\left\{ D^<(\omega) \left[n_p \left(t - \frac{t'}{2} \right) - n_{p+k}(t-t'/2) e^{\beta \hbar \omega} \right] \right\} \quad (14)$$

where (7) has been used.

Next, we use the well-known Bessel function identity,

$$e^{ia \sin X} = \sum_v J_v(a) e^{-ivX}, \quad (15)$$

to write

$$\begin{aligned} & \cos \left[\left(\omega - \epsilon_{p+k} + \epsilon_p \right) \frac{t}{\hbar} + \frac{k \cdot d}{\hbar} \left(\cos \omega_0 t - \cos \omega_0 (t-t') \right) \right] \\ &= \text{Re} \left[e^{i(\omega - \epsilon_{p+k} + \epsilon_p)t/\hbar} \sum_{\mu, \nu} J_\mu \left(\frac{k \cdot d}{\hbar} \right) J_\nu \left(\frac{k \cdot d}{\hbar} \right) e^{i\nu \omega_0 t} \right. \\ & \quad \left. e^{-i\mu \omega_0 (t-t')} e^{i(\nu - \mu)\pi/2} \right] \end{aligned} \quad (16)$$

To consider the periodicity impressed upon the system by the strong ac field, it is useful to write the distribution function as a Fourier series with fundamental frequency ω_0 , whose coefficients are slowly varying functions of time on the scale of ω_0^{-1} .

$$n_p(t) = \sum_n F_n(p, t) e^{-in\omega_0 t} \quad (17)$$

On substituting eqs. (17), (16), (13), and (14) into eq. (4), we obtain the coupled set of equations for the Fourier coefficients

$$\begin{aligned}
\frac{\partial F_n(p, t)}{\partial t} - i n \omega_0 F_n(p, t) &= \frac{e E_c}{2 \pi m^*} \int \frac{d^3 k}{k^2} \int_{-\infty}^{\infty} d\omega D^<(\omega) \\
\sum_{\mu, m} J_{\mu} \left(\frac{k \cdot d}{\hbar} \right) J_{\mu+m-n} \left(\frac{k \cdot d}{\hbar} \right) &\delta \left(\hbar \omega + \hbar(\mu + m/2) \omega_0 - \epsilon_{p+k} + \epsilon_p \right) \\
\left[F_m(p+k, t) e^{\beta \hbar \omega} - F_m(p, t) \right] &. \quad (18)
\end{aligned}$$

Approximation 6 (Weak Coupling). This is an extremely complicated infinite hierarchy of equations in general. However, if we assume that the electron-phonon interaction as measured by E_0 is weak, then the assumption

$$F_0 \gg F_n \quad \text{for } n \neq 0 \quad (19)$$

is valid. This follows since $\partial F_n / \partial t \ll n \omega_0 F_n$ for $n \neq 0$. Then if we adopt an iterative procedure starting by keeping only the $m = 0$ term on the right side of eq. (18), we see that F_n is proportional to $E_c / n \omega_0$ times F_0 ($n \neq 0$) which we assume to be small. We repeat that this procedure is valid only in the weak coupling limit for the electron-phonon approximation. In fact, the kinetic equation (18) is only valid in this case. This approximation fails for the parameters of ruby and sapphire. We use it mainly because it is the only known procedure for the nonequilibrium polar problem.

Thus, to lowest order in the electron-phonon coupling, the fundamental kinetic equation for the dc component of the electron distribution function is taken to be

$$\frac{\partial F_0(p, t)}{\partial t} = \frac{e E_c}{2\pi m^*} \int \frac{d^3 k}{k^2} \int_{-\infty}^{\infty} d\omega D^<(\omega) \sum_{\nu=-\infty}^{\infty} J_{\nu}^2\left(\frac{k \cdot d}{\hbar}\right) \delta(\hbar\omega + \nu\hbar\omega_0 - \epsilon_{p+k} + \epsilon_p) [F_0(p+k, t) e^{\beta\hbar\omega} - F_0(p, t)] . \quad (20)$$

We have not yet succeeded in obtaining a complete solution of this equation. Not the least complication is the involved dependence on the radiation intensity occurring through the Bessel functions $J_{\nu}^2(k \cdot d/\hbar)$. Examination of the requirements imposed on k by the delta function shows that values of k as large as $\sqrt{2m^*\nu\omega_0}$ can be important in the integrand. In intensity units then, $(k \cdot d/\hbar)^2 \lesssim \nu 10^{-13} I$, where I is in watts/cm². For the laser powers necessary for damage ($I \sim 10^{10}$ W/cm²), this parameter is small and the Taylor expansions of the Bessel functions can be used.

$$\begin{aligned} \frac{\partial F_0(p, t)}{\partial t} = & \frac{e E_c}{2\pi m^*} \int \frac{d^3 k}{k^2} \int_{-\infty}^{\infty} d\omega D^<(\omega) \left\{ \left(1 - \frac{1}{2} \left(\frac{k \cdot d}{\hbar} \right)^2 \right) \delta(\hbar\omega - \epsilon_{p+k} + \epsilon_p) \right. \\ & + \frac{1}{4} \left(\frac{k \cdot d}{\hbar} \right)^2 \left[\delta(\hbar\omega + \hbar\omega_0 - \epsilon_{p+k} + \epsilon_p) \right. \\ & \left. \left. + \delta(\hbar\omega - \hbar\omega_0 - \epsilon_{p+k} + \epsilon_p) \right] \right\} [F_0(p+k, t) e^{\beta\hbar\omega} - F_0(p, t)] . \quad (21) \end{aligned}$$

In this limit the various terms in the equation have a simple interpretation in terms of the transition rates for elementary processes calculated by Fermi's Golden Rule. The first term in curly brackets of order 1 can be shown to produce the difference of the rates for scattering-in and scattering-out of the state p by emission or absorption of LO phonons. The first term of order $(k \cdot d/\hbar)^2$ is the correction to these rates for the coherent possibility of absorbing and emitting a photon in this process. The second term of order $(k \cdot d/\hbar)^2$ produces the difference of the rates of scattering-in and scattering-out of the state p by either emitting or absorbing a photon and emitting or absorbing an LO phonon. The latter processes are essentially those of electron-phonon Bremsstrahlung emission and absorption.

The kinetic equation (20) is not complete for this problem because it does not contain terms which account for the process of impact ionization. We will not try to formulate these terms precisely here, but rather will discuss their qualitative features. The missing terms consist of a high-energy "sink" or loss term which accounts for those electrons whose energy exceeds the ionization threshold $\mathcal{E}_I \gtrsim \mathcal{E}_{\text{gap}}$ and lose their energy by impact ionization collisions with the lattice. There is also a low-energy "source" term which takes into account the two low-energy electrons which appear as a result of the impact ionization processes (i. e., the high-energy electron loses its energy to produce another low-energy electron plus a hole). We may consider that eq. (20) is valid for an intermediate band of energies $\mathcal{E}_{\text{max}} < \mathcal{E} < \mathcal{E}_I$ where \mathcal{E}_{max} is a measure of the maximum energy at which new electrons are created. It appears reasonable to take $\mathcal{E}_{\text{max}} < \hbar\omega_0$.

C. APPROXIMATE CONSIDERATIONS

In an effort to gain some feeling for the predictions of eq. (20) we have taken the case $k \cdot d \ll 1$, which is well satisfied by the experiments. As we have seen, the Bessel functions can be expanded in this case as in eq. (21). It is convenient to transform this equation to new variables, $\mathcal{E} = p^2/2m^*$ and μ — the cosine of the angle between the radiation polarization \underline{E}_0 and \underline{p} .

$$\frac{\partial F_0(\mathcal{E}, \mu, t)}{\partial t} = \frac{e E_c}{p} \int_{-1}^1 d\mu' \int_{-\infty}^{\infty} d\omega D^<(\omega) \left\{ \frac{1 - (1/2\hbar^2) d^2(p\mu - p_\omega \mu')^2}{r_\omega} [F(\mathcal{E} + \omega, \mu') e^{\beta \hbar \omega} - F(\mathcal{E}, \mu)] \right. \\ \left. + \frac{d^2}{4\hbar^2} \frac{(p\mu - p_\pm \mu')^2}{r_\pm} [F(\mathcal{E} + \omega \pm \omega_0, \mu') e^{\beta \hbar \omega} - F(\mathcal{E}, \mu)] \right\} \quad (22)$$

where

$$p = \sqrt{2m^* \mathcal{E}}$$

$$p_\omega = \sqrt{2m^* (\mathcal{E} + \omega)}$$

$$p_\pm = \sqrt{2m^* (\mathcal{E} + \omega \pm \omega_0)} \quad (23)$$

$$r_\sigma = [t_\sigma^2 - 2t_\sigma \mu \mu' + \mu^2 + \mu'^2 - 1]^{1/2} \quad (24)$$

$$t_\omega = \frac{1}{2} \left(\frac{p}{p_\omega} + \frac{p_\omega}{p} \right) ; \quad t_\pm = \frac{1}{2} \left(\frac{p}{p_\pm} + \frac{p_\pm}{p} \right) \quad (25)$$

The last term in eq. (22) is a shorthand notation for the sum of both the + and - indexed quantities.

Next we write $F_0(\mathcal{E}, \mu) = e^{-\beta X(\mathcal{E}, \mu)}$ and make use of the fact that X will be a more slowly varying function of \mathcal{E}, μ than F_0 . We divide the equation through by F_0 . Differences such as

$$X(\mathcal{E} + \omega \pm \omega_0, \mu') - X(\mathcal{E}, \mu)$$

are Taylor-expanded in the form

$$(\omega \pm \omega_0) X_{\mathcal{E}}(\mathcal{E}, \mu) + (\mu' - \mu) X_{\mu}(\mathcal{E}, \mu)$$

and higher derivative terms dropped. Here $X_\ell \equiv \partial X / \partial \ell$ and $X_\mu \equiv \partial X / \partial \mu$. The resulting equation can be written

$$-\beta \frac{\partial X}{\partial t} = \frac{e E_c}{p} \int_{-\infty}^{\infty} d\omega D^<(\omega) \left\{ \left[A_\omega(\ell, \mu; X_\mu) e^{-\beta \omega (X_\ell - 1)} - A_\omega(\ell, \mu; 0) \right] + \frac{d^2 p^2}{\hbar^2} \left[B_\pm(\ell, \mu; X_\mu) e^{\mp \beta \omega_0 X_\ell} - B_\pm(\ell, \mu; 0) \right] \right\}, \quad (26)$$

where we have assumed $\omega_0 \gg \omega (= \pm \omega_{LO})$ and where we define

$$A_\omega(\ell, \mu; X_\mu) = \int_{-1}^1 d\mu' \frac{e^{-\beta(\mu' - \mu)X_\mu}}{r_\omega}, \quad (27)$$

$$B_\pm(\ell, \mu; X_\mu) = \int_{-1}^1 d\mu' \frac{\left[\mu - \left(\frac{p_\pm}{p} \right) \mu' \right]^2}{r_\pm} e^{-\beta(\mu' - \mu)X_\mu}. \quad (28)$$

In the region $\ell_I > \ell \gg \omega_0 \gg \omega_{LO}$ it is clear that the parameters t_σ defined in eq. (25) all approach unity so that $A_{-\omega_{LO}} \rightarrow A_{+\omega_{LO}}$ and $B_+ \rightarrow B_-$. In this case the integration over ω (see eq. (6)) is trivial and the first factor in square brackets on the right side of eq. (22) can be written as

$$N_0 A_{\omega_{LO}}(\ell, \mu, X_\mu) \left[\left(e^{-\beta \omega_0 (X_\ell - 1)} - 1 \right) + e^{\beta \omega_{LO}} \left(e^{\beta \omega_{LO} (X_\ell - 1)} - 1 \right) \right] + (2N_0 + 1) \left[A_{\omega_{LO}}(\ell, \mu', X_\mu) - A_{\omega_{LO}}(\ell, \mu, 0) \right] \quad (29)$$

$$\cong N_0 A_{\omega_{LO}}(\ell, \mu, X_\mu) (\beta \omega_{LO})^{-1} X_\ell (X_\ell - 1) + 2N_0$$

$$\left[A_{\omega_{LO}}(\ell, \mu, X_\mu) - A_{\omega_{LO}}(\ell, \mu, 0) \right]. \quad (30)$$

In the last member of this equation we have assumed $\beta\omega_{LO} \ll 1$ and expanded. This is a good approximation for crystals above room temperature. In this limit $N_0 \cong (\beta\omega_{LO})^{-1}$. In the second term in square brackets on the right side of eq. (22), we note that since $\beta\omega_0 \cong 80$ for the cases of interest, the term with the positive exponential is likely to dominate so we neglect the other terms.

Finally we note that we are expecting exponential growth in the number of carriers during avalanche. Thus we assume that

$$F_0(p, t) = F_0(p) e^{t/\tau}, \quad (31)$$

where τ is a characteristic growth time. Then $\partial F_0 / \partial t = F_0 / \tau$. The growth is a result of the high-energy "sink" for $\ell > \ell_I$ and the low-energy "source" for $\ell < \omega_0$ which arise from the impact ionization process. These terms do not manifest themselves explicitly in the kinetic equation in the region $\omega_0 < \ell < \ell_I$ except through the time derivative term. Putting all these assumptions and approximations together leads to the equation

$$\begin{aligned} \frac{(\beta\omega_{LO}) p}{\tau c E_c} &= (\beta\omega_{LO})^2 A_{\omega_{LO}}(\ell, \mu, X_\mu) X_\ell (X_\ell - 1) \\ &+ 2 \left[A_{\omega_{LO}}(\ell, \mu; X_\mu) - A(\ell, \mu, 0) \right] + \frac{2d^2 p^2}{\hbar^2} B_+(\ell, \mu; X_\mu) e^{\beta\omega_0 X_\ell}. \end{aligned} \quad (32)$$

We have thus reduced eq. (22), which is an integro-differential-difference equation, to a nonlinear partial differential equation. Unfortunately, we also have not been able to find completely satisfactory analytic approximations to the solution of this equation. It is probably solvable by computer methods, but we have had neither time or support

for this. The boundary conditions for this equation must be determined by examining the physics of the high- and low-energy sink and source terms representing the impact ionization process. This problem is currently under study.

One very approximate conclusion can be obtained from eq. (32). First, we note that for zero radiation intensity and steady state, i. e., $d = 0$ and $\tau = \infty$, this equation has the solution $X_e = 1$, $X_\mu = 0$, corresponding to a Maxwellian distribution at the lattice temperature. Now, in the presence of the radiation the electrons will be "heated" most strongly in the $\mu = \pm 1$ directions (this follows from the dependence of the field arising as $k \cdot d$). Thus, we might expect the tail of the distribution to be drawn out, i. e., $X_e < 1$ in the $\mu = \pm 1$ directions, but to fall off faster in other directions. This implies $\beta X_\mu < -1$ for $\mu = \pm 1$.

From eqs. (27) and (28), it can be shown that for $\mu = \pm 1$ and $|\beta X_\mu| \gg 1$,

$$A_{\omega LO}(e, 1; X_\mu) = -\gamma - \log \left| \frac{\omega^2 \beta X_\mu}{8e^2} \right|, \quad (33)$$

where $\gamma = 0.5772$ (Euler's constant),

$$B_\pm(e, 1, X_\mu) = \frac{2}{(\beta X_\mu)^2}. \quad (34)$$

To a good approximation, an asymptotic relation for X_e can be obtained from eq. (32).

$$X_e = \frac{1}{\beta \hbar \omega_0} \log \left\{ \frac{(\beta X_\mu)^2}{2I_0} \cdot 10^{13} \frac{\omega_0}{e} \left[\frac{\tau_{e-ph}(e)}{\tau} + 2(\gamma + \log |2\beta X_\mu|) \right] \right\} \quad (35)$$

where $\tau_{e-ph}(e) = \sqrt{2m^*e} / N_0 E_c$ is the well-known collision time for electron-polar-optic-phonon collision. This relation is valid as long as the argument of the log is $\gg 1$. If $|\beta X_\mu| \gg 1$, we see that X_e is a decreasing function of I_0 , the radiation intensity. In fact, since $\beta \hbar \omega_0 \approx 80$, $X_e < 1$ for any reasonable assignment of parameters. Note

that for the term involving the e-folding time τ to be important requires $\tau \ll \tau_{e-ph}$ or $\tau \ll 10^{-12}$ sec using $m^* = m_e$ and $E_c \cong 2 \times 10^2$ e.s.u. for sapphire and $\mathcal{E} = \hbar \omega_0$.

If $\tau \gg \tau_{e-ph}(\mathcal{E})$, we can neglect the τ -dependent term which implies that the steady solution of the kinetic equation (i. e., eq. (4) with $\partial F / \partial t = 0$) is all we need to consider. In this case, the solution is actually independent of the magnitude of E_c , as long as it is small enough so that the weak coupling approximation which we have been using is valid. The determination of τ as a function of I_0 awaits the completion of the solution satisfying the boundary conditions imposed by the impact ionization process.

This very rough estimate of the behavior of the solution of the kinetic equation makes plausible the following model of the distribution function: The population of electrons is highly nonisotropic, being drawn out into high-energy tails in the ($\mu = \pm 1$) direction of the radiation polarization. These high-energy tails may be sufficient to trigger the strong avalanche of impact ionization events necessary for the Wasserman-Zverev model. However, considerably more analysis of the detailed solution of the kinetic equation is necessary to establish this mode. Note that the average kinetic energy in the distribution will be much lower than the ionization energy \mathcal{E}_i but there may still be a sufficient number of hot electrons to trigger the avalanche. This is consistent with Hellwarth's observation that the mean kinetic energy of electrons is much lower than the band gap energy.

REFERENCES

1. A. Wasserman, Appl. Phys. Letters **10**, 132 (1967).
2. G. M. Zverev, T. N. Mikhailova, V. A. Pashkov and N. M. Solov'eva, Soviet Phys. - JETP **26**, 1053 (1968).
3. E. Yablonovitch, private communication.
4. R. W. Hellwarth, Proceedings of the ASTM Symposium on Laser Damage (June 1970).
5. D. F. DuBois, Lectures in Theoretical Physics Vol. IXC, edited by W. E. Brittin (Gordon and Breach, New York, 1967).